UNIVERSITY OF CALIFORNIA

Santa Barbara

Constraining the variability of optical properties in the Santa Barbara Channel, CA: A phytoplankton story

A dissertation submitted in partial satisfaction of the

requirements for the degree Doctor of Philosophy

in Marine Science

by

Rebecca Katherine Barrón

Committee in charge:

Professor David Siegel, Chair

Professor Craig Carlson

Professor Mark Brzezinski

Norm Nelson

December 2014

The dissertation of Rebecca Katherine Barrón is approved.

_____

Craig Carlson

_____

Mark Brzezinksi

_____

Norman Nelson

_____

David Siegel, Committee Chair

December 2014

Constraining the variability of optical properties in the Santa Barbara Channel, CA: A phytoplankton story

Rebecca Katherine Barrón

ACKNOWLEDGEMENTS

This work was funded by the University of California Diversity Fellowship, and NASA Earth and Space Science Fellowship. The majority of the data used in this dissertation was collected as part of a larger NASA funded program, Plumes and Blooms. Other data used were collected from the NSF funded Santa Barbara Channel Long Term Ecological Research station, the CLIVAR program (Climate and Ocean Variability, Predictability and Change), and the US Gological Servey. Chapter II of this disseration, *Evaluating the importance of phytoplankton community structure to the optical properties of the Santa Barbara Channel, California*, was published by Limnology and Oceanography. Thank you L&O for acceptance of my manuscript to your journal, and for editorial help from associate editor, Dariusz Stramski.

On a personal note, where do I begin? With Dave Siegel, of course, for all of your efforts including academic, financial and personal support for me to achieve this dream. You've gone above and beyond the call of duty for me, and supported me on my journey through graduate school and motherhood. Your words of encouragement were always warmly felt, and I appreciate you never giving up on me. Thanks to my committee members, Norm Nelson, Craig Carlson and Mark Brzezinski for your guidance through the years, and speedy review of my dissertation. It's truly been a privilege to work with all of you. Huge thanks to the Plumes and Blooms team, Nathalie Guillocheau, Stuart Halewood, David Court, Erik Stassinos, Dave Menzies, Fernanda Hendrikx-Freitas, Clarissa Anderson and Tiho Kostadinov. You guys are the best, and I will miss our disgusting lunchtime conversations on the Shearwater. Thanks to my graduate student mentors from the Siegel

group, Chantal Swan for helping me with the CDOM aspect of my dissertation, Tiho Kostadinov for help with the scattering aspect, and Kyle Cavanaugh for helping me with the EOF statistics, specifically suggesting to use the standard deviation lines in my figures. Fernanda, thanks for being the best office buddy, and discussing important women in science issues with me. You are an amazing woman and scientist.

Thank you to my husband, Mike Barrón. You have been there for me every step of the way. Thanks for being my rock through so many uncertain times, and in my hours of greatest doubt. To my parents and in-laws, thank you for your love and encouragement, and for always volunteering to watch babies while I traveled. Lastly, great big thanks go to my little ones, Adeline and Santino, aka my Inspiration and my Lover Boy. Everything I do, I do for you guys. I know it was hard to be away from me for so many long hours, and you guys did AWESOME. I love you both very much. I hope Mommy made you proud.

Rebecca K. Barrón

16957 SW Cashew Way (805) 698-2187
Beaverton, OR 97006 rkb.barron@gmail.com

EDUCATION

Doctor of Philosophy, Marine Science December 2014
University of California, Santa Barbara

- Dissertation**:** Constraining the variability of optical properties in the Santa Barbara Channel: A phytoplankton story

Master of Science, Soil and Water Science September 2007
University of California, Riverside

- Thesis: Natural and artificial mixing in Lake Elsinore, CA

Bachelor of Science, Environmental Science March 2004
University of California, Riverside

- Senior project: Identification of ground water intrusion in the San Diego Creek Watershed

EXPERIENCE

Graduate Student Researcher April 2009-December 2014

University of California, Santa Barbara

- Conduct oceanographic research in with specialty in marine optics
- Attend oceanographic cruises
- Use computer programming to build multivariate statistical models
- Work with/train students and lab personel

Graduate Student Researcher September 2007-March 2009
University of California, Santa Barbara

- Design and administer research projects for Toolik Lake, AK
- Maintain and calibrate lab and field instruments.
- Mentor undergraduates in the lab and field.

Graduate Student Researcher June 2005-June 2007
University of California, Riverside

- Design and administer research projects for Lake Elsinore, CA.
- Collect and analyze lake water and soil samples for several lakes.
- Maintain and calibrate lab and field instruments.
- Mentor undergraduates in the lab and field.

BTEX Lab Technician August 2004 – May2005
Del Mar Analytical Irvine, Ca

- Analyzed soil and water samples for BTEX compounds using gas chromatography.
- Processed and reported lab data.
- Trained new employees.

Hydrology biogeochemistry Lab Technician September 2002 – July 2004
University of California, Riverside

- Analyzed water and soil samples from various watersheds in Southern California.
- Personal project: Identification of groundwater in the San Diego Creek watershed.

AWARDS

- Research Assistantship, Department of Environmental Sciences**,** University of California, Riverside, 2005 – 2006 and 2006 - 2007 academic years.
- Academic Fellowship, Graduate Division, University of California, Riverside, 2006 – 2007 academic year.
- California Lake Management Society Scholarship for Outstanding Student Research, October 2006.
- North American Lake Management Society Award for Student Poster Presentation, November 2006.
- Graduate Opportunity Fellowship, University of California, Santa Barbara, 2007-2008 academic year.
- GLEON Student Travel Fellowship, February 2008.
- Graduate Opportunity Fellowship, University of California, Santa Barbara, 2008-2009 academic year.
- GLEON Student Travel Fellowship, February 2009.
- NASA Earth and Space Science Fellowship, National Aeronautics and Space Administration, 2009-2010, 2010-2011 and 2011-2012 academic years.

GROUPS AND ACTIVITIES

- Student Committee for Hydrologist Search, University of California, Riverside, Winter 2004 and Winter 2006.
- Mini Graduate Student Association Founding Member, Department of Environmental Science, University of California, Riverside, 2006 – 2007 academic year.
- California Lake Management Society Student Member, October 2005 – current.
- North American Lake Management Society Student Member, November 2006-current.
- American Society of Limnology and Oceanography Student Member, February 2007 – current.
- Global Lake Ecology Observatory Network (GLEON) Student Member, February 2008 – current.
- GLEON student committee to help create the GLEON Site Exchange Program, 2008.
- American Society of Limnology and Oceanography Student Board Member Nominee, March 2009.

PRESENTATIONS AT NATIONAL MEETINGS AND WORKSHOPS

- *A"New" Lake Elsinore: Physical, Chemical and Ecological Changes that Resulted from the Region's Winter Storms*. North American Lake Management Society Annual Meeting. Madison, WI, November 2005. With: M.A. Anderson
- *Assessment of Stratification and Mixing in Lake Elsinore Ca***:** *Axial Flow Pumps for Improving Water Quality in a Shallow Eutrophic Lake.* California Lake Management Society Annual Meeting. Ontario, CA, October 2006. With: M.A. Anderson
- *Density driven currents in a shallow embayment in Lake Elsinore CA, resulting from differential heating and cooling.* North American Lake Management Society Annual Meeting. Indianapolis, IN, November 2006. With: M.A. Anderson
- *Density driven currents in a shallow embayment in Lake Elsinore CA, resulting from differential heating and cooling.* American Society of Limnology and Oceanography Annual Meeting. Santa Fe, NM, February 2007. With: M.A. Anderson
- *Instrumentation to Evaluate Response of Phytoplankton to Disturbances in Stratified Lakes*. Global Lake Ecological Observatory Network Workshop VI. Lake Placid, FL, February 2008. With: Arron Layns and Sally MacIntyre
- *Instrumentation to Evaluate Response of Phytoplankton to Disturbances in Stratified Lakes*. Arctic Long Term Ecological Research Annual Meeting. Woodshole, MA, March 2008. With: Arron Layns and Sally MacIntyre
- *Identifying Mixing Regimes Associated with Storm Events in Toolik Lake, AK*. Global Lake Ecological Observatory Network Workshop VIII. Hamilton New Zealand, February 2009. With: Sally MacIntyre
- *Evaluating the Importance of Phytoplankton Community Structure to Inherent Optical Properties in the Santa Barbara Channel, CA*. Ocean Science Meeting, American Geophysical Union, Portland, OR, February 2010. With: David Siegel and Nathalie Guillocheau
- *UV-absorbing substances linked to phytoplankton community dynamics in a coastal ocean*. Aquatic Science Meeting, American Society of Limnology and Oceanography, New Orleans, LA, February 2013. With: David Siegel, Norm Nelson and Nathalie Guillocheau

PUBLICATIONS

Lawson, R and M.A. Anderson (2007) Stratification and mixing in Lake Elsinore, California: An assessment of axial flow pumps for improving water quality in a shallow eutrophic lake. *Water Research* **41**: 4457-4467

Barrón, R.K., D. Siegel and N. Guillocheau (2014) Evaluating the importance of phytoplankton community structure to the optical properties of the Santa Barbara Channel, California. *Limnology and Oceanography* **59**(3): 927 - 946

ABSTRACT

Constraining the variability of optical properties in the Santa Barbara Channel, CA: A phytoplankton story

by

Rebecca Katherine Barrón

The research presented in this dissertation evaluates the direct relationships of phytoplankton community composition and inherent optical properties (IOP); that is, the absorption and scattering of light in the ocean. Phytoplankton community composition affect IOPs in both direct and indirect ways, thus creating challenges for optical measurements of biological and biogeochemical properties in aquatic systems. Studies were performed in the Santa Barbara Channel (SBC), CA where an array of optical and biogeochemical measurements were made. Phytoplankton community structure was characterized by an empirical orthogonal functional analysis (EOF) using phytoplankton accessory pigments. The results showed that phytoplankton community significantly correlated to all IOPs, e.g. phytoplankton specific absorption, detrital absorption, CDOM absorption and particle backscattering coefficients. Furthermore, the EOF analysis was unique in splitting the microphytoplankton size class into separate diatom and dinoflagellate regimes allowing for assessment optical property differences within the same size class, a technique previously

not systematically achievable. The phytoplankton functional group dinoflagellates were particularly influential to IOPs in surprising ways. Dinoflagellates showed higher backscattering efficiencies than would be predicted based on Mie theory, and significantly influenced CDOM absorption via direct association with dissolved mycosproine-like amino acid absorption (MAA) peaks in CDOM spectra. A new index was developed in this work to quantify MAA absorption peaks in CDOM spectra, and was named the MAA Index. Prior to this research dissolved MAA absorption in natural waters was never quantified, and CDOM data containing these peaks were often disregarded and discarded from analysis.

CDOM dynamics in the SBC were assessed for a 15-year study period, and this work shows that significantly large MAA Index values, e.g. MAA Index > 1, were present in approximately 16% of surface water data. Variability in CDOM spectral shape was quantified using the EOF technique, and regression analysis with EOF outputs showed that CDOM absorption intensity and spectral shape were well correlated dinoflagellate presence. Furthermore, results showed that phytoplankton biomass played a secondary role in relation to CDOM absorption, and that variability in CDOM absorption coefficients were primarily driven by community composition. CDOM quality in the SBC was also assessed using CDOM fluorescence properties via excitation emission matrix spectroscopy (EEMS). The EEMS data was analyzed using a multivariate statistical procedure, again, an EOF analysis, to identify three dominant CDOM source regimes: the surface pelagic regime, deep-water (up to 300 m) regime and kelp forest pelagic regime. This work also found that while CDOM absorption coefficient was strongly influence by which phytoplankton groups were present, DOM quality was characterized more so by the amount of phytoplankton biomass, hence indicating strong microbial component to DOM production. Lastly, with the use of the

EEMS data, and characterization of CDOM absorption properties, e.g. spectral slope, S, slope ratio, S_R, specific UV-absorbance, SUVA and MAA Index, we found that terrestrial sources of CDOM were very limited in the SBC. Based on this research, mineral particle concentrations that significantly correlated with IOPs were thought to be associated with suspended sediments from shoaling of the continental shelf rather than from stream/river influence. Thus, the SBC is a unique, optically complex ocean system where IOP dynamics, thus remote sensing reflectance, are strongly influenced by shifts in phytoplankton community structure.

I. Introduction

Phytoplankton make up the bulk of the standing stock of particulate carbon (POC) in the ocean. Understanding the phytoplankton dynamics and accurate estimation of phytoplankton biomass, e.g. carbon, are critical for answering research questions regarding the global carbon cycle, and making policy decisions. Optical measurements, such as satellite remote sensing from space borne satellites, are the best way to achieve global coverage of biomass estimation. Satellite remote sensing reflectance, R_{RS}, is a function of inherent optical properties (IOP), and IOPs are additive functions of seawater itself and the dissolved and suspended constituents in the seawater such as phytoplankton, bacteria, mineral particles, colored dissolved organic matter (CDOM), bubbles and viruses. IOPs are, in tern, affected by phytoplankton properties and community composition, both directly and indirectly.

Differences in cell size, shape, intercellular composition and intercellular density directly affect absorption and scattering properties (Stramski et al. 2001). All living phytoplankton cells contain chlorophyll *a*, which absorbs at wavelengths λ = 340 nm and 662 nm. Phytoplankton also contain accessory pigments, mostly carotenoids, and have unique absorption peaks associated with them. A small number of accessory pigments are unique to specific phytoplankton groups, thus spectral shape differences in absorption occur depending on the community composition (Bricaud et al. 2004; Stramski et al. 2001; Dierssen 2010). Furthermore, phytoplankton have the ability to increase the number chlorophyll *a* pigments per cell, called the packaging effect, thereby decreasing the overall absorption spectra (Morel and Bricaud, 1981). Diatom species are commonly

found to exhibit the packaging effect, and associated absorption spectra are lower and flattener per cell compared with cells not displaying the packing effect (Nelson et al. 1993; Bricaud 2004). Some phytoplankton groups also have the ability to produce UV-absorbing pigments as a screening protection against harmful UV-rays, thus displaying increased absorption in the associated wavebands (Roy et al. 2011;Whitehead and Vernet 2000).

Scattering properties are affected in forward and backward directions by cell size, shape and composition, e.g. density (Stramski et al. 2001, 2004). Mei theory, based on hollow, homogenous spheres, predicts that smaller particles will scatter more light in the backward direction, e.g. backscattering, than for larger particles due to the differences in the index of refraction (Stramski et al. 2004). However, recent observations have shown that nanophytoplankton groups (2 – 20 μm in size) and some microphytoplankton groups (> 20 μm in size) have much higher backscattering than predicted by Mie theory (Dall'Olmo et al. 2009; Westberry et al. 2010; Whitmire et al. 2010). Whitmire et al. (2010) found that several species of dinoflagellates had high backscattering efficiency (backscattering per unit total scattering) despite differences in cell size, and while backscattering efficiency increased in proportion to cell size for diatom species.

Secondary effects of phytoplankton community structure on oceanic IOPs are that of detrital absorption and scattering, and colored dissolved organic matter (CDOM) absorption. Phytoplankton community composition as well as biomass affects quality and shape of detrital materials and sinking rates vary depending on species. Some phytoplankton directly release CDOM into the water column, e.g. the red-tide forming dinoflagellate *L. polyedrum* (Whitehead and Vernet 2000). However, dissolved organic

material directly released by most phytoplankton species is not colored, therefore, does not absorb light (Rochelle-Newall and Fisher 2002). Most CDOM produced *in situ* is from microbial respiration and zooplankton excretion. Phytoplankton community affects CDOM absorption characteristics via food web interactions, where zooplankton and microbes have been found to excrete CDOM of differing quality based on phytoplankton or associated substrate, respectively (Rochelle-Newall and Fisher 2002; Saba et al. 2009a; b).

CDOM absorption along the coast can be further complicated by terrestrial influences. Much of CDOM is derived from higher terrestrial plants sources and carried into the ocean via stream and river inputs. CDOM absorption properties for oceanic vs. terrestrial sources are reflected in spectral shape, where terrestrially derived CDOM absorbs at higher wavelengths than CDOM produced by microbes. A fraction of CDOM also emits light, e.g. fluorescence, and can be useful in identifying CDOM sources. CDOM originally derived from phytoplankton sources in aquatic systems is protein rich, where a CDOM derived from terrestrial systems, e.g. higher plants, is rich in soil humic materials, lignin and other polyphenolic compounds. Stedmon et al. (2003) developed a multivariate statistical model, called the PARAFAC model, to identify key compounds in CDOM fluorescence spectra. Cory and McKnight (2005) refined this method and created a database for many diverse aquatic systems. However, PARAFAC doesn't work well for oceanic systems and where much of the CDOM is phytoplankton derived.

In many areas of the open ocean IOPs and chlorophyll *a* concentrations covary, thus remote sensing retrievals can be somewhat simplistic such as the standard Ocean Color (OC4) empirical algorithm (O'Reilly et al. 1998). This algorithm uses empirical

relationships between $R_{RS}(\lambda)$ and chlorophyll *a* concentrations to retrieve satellite-based measurements of phytoplankton biomass. This type of algorithm is not well suited for optically complex areas, such as many coastal areas, where IOPs may be influenced by productivity, high turbidity and/or terrestrially derived CDOM from rivers and streams. The Garver-Siegel-Maritorena (GSM) model is more well-suited for such areas, as it is a semi-analytical remote sensing algorithm that allows IOPs to vary independently from one another(Maritorena et al. 2002; Siegel 2005). Local calibration of IOP coefficients for the GSM model and chlorophyll *a* concentrations for the GSM and OC4 models, e.g. global model coefficients, has allowed for improvement in retrieving chlorophyll *a* and IOPs in some coastal areas (Mannino et al. 2008). However, Kostadinov et al. (2007) found no model improvement for local calibration of either the GSM or OC4 models for the Santa Barbara Channel, CA. This is likely because phytoplankton community structure is highly variable in this region, thus affecting IOPs in all of the ways described above.

Many more recent studies have looked directly at phytoplankton community and remote sensing reflectance (Alvain et al. 2005; Torrecilla et al. 2011). Alvain et al. (2006) found direct relationships with ocean reflectance and phytoplankton groups, identified by accessory pigment concentrations, and found that their model explained errors of the OC4 modeled and observed chlorophyll biomass. They concluded that the OC4 shortcomings are attributed to the model not accounting for independent variability of IOPs. In updates, (Alvain et al. 2012) indicated that their retrieval phytoplankton functional groups was sensitive to backscattering and CDOM absorption variability.

This research directly evaluates the relationship of phytoplankton community structure and inherent optical properties in the Santa Barbara Channel, CA. The results of this dissertation have found that phytoplankton community structure affects all IOPs in the Santa Barbara Channel. CDOM properties were closely evaluated, and have a particularly unique relationship with phytoplankton dynamics. It was observed that the microphytoplankton group, dinoflagellates, was strongly correlated with CDOM spectral characteristics due to the release of mycosporine-like amino acids (MAAs). CDOM quality was evaluated using CDOM fluorescence and was not directly related to phytoplankton community shifts, but was well correlated with phytoplankton biomass. Lastly, the results of this dissertation showed that the Santa Barbara Channel is a unique coastal ecosystem where shifts in phytoplankton community and biomass control IOP and, therefore, remote sensing reflectance values.

References

Alvain, S., H. Loisel, and D. Dessailly. 2012. Theoretical analysis of ocean color radiances anomalies and implications for phytoplankton groups detection in case 1 waters. Opt. Express **20**: 1070–1083.

Alvain, S., C. Moulin, Y. Dandonneau, and F. M. Bréon. 2005. Remote sensing of phytoplankton groups in case 1 waters from global SeaWiFS imagery. Deep Sea Res. Part I Oceanogr. Res. Pap. **52**: 1989–2004.

Alvain, S., C. Moulin, Y. Dandonneau, H. Loisel, and F. M. Breon. 2006. A species-dependent bio-optical model of case I waters for global ocean color processing. Deep. Res. PART I-OCEANOGRAPHIC Res. Pap. **53**: 917–925.

Bricaud, A. 2004. Natural variability of phytoplanktonic absorption in oceanic waters: Influence of the size structure of algal populations. J. Geophys. Res. **109**: 1–12.

Cory, R. M., and D. M. McKnight. 2005. Fluorescence Spectroscopy Reveals Ubiquitous Presence of Oxidized and Reduced Quinones in Dissolved Organic Matter. Environ. Sci. Technol. **39**: 8142–8149.

Dall'Olmo, G., T. K. Westberry, M. J. Behrenfeld, E. Boss, and W. H. Slade. 2009. Significant contribution of large particles to optical backscattering in the open ocean. Biogeosciences **6**: 947–967.

Kostadinov, T. S., D. a. Siegel, S. Maritorena, and N. Guillocheau. 2007. Ocean color observations and modeling for an optically complex site: Santa Barbara Channel, California, USA. J. Geophys. Res. **112**: 1–15.

Mannino, A., M. E. Russ, and S. B. Hooker. 2008. Algorithm development and validation for satellite-derived distributions of DOC and CDOM in the U.S. Middle Atlantic Bight. J. Geophys. Res. Ocean. **113**: n/a–n/a.

Maritorena, S., D. a Siegel, and A. R. Peterson. 2002. Optimization of a semianalytical ocean color model for global-scale applications. Appl. Opt. **41**: 2705–14.

Morel, A., and A. Bricaud. 1981. Theoretical results concerning light absorption in a discrete medium, and application to the specific absorption of phytoplankton. Deep-Sea Research, **28**: 1375-1393.

Nelson, N. B., B. B. Prezelinl, and R. Robert. 1993. Phytoplankton light absorption and the package effect in California coastal waters.

Reilly, J. E. O., S. Maritorena, B. G. Mitchell, D. A. Siegel, K. L. Carder, S. A. Garver, M. Kahru, and C. Mcclain. 1998. Ocean color chlorophyll algorithms for SeaWiFS encompassing chlorophyll concentrations between. **103**.

Rochelle-Newall, E. J., and T. R. Fisher. 2002. Production of chromophoric dissolved organic matter f luorescence in marine and estuarine environments : an investigation into the role of phytoplankton. Mar. Chem. **77**: 7–21.

Roy, S., C. A. Llewellyn, E. S. Egeland, and G. Johnsen. 2011. Phytoplankton pigments: characterization, chemotaxonomy and applications in oceanography. Cambridge.

Saba, G. K., D. K. Steinberg, and D. A. Bronk. 2009a. Effects of diet on release of dissolved organic and inorganic nutrients by the copepod Acartia tonsa. Mar. Ecol. Prog. Ser. **386**: 147–161.

Saba, G. K., D. K. Steinberg, and D. A. Bronk. 2009b. Effects of diet on release of dissolved organic and inorganic nutrients by the copepod Acartia tonsa. Mar. Ecol. Prog. Ser. **386**: 147–161.

Siegel, D. a. 2005. Independence and interdependencies among global ocean color properties: Reassessing the bio-optical assumption. J. Geophys. Res. **110**: 1–14.

Stedmon, C. a, S. Markager, and R. Bro. 2003. Tracing dissolved organic matter in aquatic environments using a new approach to fluorescence spectroscopy. Mar. Chem. **82**: 239–254.

Stramski, D., E. Boss, D. Bogucki, and K. J. Voss. 2004. The role of seawater constituents in light backscattering in the ocean. Prog. Oceanogr. **61**: 27–56.

Stramski, D., A. Bricaud, and A. Morel. 2001. Modeling the inherent optical properties of the ocean based on the detailed composition of the planktonic community. Appl. Opt. **40**: 2929–2945.

Torrecilla, E., D. Stramski, R. A. Reynolds, E. Millan-Nunez, and J. Piera. 2011. Cluster analysis of hyperspectral optical data for discriminating phytoplankton pigment assemblages in the open ocean. Remote Sens. Environ. **115**: 2578–2593.

Westberry, T. K., G. D. Olmo, E. Boss, M. J. Behrenfeld, and T. Moutin. 2010. Coherence of particulate beam attenuation and backscattering coefficients in diverse open ocean environments. Opt. Soc. Am. **18**: 15419–15425.

Whitehead, K., and M. Vernet. 2000. Influence of Mycosporine-Like Amino Acids (MAAs) on UV Absorption by Particulate and Dissolved Organic Matter in La Jolla Bay. **45**: 1788–1796.

Whitmire, A. L., W. S. Pegau, L. Karp-boss, E. Boss, and T. J. Cowles. 2010. Spectral backscattering properties of marine phytoplankton cultures. Opt. Soc. Am. **18**: 1680–1690.

II. Evaluating the importance of phytoplankton community structure to the optical properties of the Santa Barbara Channel, California

Rebecca K. Barrón,[1,*] David A. Siegel,[2] and Nathalie Guillocheau[1]

Limnology and Oceanography **59**(3): 927 - 946

[1] Earth Research Institute, University of California, Santa Barbara, California
[2] Earth Research Institute and Department of Geography, University of California Santa Barbara, California

*Corresponding author: rebecca@eri.ucsb.edu

Running head: Santa Barbara Channel optical properties

Acknowledgements

We acknowledge the Plumes and Blooms crew, especially Tihomor Kostadinov for help with the backscatter and reflectance data, and Clarissa Anderson for help with the Empirical Orthogonal Function analysis. The Plumes and Blooms project is supported by the National Aeronautics and Space Administration (NASA; NNX11AL94G) and ship time is provided by the National Oceanic and Atmospheric Administration Channel Islands National Marine Sanctuary. RKB was also supported by a NASA Earth and Space Science Fellowship. The authors would also like to thank the anonymous reviewers and associate editor Dariusz Stramski for their efforts in helping to improve our manuscript.

Abstract

Observations from the Santa Barbara Channel (SBC) California were used to evaluate relationships among optical properties and phytoplankton community structure. Phytoplankton community structure was determined by statistically analyzing ten diagnostic phytoplankton pigment concentrations using empirical orthogonal function (EOF) analysis. The first four EOF modes explained 82% of phytoplankton community structure variability and were interpreted as a mixed community mode composed mostly of nanoplankton, a mode dominated by microplankton (diatoms and dinoflagellates), a mode describing alternating diatom and dinoflagellate dominance and a mode reflecting picoplankton presence. Variations in colored dissolved organic matter (CDOM) and phytoplankton absorption spectra were related to changes of the mixed microplankton modal amplitudes. Characteristics of the CDOM spectrum were further dependent on whether diatoms or dinoflagellates were dominant. The particle backscattering coefficient was significantly correlated with EOF modes describing the mixed microplankton and the picoplankton communities. The influence of phytoplankton community structure was also seen in the performance of standard ocean color algorithms using the in situ data set. The present results demonstrate that many optical characteristics vary significantly with changes in phytoplankton community structure and suggest that improvements in remote sensing algorithms will require model coefficients to vary accordingly. Further, changes in phytoplankton community composition affect both dissolved and particle absorption and scattering properties, not simply the phytoplankton specific properties, creating challenges for the development of algorithms aimed at assessing phytoplankton community structure from satellite observations.

Introduction

Ocean color remote sensing has revolutionized our understanding of the global ocean by providing information about phytoplankton distributions, rates of net primary production and particle characteristics of the surface ocean. Space-borne instrumentation quantifies the reflectance spectrum of the sea surface, and the information it contains, on spatial and temporal scales impossible to achieve by any other means. Remote-sensing reflectance of ocean waters, $R_{RS}(\lambda)$, or equivalently normalized water-leaving radiance, $L_{wN}(\lambda)$, can be modeled as a function of the absorption and backscattering coefficients of seawater, termed inherent optical properties (IOPs). Inherent optical properties are additive functions of seawater itself as well as suspended and dissolved constituents such as phytoplankton, detritus, mineral particles, colored dissolved organic matter (CDOM), bacteria, viruses and air bubbles (Mobley 2002; Stramski et al. 2004). Thus, understanding the link between IOPs and $R_{RS}(\lambda)$ is critical for studying and monitoring biological and biogeochemical change in the world oceans.

Ocean color algorithms model biological and optical properties from remotely sensed observations of ocean reflectance spectra (O'Reilly et al. 1998; Maritorena et al. 2002; Lee et al. 2002). The Ocean Color algorithm (OC4) quantifies chlorophyll *a* concentration from ocean reflectance using an empirical relationship between ratios of $R_{RS}(\lambda)$ bands and in situ measurements of chlorophyll *a* (O'Reilly et al. 1998). This algorithm is adequate for the open ocean where ocean color is dominated by phytoplankton properties and other constituents are assumed to roughly covary with changes in chlorophyll *a* (IOCCG 2000; Siegel et al. 2013). However in complex ocean optical environments, the contributions of other optical properties relative to

phytoplankton chlorophyll concentrations vary, which makes this empirical approach fraught with difficulties (Dierssen 2010; Szeto et al. 2011). Semi-analytical models break the assumption of common proportions among IOPs that plague empirical relationships (Maritorena et al. 2002; Lee et al. 2002); however they have yet to include the influences that variations in phytoplankton community structure may create.

Coastal areas are often optically complex due to high and highly variable levels of turbidity, phytoplankton productivity and CDOM from upwelling and/or terrestrial inputs and the associated IOPs may vary independently (IOCCG 2000; Toole and Siegel 2001). Such areas of optical complexity, termed Case II conditions, often require local calibration for empirical coefficients used in remote sensing algorithms. Magnuson et al. (2004) found that local tuning of the Garver-Siegel-Maritorena (GSM) semi-analytical and the SeaWiFS operational (OC4) empirical models for the Chesapeake Bay and the Mid-Atlantic Bight resulted in better chlorophyll *a* retrieval statistics than the respective global models. Kostadinov et al. (2007) locally optimized the GSM model for the Santa Barbara Channel (SBC) but found no significant improvement in model performance. The lack of improvement was attributed to the assumption that the IOP spectral shapes were constant in time. Changes in the seawater constituents can cause changes in IOP spectral shape.

Changes in phytoplankton functional type affect inherent optical properties directly due to differences in size, shape, density and cellular composition, and indirectly due to excretions and biological relationships, e.g. nutrient cycling, affecting the local environment. For example, Stramski et al. (2001) showed that both the magnitude and spectral shapes of absorption and scattering varied significantly for particulate

assemblages with the same total chlorophyll *a* concentration. Cell size, shape and composition all affect the relative proportions of light scatter in the forward and backward directions (Morel and Ahn 1990; Stramski et al. 2001, 2004). Over a significant portion of the size range, Mie theory predicts that smaller homogeneous spheres will scatter proportionally more light in the backwards direction than largeer ones. However, recent observational and laboratory studies have found that larger phytoplankton contribute significantly to particulate backscattering (Dall'Olmo et al. 2009; Whitmire et al. 2010; Westberry et al. 2011). Differences in cellular composition and shape also affect light scatter. This can lead to differences in the amount of light backscattered for organisms with the same assumed scattering cross sections. Vaillancourt et al. (2004) found that dinoflagellates had the highest backscattering efficiency of all of the phytoplankton species in their 12-culture study. Whitmire et al. (2010) showed that backscattering ratios for diatoms were largely a function of size, whereas dinoflagellate backscattering ratios were high regardless of size.

Different species of phytoplankton can have unique absorption spectra due to the differences in the amount of chlorophyll *a* per cell as well as the presence of various accessory pigments unique to their functional type (Kirk 1994; Stramski et al. 2001; Dierssen 2010). Phytoplankton species have the ability to increase the intracellular pigment concentration thereby increasing the chlorophyll *a* content per cell and effectively decreasing the absorption per pigmented particle with respect to the same concentration of pigment suspended in solution (Morel and Bricaud, 1981). This is referred to as pigment packaging and is common among diatom species (Nelson et al. 1993). Bricaud et al. (2004) concluded that pigment packaging, attributed to differences

in size class, was an important source of variability of phytoplankton absorption in the global ocean. In addition to chlorophyll *a*, phytoplankton contain many accessory pigments that absorb light at various wavelengths to aid in photosynthetic processes and/or provide protection from ultraviolet (UV) light (Roy et al. 2011). Accessory pigment content may be unique to various phytoplankton groups and can be observed as differences in the absorbance spectra (Dierssen 2010).

Secondary effects of phytoplankton functional types on IOPs include that of colored dissolved organic matter (CDOM) and particulate detritus associated with a given phytoplankton community. CDOM accounts for the majority of UV and blue spectral light absorption in the ocean (Nelson and Siegel 2013). Phytoplankton community structure may also affect the CDOM composition in the ocean. In particular, some phytoplankton species have been directly linked to increases in CDOM absorption via the release of photo protective pigments called mycosporine-like amino acids (MAAs) (Vernet and Whitehead 1996). Absorption and scattering of detritus can be significant and correlate to phytoplankton assemblage, especially during or following a phytoplankton bloom (Antoine et al. 2011). Associated biogeochemical cycling of the detrital matter can also have an effect on CDOM absorption.

For all the reasons listed above, phytoplankton community composition should play a significant role in determining IOP characteristics, and therefore should affect ocean reflectance spectra (Mobley and Stramski 1997; Dierssen, 2010). Over the last decade, several studies have used ocean color reflectance determinations to assess phytoplankton community structure (Sathyendranath et al. 2001; Alvain et al. 2005; Torrecilla et al. 2011). Alvain et al. (2006) explained the variability in chlorophyll *a*

concentrations modeled with the OC4 band-ratio algorithm by the direct relationship of $L_{wN}(\lambda)$ spectral shape with phytoplankton community composition. Although this novel approach explained chlorophyll variability well, shortcomings with this approach are manifested in the fact that the OC4 algorithm does not consider the independent variability of IOPs. More recently, Alvain et al. (2012) evaluated their original model and found it to be sensitive to variations in particle backscattering as well as CDOM and phytoplankton absorption. Therefore, constraining IOP variability, and in particular the roles of phytoplankton community structure changes, is needed to advance ocean color models.

Here, we will evaluate the relationship of phytoplankton community structure to the optical properties in a complex coastal ocean. We identify phytoplankton communities by applying a multivariate statistical procedure to phytoplankton indicator pigment concentrations collected over a 4 year period along side apparent and inherent optical property measurements. The goal of this work is to ultimately assess relationships between IOPs and phytoplankton community structure that can help us identify sources of error for remote sensing algorithms for areas with high biological and biogeochemical diversity. The shifts in biological and biogeochemical properties observed span those of the global ocean, thereby making this study relevant to a diverse array of oceanic systems.

Methods

Study site

The Santa Barbara Channel, California, is a dynamic coastal system with near-surface chlorophyll *a* concentrations ranging from 0.3 to 28 mg m^{-3} while stream and

river inputs only episodically influence overall particle loads (Toole and Siegel 2001; Otero and Siegel 2004; Kostadinov et al. 2012). Phytoplankton community composition in the SBC varies seasonally from a micro-phytoplankton community, indicative of a eutrophic coastal upwelling system, to a community comprised of nano- and pico-phytoplankton resembling a more oceanic, oligotrophic system (Anderson et al. 2008). Due to the low stream water inputs during most of the year, changes in phytoplankton abundances and characteristics dominate the variability of all IOPs in the Santa Barbara Channel (Toole and Siegel 2001; Kostadinov et al. 2007; Antoine et al. 2011).

Data for this paper were collected as part of the Plumes and Blooms (PnB) program, which conducts monthly cruises across the Santa Barbara Channel at seven stations from Goleta Point to Santa Rosa Island (Fig. 1). The surveys consist of conductivity-temperature-depth measurements, optical parameters measured in situ with profiling instruments and in the laboratory from discrete samples, as well as various chemical and biological determinations. A brief description of measurement methodologies are described below and more detailed descriptions are available from the PnB website (http://www.icess.ucsb.edu/PnB/) and in previous studies (Toole and Siegel 2001; Anderson et al. 2008; Kostadinov et al. 2012). The data set used for this paper spans from November 2005 – August 2009 and is a subset of the entire record that began in 1996 and continues presently.

Discrete water sample analyses

Discrete samples were taken using 5 liter Niskin bottles deployed on a rosette with a Seabird 9/11 conductivity-temperature-depth system. Samples that were taken at

discrete depths were analyzed for nutrients, biogenic and lithogenic silica (BSi and LSi), particulate organic carbon (POC), phytoplankton accessory pigments, chlorophyll *a,* and CDOM. Nutrient samples were collected directly from the Niskin bottles and stored in a shipboard freezer, then transferred to the laboratory freezer until analysis on a Lachat QuikChem 8000 Flow Injection Analyzer (http://www.msi.ucsb.edu/services/analytical-lab/instruments/flow-injection-analyzer). BSi and LSi samples were filtered shipboard onto 0.4 μm membrane filters and frozen until analysis using an NaOH extraction procedure described in Shipe and Brzezinski (2001) and, more recently, in Krause et al. (2013). POC samples were filtered onto GF/F filters shipboard and immediately stored in liquid nitrogen until analysis on a CE440 Elemental Analyzer.

The phytoplankton pigments were determined via high performance liquid chromatography (HPLC) analysis (described in more detail below) and included chlorophyll *a* in the pigment suite. Fluorometric chlorophyll *a* analysis using a standard acetone extraction method were also conducted, although only chlorophyll *a* concentrations determined via HPLC are presented here to provide consistency.

Inherent optical properties (IOPs)

The coefficient of absorption for colored dissolved organic matter (CDOM), $a_g(\lambda)$, was determined using surface water samples that were collected in glass amber bottles preconditioned for carbon analysis. Samples were immediately stored in a shipboard refrigerator at 4^{o}C. Samples were filtered through a 0.2 μm membrane filter in the laboratory and analyzed on a Shimadzu 2401-PC spectrophotometer within 24 hours of collection.

Several large peak-like features in the ultraviolet spectral region were found in the CDOM spectra from PnB (Fig. 2a). The features are a departure from a typical CDOM spectrum, a spectrum decreasing exponentially with increasing wavelength, and were similar in shape to mycosporine-like amino acid (MAA) absorption signatures presented in other studies (Whitehead and Vernet 2000). The (presumably) MAA peaks in this study were quantified by modeling a 'baseline' CDOM spectrum by log-transforming the $a_g(\lambda)$ data (*see* Fig. 2), then making a linear regression fit to the data points surrounding the MAA absorption region (300-310 nm and 390-400 nm). The procedure was similar to that of calculating the spectral slope, *S* (Nelson et al. 2007; 2010), but was used here to estimate what the CDOM spectra would appear to be if the MAA-like signal was not present. The modeled baseline spectra were then subtracted from the real $a_g(\lambda)$ data. The term 'MAA index' is defined here as the summation of the residual between $a_g(\lambda)$ and the modeled baseline between λ = 310 – 390 nm (Fig. 2b).

Samples for determining the particle absorption coefficient, $a_p(\lambda)$ were collected by filtering seawater onto a GF/F filter and then stored immediately in liquid nitrogen until laboratory analysis. The $a_p(\lambda)$ samples were analyzed on the Shimadzu 2401-PC using the quantitative filtration technique (Mitchell, 1990). The optical pathlength amplification factor was determined using natural phytoplankton samples collected from Plumes and Blooms cruises (Guillocheau 2003). The filters were then extracted in methanol over night to remove extractable phytoplankton products and re-analyzed on the spectrophotometer for absorption of detrital material, $a_d(\lambda)$. This allowed for the quantification of phytoplankton specific absorption, as $a_{ph}(\lambda) = a_p(\lambda) - a_d(\lambda)$.

Vertical profiles of the beam attenuation coefficient, $c(\lambda)$, and absorption coefficient, $a(\lambda)$, spectra were collected at each station using a Wetlabs AC-9 profiling instrument at wavelengths λ = 440, 488, 510, 555, 630, and 676 nm, which were linear interpolated to match those captured by the Hydroscat (described below). Correction algorithms and data analysis procedures for this instrument are presented in Kostadinov et al. (2012). Surface values were obtained by averaging the upper 15 m of the vertical profiles. Total scattering coefficient, $b(\lambda)$, was calculated as the difference between the beam attenuation and absorption coefficients, or $b(\lambda) = c(\lambda) – a(\lambda)$. The particle scattering coefficient, $b_p(\lambda)$, was determined by $b_p(\lambda) = b(\lambda) – b_w(\lambda)$ where $b_w(\lambda)$ is the scattering coefficient of pure seawater taken from Smith and Baker (1981).

Vertical profiles of volume scattering function at 140°, $\beta(140^o,\lambda)$, were measured at wavelengths λ = 442, 470, 510, 589, and 671 nm using a HobiLabs Hydroscat-6 profiling instrument. The data were filtered with a moving average and then binned to 1m. The Hydroscat data was corrected for light attenuated in the measurement path of the instrument, called a $\sigma(\lambda)$ correction, using data collected simultaneously by the AC-9 (Kostadinov et al. 2007, 2012). $\beta(140^o,\lambda)$ was then converted to particle backscattering coefficient, $b_{bp}(\lambda)$ using:

$$b_{bp}(\lambda) = 2\pi\chi_p\,[\beta(140^o,l) - \beta_w(140^o,l)] \qquad (1)$$

The value of χ_p = 1.14 was determined from the results of Dall'Olmo et al. (2009), and $\beta_w(140^o,l)$ was determined from Morel et al. (1974). The data were then averaged for the upper 15 m of the water column to estimate average surface $b_{bp}(\lambda)$ values.

Remote sensing reflectance spectra

Light reflectance was determined using a free-falling Biospherical Instruments Profiling Reflectance Radiometer, PRR-600. The instrument captured vertical profiles of upwelling radiance, $L_u(\lambda)$, and downwelling irradiance, $E_d(\lambda)$, at wavelengths λ = 412, 443, 490, 510, 555, and 656 nm. Values of the remote-sensing reflectance spectrum, $R_{rs}(\lambda)$, were calculated from the ratio of the upwelling radiance just beneath the sea surface, $L_u(0^-,\lambda)$, to the corresponding downwelling irradiance spectrum, $E_d(0^-,\lambda)$, and then propagated across the sea surface using the relationship described in Lee et al. (2002). Further data processing details can be found in Kostadinov et al. (2012). Estimates of $R_{rs}(\lambda)$were then used to retrieve IOPs and chlorophyll *a* concentrations. The GSM model uses a semi-analytical algorithm that relates $R_{rs}(\lambda)$ to the absorption and scattering properties of seawater and retrieves b_{bp}(443), a_g(443) and chlorophyll *a* concentration as outputs (Maritorena et al. 2002). The OC4 model is an empirical algorithm that uses band ratios of R_{rs} (λ) at blue to green wavelengths to derive chlorophyll *a* concentrations (O'Reilly et al. 1994). The globally optimized versions of the GSM model (Maritorena et al. 2002) and OC4v6 model were used (http://oceancolor.gsfc.nasa.gov/REPROCESSING/R2009/ocv6/).

Phytoplankton community composition

Phytoplankton community composition was determined using a multivariate statistical approach applied to phytoplankton pigment concentrations collected at each PnB station. Pigment samples were collected from surface waters, immediately concentrated by filtration onto GF/F filters, and stored in liquid nitrogen. Samples were

shipped in liquid nitrogen to the Horn Point Laboratory for HPLC analysis (Hooker et al. 2009). The ten pigments chosen for this analysis are considered diagnostic pigments and represent the presence of different phytoplankton functional groups (Table 1; following Vidussi et al. 2001). We added chlorophyll *a* and lutein (a photo-protective pigment for many species) to our pigment suite in attempt to better characterize phytoplankton community responses under bloom conditions and changing light conditions.

Following Anderson et al. (2008), we performed an empirical orthogonal function (EOF) analysis using the diagnostic pigment data set after removing the mean and standardizing to unit variance. An EOF analysis decomposes spatial and temporal variability of a data set containing several variables into a set of independent orthogonal functions, or modes (Emery and Thomson 1997). The modes of variability determined for the diagnostic pigment data represent a phytoplankton 'community,' and the amplitude function associated with each mode indicates the intensity of presence of the given community (Anderson et al. 2008). We chose to use the EOF method rather than CHEMTAX method (Mackey et al. 1997), a commonly used chemotaxonomic method for determining phytoplankton community compositions, because the EOF method is well suited for understanding covariability among the diagnostic pigments. The CHEMTAX program requires a priori ratios of pigment concentrations and does not allow those pigment ratios to vary in either time or space. Hence, the multivariate statistical approaches are more flexible in that respect.

Anderson et al. (2008) performed a statistical analysis using PnB diagnostic pigment data from 1998 – 2003. The pigment samples used in that study were analyzed by a team at the San Diego State University (SDSU) Center for Hydro-Optics and

Remote Sensing (CHORS). Quality assurance discrepancies in the HPLC procedures from the CHORS lab surfaced shortly after the Anderson et al. (2008) paper was published (Hooker et al. 2009). The calibration issues in the CHORS HPLC phytoplankton pigment data set resulted in over estimating pigment concentrations that were typically found in relatively higher concentrations, and under estimating pigments that were found in lower concentrations. We chose to omit the CHORS data for this work and use here only data from the Horn Point Laboratory. It should be noted that the methodological discrepancies between the two data sets were unlikely to have affected the outcome of the analysis in Anderson et al. (2008) due to the nature of the statistical procedure. That is, quantification issues would not necessarily affect the patterns of covariability among pigments to first order and the EOF method would assess these patterns nearly independent of the issues in their individual quantification and the interpretations made by Anderson et al. (2008) are fully supported by the present analysis.

Results

Oceanographic conditions

Sea surface temperature during this study ranged from 10^{o}C to nearly 22^{o}C (mean 14.7^{o}C), where maximum temperatures occurred in the early fall of each year, and the minimum temperatures occurred in the spring (Fig. 3a). This is driven by upwelling-favorable winds in the spring causing the vertical transport of cool, nutrient-rich waters to the surface, and more stratified conditions with a shallow, warm surface layer occur in the fall (Toole and Siegel 2001; Brzezinski and Washburn 2011). Although seasonal patterns of upwelling and stratification occur, physical mixing processes in the SBC are

more so influenced by lateral advection driven by wind forcing and relaxation along the California coast (Harms and Winant 1998; Washburn et al. 2011). Synoptic scale wind forcing and relaxations have a significant effect on changes in biogeochemistry, e.g., nutrient status in the SBC. Brzezinski and Washburn (2011) found that wind-driven upwelling was responsible for the highest levels of phytoplankton productivity and nutrient concentrations in the SBC, and that cyclonic eddies enhance productivity either by entrainment of upwelled water, isopycnal uplift, or a combination of both. Eddy-enhanced productivity was most prominent in the fall (Brzezinski and Washburn 2011).

Dissolved nitrate + nitrite (NO_3+NO_2) concentrations at the sea surface, referred to hereafter just as nitrate, were highest in the spring, also consistent with upwelling-favorable conditions (Fig. 3b). Surface chlorophyll *a* concentrations determined via HPLC analysis are shown in Fig. 3c. The mean chlorophyll *a* concentration was 2.96 μg L^{-1} and the median was 2.06 μg L^{-1}. An extremely high concentration of 28.3 μg L^{-1} was observed in May 2008 and was coincident with high levels of biogenic silica (Fig. 3d) – indicating the presence of diatom populations (Shipe and Brzezinski 2001; Krause et al. 2013). Patterns in biogenic silica tended to mimic patterns in chlorophyll *a* through much of the time series. Diatom populations are typically abundant during or just following periods of strong upwelling accompanied by higher rates of primary productivity and chlorophyll *a* concentrations, whereas increased dinoflagellate abundance have been observed in response to more shallow eddy-driven mixing processes together with low levels of dissolved silicate concentrations (Anderson et al. 2008; Brzezinski and Washburn 2011).

Phytoplankton community structure

Phytoplankton community structure was quantified using an EOF analysis of phytoplankton pigment concentrations following Anderson et al. (2008). The first four EOF modes explained 82% of community structure variability. Fig. 4 shows bar plots of the eigenvector loadings for the four most significant EOF modes. The phytoplankton community composition associated with each mode is interpreted by the relative value of the eigenvectors (height of the bars) and the relationship between the individual pigment concentrations and the EOF amplitude functions for each mode (i.e., the values of $100 \cdot r^2$ are the numbers above each bar). The amplitude function (AF) for each mode is a value that indicates the intensity of the overall pattern of community structure for every time and space point analyzed (Fig. 5). The dashed lines on Fig. 5a-d indicate the first and second standard deviations of the mean AF for each mode. Data outside these lines represent extreme AF values and are interpreted as community presence in its strongest form in either the positive or negative directions. The closer the AF values are to zero, the less relevant that EOF mode is for that time and location. Extreme AF values are most frequently observed at Sta. 5 and 6; these stations are near the center of the cyclonic eddy frequently present in the SBC, thus located where upwelling is thought to persistently occur (Harms and Winant 1998; Washburn et al. 2011).

Mode 1 of the EOF analysis captured 37% of the co-variability of the pigment data (Fig. 4). The eigenvector loadings for Mode 1 were positive for all pigments indicating all pigment levels increase and decrease in concert as the Mode 1 AF changes. The amplitude functions are well correlated with indicator pigments for the functional types: green flagellates, prochlorophytes, chromophytes, nanoflagellates, and others in

the nanoplankton size class (Table 1). AF did not correlate well with chlorophyll *a* (r^2=0.05), indicating that large changes in chlorophyll *a* (i.e., blooms) are not typically associated with these phytoplankton assemblages. These results are broadly consistent with the results of Anderson et al. (2008), who interpreted their Mode 1 as an early upwelling nanoplankton community. Mode 1 AF did not correlate well with nutrient concentrations, with the exception of a weak correlation with SiO_4 (r = 0.22), and only a weak correlation is found with sea surface temperature (SST) (r = -0.16). This shows that the present Mode 1 community possesses some of the traits of that found in the previous study (Table 2). However in this study, extreme AF values of Mode 1 did not seem to occur seasonally, e.g., early spring such as in Anderson et al. (2008), but were present at various times of the year (Fig. 5a). Here, Mode 1 was interpreted as a baseline community rather than a more characteristic upwelling indicator. Differences between Anderson et al. (2008) and the present study may simply be due to lack of overlap in the observational periods for the two studies.

The EOF loadings for Modes 2 through 4 occurred both in the positive and negative direction indicating opposing relationships among some of the pigments. Mode 2 captured 22% of the co-variability of the pigment data set. Mode 2 AF values correlated strongly with chlorophyll *a* (r^2 = 0.82) and fucoxanthin (r^2 = 0.72) concentrations, suggesting that diatom blooms drive variability of this second mode. A positive correlation was also seen with peridinin (r^2 = 0.16), the marker pigment for dinoflagellates. Hence, this mode was interpreted as a 'mixed' microplankton community as the fucoxanthin and peridinin eigenvectors have the same sign, indicating the co-occurrence of diatoms and dinoflagellates. The eigenvectors for many of the

indicator pigments of the smaller functional types, e.g., prochlorophytes, cyanobacteria, nanoflagellates, chromophyte, and green flagellates, were negative, showing that the smaller phytoplankton groups alternate in importance with microplankton. Mode 2 AF showed a strong negative correlation with sea surface temperature, and strong positive correlations with B-Si, POC, Chl *a* and the mycosporine-like amino acid (MAA) index (Table 2). High values of the MAA index indicate the optical presence of mycosporine-like amino acids in the dissolved phase of the seawater. Positive extreme values of Mode 2 AF, e.g., indicating strong microplankton presence, occurred mostly in the spring further aiding our interpretation of Mode 2 as the spring bloom mode. Negative extreme AF values of Mode 2 indicated the lack of microplankton in the community, the strongest of which occurred in late spring and early summer 2009 (Fig. 5b).

Mode 3, representing 13% of the variance in the pigment data set, was interpreted as an alternating microplankton community dominance between diatom (positive) and dinoflagellate (negative) populations. Negative loadings for this mode indicated a phytoplankton community dominated by dinoflagellates (Mode 3 AF vs. peridinin r^2 = 0.52) and positive loadings indicated a community dominated by diatoms (Mode 3 AF vs. fucoxanthin r^2 = 0.25). Mode 3 AF showed strong positive correlations with concentrations of B-Si, POC, Chl *a* and salinity (Table 2), consistent with conditions during a diatom blooms in the SBC (Anderson et al. 2008; Brzezinski and Washburn 2011). Mode 3 AF correlated well in the negative direction with MAA index, thus indicating a positive relationship with the dinoflagellate-dominated community and MAAs (*see* discussion to follow). Negative extreme values of Mode 3 co-occurred with positive extreme values of Mode 2 in the spring of 2006, and again in winter of 2006-

2007 indicating dinoflagellate-dominated blooms. Positive extreme AF of Mode 3 co-occurred with Mode 2 positive AF in the spring of 2007, and, more so, in 2008 indicating the strong dominance of diatoms during these blooms.

Mode 4 captured 10% of co-variability in the data set. Values of the Mode 4 AF were well correlated with SST and inversely correlated with nutrient concentrations (Table 2). Mode 4 showed positive extremes in the amplitude function during stratified conditions and negative extremes when turbulent mixing was occurring. Indicator pigments most highly correlated with AF of Mode 4 were zeaxanthin ($r^2 = 0.38$), an indicator for picoplankton, and violaxanthin ($r^2 = 0.32$), a photo protective pigment. Mode 4 was interpreted as a picoplankton dominated or stratified mode and the most strongly positive AF occurred in the summer, and negative AF in the winter. The eigenvector for peridinin was also on the positive side while the eigenvectors for all of the other phytoplankton functional types were opposite. It makes sense that the indicator pigments for dinoflagellates co-vary positively with those for other stratified functional types as they are also found in the summer-fall in the SBC (Brzezinski and Washburn, 2011). Mode 4 AF correlated well in the positive direction with temperature and MAA index, and negatively with dissolved nutrients - further confirming the relationship with warm, stratified conditions (Table 2).

Inherent optical properties (IOP)

Mean component absorption spectra from Plumes and Blooms cruises (November 2005 – August 2009) are shown in Fig. 6. Variability about the mean is displayed here as one standard deviation (shaded areas). Phytoplankton absorption coefficient ($a_{ph}(l)$) was

more variable at shorter wavelengths and particularly variable in the UV portion of the spectrum. The absorption peaks at $a_{ph}(440)$ and $a_{ph}(675)$ nm are due to chlorophyll *a* absorption. The shoulders seen in the mean $a_{ph}(l)$ spectrum surrounding the chlorophyll *a* blue peak are due to accessory pigments, mostly carotenoids. Variability about the mean is a result of the variability in phytoplankton community composition and abundance and can be attributed to the presence of different accessory pigments contained by various species (e.g., diagnostic pigments) as well as size differences between phytoplankton groups (Nelson et al. 1993; Ciotti et al. 2002; Bricaud et al. 2004). The above previous studies have shown that lower absorption coefficient values as well as flatter spectra have been observed by microplankton, whereas smaller phytoplankton groups have shown higher overall absorption coefficient values with sharper absorption peaks. This reduction in the magnitude and flattening of phytoplankton absorption spectra as intracellular pigment concentrations or cell size increase is referred to as the package effect (Morel and Bricaud, 1981; Nelson et al. 1993). The effects of pigment packaging can be better assessed by normalizing the spectra to the chlorophyll *a* concentration ($a_{ph}^*(\lambda) = a_{ph}(\lambda)/$[Chl *a*]; Fig. 6b). Here, the standard deviations fit more tightly around the mean spectrum, particularly at higher wavelengths. The change in mean spectral shape and tightening of the standard deviation for $a_{ph}(\lambda)^*$ reflect the strong presence of microplankton in the SBC due to the high chlorophyll *a* concentrations associated with microplankton groups.

The average detrital absorption coefficient spectrum, $a_d(\lambda)$, increases towards shorter wavelengths (Fig. 6c). Overall, $a_d(\lambda)$ accounts for only a small portion of the total particle absorption. Increasing standard deviations towards decreasing wavelengths are

indicative of changes in the spectral decay slope within the data set. The mean CDOM absorption coefficient, $a_g(\lambda)$, also decays with increasing wavelength (Fig. 6d). Mean value of $a_g(400)$ are much greater than the other component absorption coefficients following global patterns (Nelson and Siegel, 2013). The standard deviations in $a_g(\lambda)$ are for the most part relatively small with the exception of a bulge found between λ = 300-400 nm. This is due to peak-like features near λ = 335 nm in several samples from the PnB cruises (*see* Fig. 2 for an example).

Mean particulate total and backward scattering spectra are relatively flat, yet are highly variable in magnitude (Fig. 7a, b). Average values of particle scattering coefficient, $b_p(\lambda)$, of the surface ocean resulted in a fairly flat spectrum with values ranging spectrally between 0.45 and 0.5 m^{-1} (Fig. 7a). Average particulate backscattering coefficient spectra, $b_{bp}(\lambda)$, ranged from 0.0039 – 0.0059 m^{-1}. The spectral shape for $b_{bp}(\lambda)$ observed in this study is typical for coastal, eutrophic regions (Kostadinov et al. 2012). Mean values of the particulate backscattering ratio, b_{bp}:b_p, often referred to as $\tilde{b}_{bp}(\lambda)$, was 1% to 1.2% with a slight decreasing trend in the blue spectral region (Fig. 7c). Values of b_{bp}:b_p is governed by the index of refraction and the slope of particle size distribution, where low values of b_{bp}:b_p are indicative of large particles. The values presented here (Fig. 7c) and in other studies for the SBC (Kostadinov et. al. 2010, 2012; Antoine et al. 2011) are typical for coastal systems where the particle load is dominated by larger phytoplankton species (also observed through laboratory studies, Whitmire et al. 2010).

Remote sensing reflectance spectrum, $R_{rs}(\lambda)$, is a function of the absorption and backscattering spectra presented above. The values of $R_{rs}(\lambda)$, obtained in situ using the PRR instrument, were indicative of a productive, coastal ocean where the reflectance is

highest in the green portion of the spectrum (Fig. 7d). The data presented here are a subset of the PnB IOP dataset used in Kostadinov et al. (2012) as only Horn Point Laboratory-analyzed HPLC data are used.

Relationship of IOPs to phytoplankton community structure

The data series of each IOP were linearly regressed with the AFs for each of the EOF modes where the AF values are used as a proxy for different phytoplankton communities. Linear regression analyses were done for every wavelength of the IOPs in effort to characterize spectral relationships between the optical parameters and phytoplankton community structure. Relationships were examined using slope diagrams, where the y-axis in Figs. 8 and 9 display the slope, m, for the linear regression, $y = mx + n$, of IOP vs. AF data series for each available wavelength (following Kostadinov et al. 2007). Fig. 8 show the spectral slope values for the regression between $a_{ph}(\lambda)$, $a_d(\lambda)$, $a_{ph}^*(\lambda)$, and $a_g(\lambda)$ and the top four EOF AF values ($m_{aph}(\lambda)$, $m_{ad}(\lambda)$, $m_{aph^*}(\lambda)$, and $m_{ag}(\lambda)$; in the following we will denote the slope spectra without the explicit spectral notation). Similar regressions were performed between $b_{bp}(\lambda)$, $b_p(\lambda)$, and $R_{rs}(\lambda)$ observations and the pigment EOF AF values (Fig. 9). The n-value shown in the figures indicates the number of independent observations used in each linear regression. The linear relationships represented by the slope diagrams were interpreted to be significant when the 95% confidence intervals surrounding the regression slope values are divergent from zero.

Slope spectra for the Mode 1 AF (the nanoplankton community) showed significant positive relationships with $a_{ph}(\lambda)$ and $a_{ph}^*(\lambda)$ at approximately λ = 400-500 nm and λ = 660-685 nm, capturing the regions of maximum chlorophyll *a* absorption.

Mode 1 m_{ag} and m_{ad} were not significantly different from zero at any wavelength, indicating there were no significant relationships between the non-living fraction of the absorption spectrum when the phytoplankton community was comprised of mostly nanoplankton.

Linear regressions with Mode 2 AF were significant for all absorption properties over large portions of the spectrum. The slope diagrams for m_{aph} and m_{ad} display positive relationships for the entire spectra, indicating that absorption due to phytoplankton, e.g., 'living' particles, as well as absorption due to non-living particles values were higher overall when microplankton groups dominated the phytoplankton community. The spectral shape of the m_{aph} and m_{ad} slope diagrams mimic the shape of the average absorption spectra, reinforcing the notion that microplankton groups are strongly influencing these properties. Values of $a_{ph}^*(\lambda)$ were negatively related to Mode 2 AF at λ = 663 nm and λ = ~380-500 nm, capturing the chlorophyll *a* absorption peaks as well as some of the surrounding accessory pigments. Negative slopes at the chlorophyll *a* absorption peaks are indicative of the package effect. That is, chlorophyll specific phytoplankton absorption decreases due to the package effect. The package effect is a common physiological strategy for large phytoplankton species such as diatoms (Kirk, 1994). Values of m_{aph^*} were positive for wavelengths approximately less than λ = 380nm. This is likely due to the presence of MAAs associated with one or more of the microplankton groups.

Positive linear relationships were observed for Mode 2 m_{ag} starting λ = 400 nm and continuing into the UV portion of the spectrum. The slope diagram does not reflect that of the average CDOM absorption spectra (Fig. 6d), but shows 'peaks' in this

relationship around λ = 335 nm. The increased absorption in the UV wavelengths, in both the particulate and dissolved phase, may have been due to MAAs. The linear relationships indicated a positive correlation of the MAA index with microplankton groups.

The EOF loadings for Mode 3 indicated an alternation in community dominance between diatom (positive) and dinoflagellate (negative) groups. Alternating positive and negative AF was interpreted as the progressive alternation of these groups in time and space; thus, the interpretation of the slope diagrams was so. Positive linear regression slopes were generally interpreted as positive linear relationships of IOPs vs. diatoms, and negative linear regression slopes were interpreted as positive relationships of IOPs vs. dinoflagellates. However, some logical exceptions were made below as the EOF leaves room for objectivity. Mode 3 m_{aph} were significantly positive for wavelengths λ = 400 - 700 nm with the characteristic phytoplankton absorption spectrum. This portion of the slope diagram had a similar shape to that for Mode 2, indicating that diatoms largely influence the relationship for this wavelength range. At wavelengths less than 400 nm, the linear regression slope became negative and showed a significant relationship at about λ = 360 nm. UV peaks, e.g. MAAs, were observed in several CDOM spectra, and the relationship here indicates that increased UV absorption was associated with the dominance of dinoflagellate groups.

Values of mode 3 m_{aph*} were significantly negative for the entire spectra and from 400-700 nm look similar to that for Mode 2. For wavelengths less than 400 nm, the slope diagram shows a strengthening negative relationship into the UV portion of the spectrum, indicating a positive correlation with dinoflagellates and UV absorption. Based on the

shape of the slope diagram for Mode 3 m_{aph}, the $a_{ph}(\lambda)$ relationship is likely reflecting the pigment packaging effect due to diatoms from λ = 400 to 700 nm, rather than increased phytoplankton specific absorption due to dinoflagellate presence. Negative m_{aph} and m_{aph*} in the UV portion of the spectrum, however, are more likely indicative of the strong UV absorbing capability of some dinoflagellate species, therefore, are interpreted as positive linear relationships between $a_{ph}(\lambda)$ and $a_{ph}^*(\lambda)$ and dinoflagellate functional type. The linear regressions for $a_g(\lambda)$ vs. AF also resulted in significantly negative m_{ag} in the UV portion of the spectrum. Slight peak-like features around λ = 335 and 360 nm, like those in Mode 2, are observed also in the negative direction for this mode. The shape of the slope diagram slightly resembles the shape of the average CDOM absorption spectra in that the relationship increases further into the UV, rather than decreasing like for Mode 2. This shows that the baseline CDOM concentrations as well as the UV peaks are both correlated with dinoflagellate presence.

Significant positive linear regression slope spectra for the absorption properties vs. Mode 4 AFs were observed for $a_{ph}(\lambda)$, $a_{ph}^*(\lambda)$, and $a_g(\lambda)$ only in the UV portion of the spectrum. The slope diagrams for particulate absorption properties make sense for this mode, which is indicative of high light adapted, small phytoplankton groups. Many high light adapted species contain MAAs in their cytoplasm (Roy et al. 2011). The shape of the slope diagram for m_{ag} looks like an inverted version of the slope diagram for Mode 3, e.g., the linear relationship strengthens further into the UV portion of the spectrum, indicating a strong relationship with CDOM absorption coefficient.

Linear regression spectral slopes for particle scattering properties vs. AF and $R_{rs}(\lambda)$ vs. AF are shown in Fig. 9. Mode 1 m_{bbp} was not significant at any wavelength,

however m_{bp} were significantly positive and $m_{bbp:bp}$ were significantly negative across all wavelengths. This shows that the nanoplankton community is significantly correlated to higher total scattering, and backscattering efficiency is lower when these groups are present. m_{bbp} was positive across the entire spectra for Mode 2, indicating that larger backscattering coefficient values are observed when the phytoplankton community is dominated by microplankton and chlorophyll *a* concentrations are high. Values of Mode 2 m_{bp} were significantly positive at longer wavelengths. Mode 2 AF also showed a significant positive relationship with b_{bp}:b_p at all wavelengths. Mode 3 m_{bbp} values were significantly positive for wavelengths 442, 589, and 671 nm. Mode 3 spectra for m_{bp} were significantly positive for the entire spectral range, while $m_{bbp:bp}$ was weakly significantly negative for only 510 nm. All of the linear regressions for scattering properties with Mode 4 AF were insignificant.

Linear regressions for $R_{rs}(\lambda)$ vs. AF resulted in significantly negative relationships in the blue and green part of the spectrum for Modes 1, 2, and 3. m_{Rrs} for Modes 2 and 3 were both significantly positive at $\lambda = 656$ nm. $R_{rs}(\lambda)$ is to first order is related to the ratio of backscattering coefficient divided by the absorption coefficient. The first three modes are consistent with the results of changes due to absorption being the dominant process. AF for Mode 4 looks more like a backscattering signal with its positive slope values throughout the spectrum (Toole and Siegel 2001). High AF values for Mode 4 indicate a higher picoplankton presence, but also a clearer ocean. The relationship with $R_{rs}(\lambda)$ could simply be due to lower absorption. Backscattering is also driving variability in $R_{rs}(\lambda)$ for longest wavelengths in slope spectra with Mode 2 and 3 AFs.

Discussion

Comparison with previous studies

The results above show that changes in phytoplankton community structure will affect inherent optical properties. An EOF analysis of a suite of phytoplankton pigment concentrations is performed and shows that the first 4 modes accounted for 82% of the variability in the pigment data. The 4 modes of variability presented encompassed all of the phytoplankton community regimes in the SBC consistent with previous studies (Toole and Siegel 2001; Anderson et al. 2008; Brzezinski and Washburn, 2010). Several recent studies have related IOPs and remote sensing reflectance to chemotaxonomic phytoplankton functional types and/or size classes determined via HPLC pigment concentrations. Bricaud et al. (2004) found that deviations from average a_{ph}*(440) in oceanic waters were driven by phytoplankton size classes, determined using the methods outlined in Vidussi et al. (2001) and Uitz et al. (2004). Kostadinov et al. (2012) used size classifications also determined from phytoplankton pigment concentrations to explain the variability of particle scattering in the SBC. The novelty of the approach of this study is that it objectively analyzed phytoplankton community variability using the covariance structure contained within the pigment data rather than pre-set ratios. This approach splits the microplankton size class into two separate regimes (e.g., EOF Mode 3) whereas in the phytoplankton pigment concentration size class approaches, the diatom and dinoflagellate functional groups are often combined into a single class. Diatom and dinoflagellate functional types may play very different roles in aquatic environment with regards to biogeochemical cycling (Nair et al. 2008) and, as shown in this work, affect the optical environment in different ways. Alvain et al. (2005) statistically examined

accessory pigment concentrations in relation to in situ $L_{wN}(\lambda)$and $R_{rs}(\lambda)$ from satellite measurements, so their method is also not limited by predetermined ratios (Alvain et al. 2005, 2006). However, peridinin concentrations are below detection in the open ocean (Case 1) and the effects of dinoflagellates on light reflectance and satellite-derived chlorophyll were omitted in those studies.

The linear regression results for Mode 1 AF vs. the various IOP parameters showed that changes in the chlorophyll *a* concentrations were only slightly represented by this community, a nanoplankton dominated community, by weak positive correlations with $a_{ph}(\lambda)$ and $a_{ph}^*(\lambda)$ from approximately $\lambda = 400 – 500$ nm. However, detrital and CDOM absorption properties were not well constrained by the dynamics of this mode at all. This was not surprising considering that Mode 1 did not include any bloom events, which would be expected to have a higher effect on changes in detritus and carbon biogeochemistry in the surface water. Similarly $b_{bp}(\lambda)$ was also not constrained by Mode 1 AF. Antoine et al. (2011) used data from the SBC as well as from the Mediterranean Sea and found that $b_{bp}(\lambda)$ was a good indicator for chlorophyll *a*, thus phytoplankton abundance, only when strong changes in abundance occurred such as a bloom or a dilution event. Their results relate well to Mode 1 results considering that it is representing background community assemblage.

IOPs were most strongly correlated with the importance of the microplankton groups, Mode 2, and the differences between diatom and dinoflagellate functional types, Mode 3. Characteristics of the diatoms captured in the IOP properties were consistent with the package effect as shown by the negative linear relationships with $a_{ph}^*(\lambda)$; yet positive correlations were observed with scattering coefficients, $b_{bp}(\lambda)$ and $b_p(\lambda)$. Positive

correlations with scattering properties were somewhat counterintuitive. Mie theory shows that larger homogeneous spheres will scatter proportionally more light in the forward direction than smaller ones. In general, larger phytoplankton may have lower indices of refraction than smaller ones (e.g., Stramski, 1999). However, Mode 2 was most highly correlated with chlorophyll *a* concentrations and the higher backscatter associated with this mode may have been a reflection of the sheer increase in phytoplankton abundances from baseline conditions (Antoine et al., 2011). Several recent studies have found that larger phytoplankton size classes contribute much more to bulk backscattering than previously thought (Dall'Olmo et al. 2009; Westberry et al. 2010; Whitmire et al. 2010). Mode 2 was also correlated positively with $a_d(\lambda)$ and $a_g(\lambda)$, indicating an increase in detrital particulates during blooms. The positive correlations of $b_{bp}(\lambda)$ with Mode 2 likely was caused by a combination of phytoplankton sized particles, detritus and any other increased particle abundance, e.g., bacteria as consumers in response to increased detritus, which may have covaried with bloom conditions.

The influence of dinoflagellates on IOP properties is manifested in numerous ways as shown through positive correlations, presented as negative correlations due to the sign of the amplitude function, with the Mode 3 AF vs. $a_{ph}(\lambda)$ and $a_{ph}^*(\lambda)$ in the UV region, positive correlation with $a_g(\lambda)$ in what appears to be a UV absorbing substance as well as background CDOM absorption, and positive correlations to $b_{bp}(\lambda)$ at select wavelengths. Whitmire et al. (2010) found that dinoflagellate species had higher backscattering ratios than diatom species, which is consistent with the results found in this paper considering the slight negative correlation of Mode 3 AF with b_{bp}:b_p (510). The authors attribute their observations to the complex cellular composition and dense DNA

content of dinoflagellates. Vaillancourt et al. (2004) found that dinoflagellates had the highest b_{bp}:$b_p(\lambda)$ values of 20 species of phytoplankton examined, consistent with the analysis on the EOF Modes in this study. Overall, this study was able to constrain much of the variability in the IOPs based on phytoplankton community structure. The main microplankton functional types in the SBC, diatoms and dinoflagellates, explained notable differences in all IOPs.

Phytoplankton community and CDOM absorption spectra

Absorption properties in both the particulate and dissolved phase were strongly influenced by phytoplankton community structure in the UV portion of the spectrum, as shown in Fig. 8. This feature was particularly noteworthy for CDOM absorption coefficients, with stronger correlations peaking between λ = 300-400 nm. The characteristic was due to the presence of peak-like features in the CDOM spectra that were observed as deviations from the baseline CDOM curve, and peak around λ = 335 nm and often, but not always, a peak is found at approximately λ = 360 nm as well (*see* example in Fig. 2). This spectral region is where the largest variability among the $a_g(\lambda)$ spectra was found (Fig. 5d). Large peaks, e.g., visible to the eye in individual spectral plots, were found in 33% of the CDOM spectra in the PnB data set used for this analysis. The peaks may be indicative of a UV absorbing substance related to, and potentially derived from, phytoplankton as they co-occurred with strong UV absorption in the $a_{ph}(\lambda)$ spectra as well. Vernet and Whitehead (1996) observed increased UV absorbance in the particulate and dissolved phase during a red-tide bloom of the dinoflagellate, *Lingulodinum polyedra,* off the Southern California coast in conjunction with increased

MAA concentrations. Absorbance peaks were observed at $a_p(360)$ as well as $a_g(360)$ for samples collected in situ during the bloom, and a shoulder in the absorbance spectra for filtrate of growth media was observed around $\lambda = 310$ nm when the species was grown in isolation. Recently, Tilstone et al. (2010) observed increased UV absorption for in situ CDOM in the Iberian Peninsula with similar spectral shoulders as observed in this study. The UV peaks observed in their study correlated well with increased MAA concentrations, peridinin concentrations, and dinoflagellate presence. There are no measurements of MAAs for the PnB data set, but it is likely that the peaks in UV absorption observed in this study were due to the presence of MAAs based on the similarity to previous studies (Vernet and Whitehead 1996; Whitehead and Vernet 2000; Tilstone et al. 2010). Therefore, the peak-like features are referred to as MAAs in this paper.

Residual CDOM spectra, a step in quantifying MAA index (*see* Methods section above; Fig. 2b), surprisingly revealed characteristic peaks at very low absorption in many spectra, totaling 55% of the PnB data used for this study. Values of the MAA index were significantly correlated with Modes 2, 3 and 4 (Table 2). The strongest relationship occurred with Mode 2 ($r = 0.64$), the mixed microplankton mode, however the negative correlation with Mode 3 ($r = -0.32$) indicates that dinoflagellates drive the relationship. The MAA index is also correlated well with peridinin concentrations, $r^2 = 0.70$ (Fig. 10), supporting the speculation that the MAAs are related to dinoflagellates. It was also not surprising that a significant correlation was observed with Mode 4 ($r = 0.24$), as this mode indicates stratified, high light conditions – conditions that would be prime for species whom are able to produce MAAs as a UV-shading mechanism.

Many phytoplankton species contain MAAs for presumably photoprotective purposes including the picoplankton *Prochlorococcus,* and the harmful algal diatom *Pseudo-nitzschia* (Roy et al. 2011). However, dinoflagellates are the only functional group documented to date that have co-occurred with dissolved MAAs in the water column (Vernet and Whitehead 1996; Tilestone et al. 2010). In the EOF analysis, peridinin is found on the positive side of our eigenvectors for Mode 4 – the mode that signals the presence of a stratified water column. Although peridinin is weakly correlated with the Mode 4 AF ($r^2 = 0.09$), it is only influential for Mode 3 ($r^2 = 0.52$), indicating how prevalent this functional group is in the SBC.

Roles of phytoplankton community structure on remote sensing retrievals

Coastal areas can be optically complex due to a number of factors including terrestrial runoff, phytoplankton blooms, and, as the SBC data set has shown, high variability in the phytoplankton community structure. Model performance for ocean color remote sensing in coastal areas can sometimes be improved by local calibration. That is, site-specific characterization of IOPs in coastal areas can be incorporated into the models, such as the GSM model that requires IOP spectral slopes as constants. In attempt to improve model performance, Kostadinov et al. (2007) executed local calibration of the GSM and OC4 models for the SBC. However, the locally tuned models did not perform substantially better than the globally tuned models. Here we examine the roles that phytoplankton community structure may play on bio-optical model performance. The globally tuned GSM model retrieved $a_{cdm}(443)$, $b_{bp}(443)$ and chlorophyll *a* concentration using measured $R_{rs}(l)$ spectra. Measured reflectance spectra were also used to retrieve

chlorophyll *a* concentrations using the empirical OC4v6 algorithm. Model-data residuals were calculated comparing the measured IOPs or chlorophyll *a* concentrations with the modeled parameters. Fig. 11 shows the data-model residuals, where negative residuals indicate an over-estimation from the model and a positive residual indicates model under-estimation of the given constituent.

A sub-sample of the residuals were extracted that corresponded to the extreme amplitude functions of the EOF analysis to assess the effects of phytoplankton community structure on model performance. Extreme AF values are represented in Fig. 5 as values $\pm$ 1 or 2 standard deviations from the mean AF, and indicate a time when a particular EOF mode was at its maximum intensity. Model residuals corresponding to the extreme AFs were then analyzed with a Student's two sample *t*-test against the total residuals for the given IOP or chlorophyll *a* concentrations. This analysis allows us to determine if the mean GSM or OC4 model error associated with the extreme AFs is significantly different from the total mean model residuals, thus leading us to speculate whether the model may be over or under predicting IOPs and chlorophyll *a* concentrations when a particular phytoplankton community is present.

In general, larger errors in chlorophyll *a* from both the OC4 and GSM models tended to occur in the negative direction, indicating the models are over-estimating chlorophyll *a* concentration. The exception to this was during the spring of 2006 and early summer of 2008, where considerable under-prediction occurred (model time series data not shown). The *t*-test results (Table 3) indicated that there were no significant errors for the OC4 model associated with phytoplankton communities for Modes 1 and 2. Model errors were significantly related to Mode 3, where residuals co-occurring with

negative AFs, e.g., dinoflagellate bloom, corresponded with significant over-prediction of chlorophyll *a* concentrations, and residuals co-occurring with positive AFs, e.g., diatom bloom, corresponded with significant under-prediction of chlorophyll *a* concentrations. The OC4 model residuals coinciding with extreme values of Mode 4 were also significantly less than the mean, indicating an over-prediction of chlorophyll *a* concentrations associated with the picoplankton dominated community. Chlorophyll *a* residuals from the GSM model were significantly less that the mean residual corresponding to extreme AF of Modes 2 and 3 both in the positive direction, e.g., + 1 and/or 2 standard deviations from the mean AF. This shows that the GSM model is significantly over-estimating chlorophyll *a* concentrations for microplankton, and specifically when diatoms are present. The differences in the OC4 and GSM model for Mode 3 are reflected by the sample means in Table 3 indicate that the GSM much more strongly over-estimates chlorophyll *a* concentrations when diatoms are present. The difference was driven largely by a single diatom bloom event on 11 April 2007. Oceanographic conditions (Fig. 2) and EOF amplitude functions indicate that it was not one of the strongest diatom blooms presented here, but beyond that it is unclear why the GSM over-estimation was so severe for this date.

The *t*-test results for the $a_{cdm}(443)$, calculated with the GSM model, for Modes 1, 2 and 3 indicate that the model is over predicting $a_{cdm}(443)$. The *t*-test also indicated that the model significantly over estimated $a_{cdm}(443)$ at times and locations co-occurring with Mode 3 extreme AFs, e.g., corresponding to dinoflagellate blooms. This was a bit surprising considering that results above show that higher absorbance of CDOM correlated to Mode 3. The spectral slopes in the GSM model are fixed, which may be

responsible for discrepancies between the modeled and observed IOPs. The results from this comparison need to consider that the observed influences of phytoplankton community structure on $a_g(\lambda)$ and $a_d(\lambda)$ occurred mostly below 400 nm (Fig. 6), and the GSM model does not consider the UV portion of the spectrum. Mode 2 was only slightly correlated with $a_g(\lambda)$ between 400-450, and very weakly at that. Furthermore, absorbance is very low in general above 400 nm in the dissolved and detrital fraction of the water column; therefore statistics are difficult to interpret.

Model errors for the GSM estimation of $b_{bp}(443)$ were more variable about the mean than for chlorophyll *a* concentrations and $a_{cdm}(443)$. The *t*-test results indicate that the GSM model is over-estimating $b_{bp}(443)$ when microplankton groups are dominating the phytoplankton community. This is shown by significant results for residuals corresponding to Modes 2 and 3 positive extreme AFs, as well as Mode 3 negative extreme AFs (Table 3) tested against the residual mean. The *t*-test was significant for residuals associated with positive extreme AFs of Mode 4, indicating model is over estimating $b_{bp}(443)$ when picoplankton groups are dominating the community. Significant results were also observed for residuals corresponding to negative extreme AFs of Mode 4, indicating under prediction of backscattering values when the inverse community is observed, loosely defined by larger groups of phytoplankton or simply when the picoplankton groups are less dominant.

Implications for future research

We have explored the roles that phytoplankton community structure has on the optical properties of the Santa Barbara Channel, an optically complex coastal system. We show that the phytoplankton community structure is important for all optical properties, not simply those specific to phytoplankton. This has many implications for remote sensing approaches for retrieving phytoplankton functional types. System approaches, such as Alvain et al. (2005), will likely have better capability of capturing community dynamics rather than reductionist approaches which focus solely on phytoplankton specific properties. Clearly, the entire planktonic community will respond to changes in phytoplankton functional types and this in turn will influence IOP values and characteristics. Looking ahead, there are enormous challenges for building remote sensing models that incorporate phytoplankton functional types.

References

Alvain, S., C. Moulin, Y. Dandonneau, and F. M. Bréon. 2005. Remote sensing of phytoplankton groups in case 1 waters from global SeaWiFS imagery. Deep-Sea Research I **52**: 1989-2004.

Alvain, S., C. Moulin, Y. Dandonneau, H. Loisel, and F. M. Bréon. 2006. A species-dependent bio-optical model of case I waters for global ocean color processing. Deep-Sea Research I **53**: 917-925.

Alvain, S., C. Moulin, Y. Dandonneau, and H. Loisel. 2008. Seasonal distribution and succession of dominant phytoplankton groups in the global ocean: A satellite view. Global Biogeochemical Cycles **22**: GB3001, doi:10.1016/j.dsr.2006.01.011

Alvain, S., H. Loisel, and D. Dessailly. 2012. Theoretical analysis of ocean color radiances anomalies and implications for phytoplankton groups detection in case 1 waters. Optics Express **20**: 1070-1083.

Anderson, C. R., D. A. Siegel M. A. Brzezinski, and N. Guillocheau. 2008. Controls on temporal patterns in phytoplankton community structure in the Santa Barbara Channel, California. Journal of Geophysical Research **113**: C04038, doi:10.1029/ 2007JC004321

Antoine, D., D. A. Siegel, T. Kostadinov, S. Maritorena, N. B. Nelson, B. Gentili, V. Vellucci, and N. Gillocheau. 2011. Variability in optical particle backscattering in constraining bio-optical oceanic regimes. Limnology and Oceanography **56**: 955-973.

Bhaud, Y., D. Guillebault, J. Lennon, H. Defaque, M. O. Soyer-Gobillard, and H. Moreau. 2000. Morphology and behaviour of dinoflagellate chromosomes during the cell cycle and mitosis. Journal of Cell Science **113**: 1231-1239.

Bricaud, A., M. Babin, A. Morel, and H. Claustre. 1995. Variability in the chlorophyll-specific absorption coefficients of natural phytoplankton: Analysis and parameterization. Journal of Geophysical Research **100**: 13,321-13,332.

Bricaud, A., A. Morel, M. Babin, K. Allali, and H. Claustre. 1998. Variations of light absorption by suspended particles with chlorophyll *a* concentration in oceanic (case 1) waters: Analysis and implications for bio-optical models. Journal of Geophysical Research **103**: 31,033-31,044.

Bricaud., A., H. Claustre, J. Ras, and K. Oubelkheir. 2004. Natural variability of phytoplanktonic absorption in oceanic waters: Influence of the size structure of algal populations. Journal of Geophysical Research. **109:** C11010, doi:10.1029/98JC02712.

Brzezinksi, M. A., and L. Washburn. 2011. Phytoplankton primary productivity in the Santa Barbara Channel: effects of wind-driven upwelling and mesoscale eddies. Journal of Geophysical Research: Oceans **116**: C12013, doi:10.1029/2011JC007397.

Clavano, W. R., E. Boss, and L. Karp-Boss. 2007. Inherent optical properties of non-spherical marine-like particles – from theory to observation. Oceanography and Marine Biology **45**: 1–38.

Ciotti, A. M., M. R. Lewis, and J. J. Cullen. 2002. Assessment of the relationships between dominant cell size in natural phytoplankton communities and the spectra shape of the absorption coefficient. Limnology and Oceanography. **47**: 404-417.

Dall'Olmo, G., T. K. Westberry, M. J. Behrenfeld, E. Boss, and W. H. Slade. 2009. Significant contribution of large particles to optical backscattering in the open ocean. Biogeosciences. **6**: 947-967.

Dierssen, H. M. 2010. Perspectives on empirical approaches for ocean color remote sensing of chlorophyll in a changing climate. Proceedings of the National Academy of Sciences of the United States of America. **107**: 17073-17078.

Emery, W. J., and R. E. Thomson. 1997. Data analysis methods in physical oceanography. Pergamon.

Guillocheau, N. 2003. β-correction experiment report, University of California, Santa Barbara internal report.

Harms, S., and C. D. Winant. 1998. Characterisitc patterns of the circulation in the Santa Barbara Channel. Journal of Geophysical Research: Oceans **103**: 3041-3065.

Hooker, S., L. Van Heukelem, J. Perl, J. Dolan, and R. Farnbach. 2009. NASA report. NASA Ocean Biology and Biogeochemistry GSFC Calibration and Validation Office. Available at http://oceancolor.gsfc.nasa.gov/DOCS/CHORS_Final_Report_Sec.pdf

International Ocean Colour Coordinating Group (IOCCG). 2000. Remote sensing of ocean colour in coastal, and other optically-complex waters. Sathyendranath, S. (ed.), Reports of the International Ocean-Colour Coordinating Group, No. 3, IOCCG, Dartmouth, Canada.

Kirk, J. T. O. 1994. Light and photosynthesis in aquatic ecosystems. 2nd Editon. Cambridge University Press.

Kostadinov, T. S., D. A. Siegel, S. Maritorena, and N. Guillocheau. 2007. Ocean color observations and modeling for an optically complex site: Santa Barbara Channel, California, CA. Journal of Geophysical Research **112**: C07011, doi:10.1029/2006JC003526

Kostadinov, T. S., D. A. Siegel, and S. Maritorena. 2010. Global variability of phytoplankton functional types from space: Assessment via the particle size distribution. Biogeosciences **7**: 3239-3257.

Kostadinov, T. S., D. A. Siegel, S. Maritorena, and N. Guillocheau. 2012. Optical assessment of particle size and composition in the Santa Barbara Channel, California. Applied Optics **51**: 3171-3189.

Krause, J. W., M. A. Brzezinski, D. A. Siegel, and R. C. Thunell. 2013. Biogenic silica standing stock and export in the Santa Barbara Channel ecosystem. Journal of Geophysical Research **118**: 736-749, doi: 10.1029/2012JC008070.

Lee, Z, K. L. Carder, and R. A. Arnone. 2002. Deriving inherent optical properties from water color: A multiband quasi-analytical algorithm for optically deep waters. Applied Optics **41**: 5755-5772

Magnuson, A., L. W. Harding, M. E. Mallonee, and J. E. Adolf. 2004. Bio-optical model for Chesapeake Bay and the Middle Atlantic Bight. Estuarine, Coastal and Shelf Science **61**: 403-424.

Mackey, M. D., H. W. Higgins, D. J. Wright, and W. Simon. 1997. CHEMTAX user's manual, a program for estimating class abundances from chemical markers: Application to HPLC measurements of phytoplankton pigments. Report 229: 47. CSIRO Marine Laboratory.

Maritorena, S., D. Siegel, A. Peterson. 2002. Optimization of a semi-analytical ocean color model for global-scale applications. Applied Optics **41**: 2705-2714.

Mitchell, B. G. 1990. Algorithms for determining the absorption coefficient of aquatic particulates using the quantitative filter technique (QFT), p. 137-148. In Ocean Optics

10, Proc. SPIE 1302.

Mobley, C. D. 1994. Light and water: Radiative transfer in natural waters. Academic Press.

Mobley, C. D. and D. Stramski. 1997. Effects of microbial particles on oceanic optics: Methodology for radiative transfer modeling and example simulations. Limnology and Oceanography **42**: 550-560.

Mobley, C. D., L. K. Sundman, and E. Boss. 2002. Phase function effects on oceanic light fields. Applied Optics. **41**: 1035-1050.

Morel, A. 1974. Optical properties of pure water and pure seawater. In: *Optical Aspects of Oceanography,* N.G. Jerlov and E.S. Nielsen Eds., Academic Press, p. 1-24..

Morel, A. and Y. Ahn. 1990. Optical efficiency factors of free-living marine bacteria: Influence of bacterioplankton upon the optical properties and particulate organic carbon in oceanic waters. Journal of Marine Research **48**: 145-175.

Morel, A., and A. Bricaud. 1981. Theoretical results concerning light absorption in a discrete medium, and application to the specific absorption of phytoplankton. Deep-Sea Research, **28**: 1375-1393.

Nair, A., S. Sathyendranath, T. Platt, J. Morales, V. Stuart, M. Forget, E. Devered, and H. Bouman. 2008. Remote sensing of phytoplankton functional types. Remote Sensing of Environment **112**: 3366 – 3375.

Nelson, N. B., Prézelin, B. B., and R. R. Bidigare. 1993. Phytoplankton light absorption and the package effect in California coastal waters. Marine Ecology Progress Series **94**: 217-227.

Nelson, N. B., D. A. Siegel, C. A. Carlson, C. Swan, W. M. Smethie, Jr., and S.

Khatiwala. 2007. Hydrography of chromophoric dissolved organic matter in the North Atlantic. Deep-Sea Research I **54**: 710-731.

Nelson, N. B., D. A. Siegel, C. A. Carlson, and C. M. Swan. 2010. Tracing global biogeochemical cycles and meridional overturning circulation using chromophoric dissolved organic matter. Geophysical Research Letters **37**: L03610, doi:10.1029/2009GL042325

Nelson, N. B., and D. A. Siegel. 2013. Global distribution and dynamics of chromophoric dissolved organic matter. Annual Review of Marine Science **5**: 447-476.

O'Reilly, J. E., S. Maritorena, B. G. Mitchell, D. A. Siegel, K. L. Carder, S. A. Garver, M. Kahru, and C. R. McClain. 1998. Ocean color chlorophyll algorithms for SeaWiFS. Journal of Geophysical Research **103**: 24937–24953.

Otero, M. P., and D. S. Siegel. 2004. Spatial and temporal characteristics of sediment plumes and phytoplankton blooms in the Santa Barbara Channel. Deep Sea Research II **51**: 1129-1149.

Roy, S., C. A. Llewellyn, E. S. Egeland, and G. Johnsen. 2011. Phytoplankton pigments: characterization, chemotaxonomy and applications in oceanography. Cambridge.

Sathyendranath, S., G. Cota, V. Stuart, H. Maass, and T. Platt. 2001. Remote sensing of phytoplankton pigments: a comparison of empirical and theoretical approaches. International Journal of Remote Sensing **22**: 249-273.

Shipe, R. F., and M. A. Brzezinski. 2001. A time series study of silica production and flux in an eastern boundary region: Santa Barbara Basin, California. Global Biogeochemical Cycles **15**: 516-531.

Siegel, D. A., M. J. Behrenfeld , S. Maritorena, C. R. McClain, D. Antoine, S. W. Bailey,

P. S. Bontempi, E. S. Boss, H. M. Dierssen, S. C. Doney, R. E. Eplee Jr., R. H. Evans, G. C. Feldman, E. Fields, B. A. Franz, N. A. Kuring, C. Mengelt, N. B. Nelson, F. S. Patt, W. D. Robinson, J. L. Sarmiento, C. M. Swan, P. J. Werdell, T. K. Westberry, J. G. Wilding, and J. A. Yoder. 2013. Regional to global assessments of phytoplankton dynamics from the SeaWiFS mission. Remote Sensing of Environment **135**: 77-91, doi: 10.1016/j.rse.2013.03.025

Smith, R. C., and K. S. Baker. 1981. Optical properties of the clearest natural waters (200-800 nm). Applied Optics **20**: 177-184.

Stramski, D. 1999. Refractive index of planktonic cells as a measure of intracellular carbon and chlorophyll *a* content. Deep-Sea Research I, **46**: 335-351.

Stramski, D., A. Bricaud, and A. Morel. 2001. Modeling the inherent optical properties of the ocean based on the detailed composition of the planktonic community. Applied Optics **40**: 2929-2945.

Stramski, D., E. Boss, D. Bogucki, and K. J. Voss. 2004. The role of seawater constituents in light backscattering in the ocean. Progress in Oceanography **61**: 27-56.

Szeto, M., P. J. Werdell, T. S. Moore, and W. Campbell. 2011. Are the world's oceans optically different? Journal of Geophysical Research: Oceans **116**: C00H04, doi:10.1029/2011JC007230

Tilstone, G. H., R. L. Airs, V. Martinez-Vicente, C. Widdicombe, and C. Llewellyn. 2010. High concentrations of mycosporine-like amino acids and colored dissolved organic matters in the sea surface microlayer off the Iberian Peninsula. Limnology and Oceanography **55**: 1835-1850, doi: 10.4319/lo.2010.55.5.1835

Toole, D. A., and D. A. Siegel. 2001. Modes and mechanisms of ocean color variability in the Santa Barbara Channel. Journal of Geophysical Research: Oceans **106**: 26985-27000.

Torrecilla, E., D. Stramski, R. A. Reynolds, E. Millan-Nunez, and J. Piera. 2011. Cluster analysis of hyperspectral optical data for discriminating phytoplankton pigment assemblages in the open ocean. Remote Sensing of Environment **115**: 2578-2593, doi:10.1016/j.rse.2011.05.014

Uitz., J., H. Claustre, A. Morel, and S.B. Hooker. 2006. Vertical distribution of phytoplankton communities in open ocean: An assessment based on surface chlorophyll. Journal of Geophysical Research: Oceans **111**: C08005, doi:10.1029/2005JC003207

Vaillancourt, R. D., C. W. Brown, R. R. L. Guillard, and W. M. Balch. 2004. Light backscattering properties of marine phytoplankton: relationships to cell size, chemical composition and taxonomy. Journal of Plankton Research **26**: 191-212.

Vernet, M., and K. Whitehead. 1996. Release of ultraviolet-absorbing compounds by the red tide dinoflagellate *Lingulodinium ployedrum*. Marine Biology **127**: 34-44.

Vidussi, F., H. Claustre, B. B. Manca, A. Luchetta, and J. C. Marty. 2001. Phytoplankton pigment distribution in relation to upper thermocline circulation in the eastern Mediterranean Sea during winter. Journal of Geophysical Research **106**: 19,939-19,956.

Washburn, L., M. R. Fewings, C. Melton, and C. Gotschalk. 2011. The propagating response of coastal circulation due to wind relaxations along the central California coast. Journal of Geophysical Research **116**: C12028, doi:10.1029/2011JC007502

Westberry, T. K., G. Dall'Olmo, E. Boss, M. J. Behrenfeld, and T. Moutin. 2010. Coherence of particulate beam attenuation and backscattering in diverse open ocean environments. Optics Express **18**: 15419:15425.

Whitehead, K., and M. Vernet. 2000. Influence of mycosporine-like amino acids (MAAs) on UV absorption by particulate and dissolved organic matter in La Jolla Bay. Limnology and Oceanography **45**: 1788-1796.

Whitmire, A. L., W. S. Pegau, L. Karp-Boss, E. Boss, and T.J. Cowles. 2010. Spectral backscattering properties of marine phytoplankton cultures. Optics Express **18**: 15073-15093.

Table 1. Diagnostic phytoplankton pigments for chemotaxonomy

Pigments	Abbreviation	Taxonomic Significance	Size class
Peridinin	Per	dinoflagellate	micro (>20
19'butanoyloxy-fucoxanthin	But	chromophytes nanoflagellates	nano (2 - 20 μm)
Fucoxanthin	Fuco	Diatoms	micro (>20
Violaxanthi	Viol	photo-	
19'hexanoyloxy-fucoxanthin	Hex	chromophytes nanoflagellates	nano (2 - 20 μm)
Alloxanthin	Allo	cryptophytes	nano (2 - 20
Zeaxanthin	Zea	cyanobacteria prochlorophytes	pico (>2 μm)
Lutien	Lut	photo-	
Chlorophyll *b*	Chl *b*	green flagellates prochlorophytes	nano (2 - 20 μm)
Chlorophyll	Chl *a*		

Modified from Vidussi et al. 2001

Table 2. Linear regression results from EOF amplitude functions (AF) vs. seawater properties.

	Linear regression correlation coefficient (*r*)				
Property	Mode 1	Mode 2	Mode 3	Mode 4	*n*
Salinity	0.04	-0.11	**0.46**	**-0.34**	207
Temperature	**-0.16**	**-0.50**	**-0.15**	**0.49**	210
NO_3+NO_2	0.01	0.07	0.03	**-0.50**	195
PO_4	0.13	0.11	0.02	**-0.55**	195
SiO_2	**0.22**	0.13	-0.10	**-0.41**	195
L-Si	-0.09	**0.21**	-0.03	-0.05	225
B-Si	**-0.16**	**0.40**	**0.77**	**-0.15**	225
POC	**-0.06**	**0.55**	**0.82**	0.15	125
Chl *a*	**0.14**	**0.54**	**0.70**	-0.04	225
MAA	0.05	**0.64**	**-0.32**	**0.24**	225

Bold numbers indicate significant results with p-value ≤ 0.05.

Table 3. Two Sample T-test - Model residual corresponding to 1 & 2 standard deviations (SD) from the AF mean vs. average IOP model residual. Numbers in bold indicate significant results with $p < 0.10$.

	Mode 1			Mode 2			Mode 3			Mode 4		
	Sample mean	**N**	**p-value**	**Sample mean**	**(N)**	**p-value**	**Sample mean**	**(N)**	**p-value**	**Sample mean**	**(N)**	**p-value**
[Chl *a*] - OC4												
+1 std AF	0.33	24	0.26	-0.14	30	0.49	-1.89	11	0.62	**-3.78**	**13**	**0.09**
-1 std AF	-0.30	15	0.66	-0.09	16	0.52	**-6.10**	**14**	**2.73E-03**	-0.52	21	0.71
+2 std AF	-1.50	12	0.73	-1.72	9	0.69	**6.94**	**6**	**7.78E-04**	0.79	2	0.65
-2 std AF	NaN	0	NaN	-0.37	3	0.85	3.38	2	0.26	-0.24	2	0.85
[Chl *a*] - GSM												
+1 std AF	-2.02	24	0.44	-2.55	30	0.16	**-8.68**	**11**	**3.17E-07**	-2.36	13	0.38
-1 std AF	-0.68	15	0.51	-1.21	16	0.89	-2.91	14	0.16	-1.77	21	0.63
+2 std AF	-2.61	12	0.27	**-3.85**	**9**	**0.08**	**-6.04**	**6**	**0.01**	0.49	2	0.50
-2 std AF	NaN	0	NaN	-2.39	3	0.64	2.77	2	0.14	-2.01	2	0.81
a_{cdm}(443)												
+1 std AF	**-0.08**	**24**	**0.05**	**-0.12**	**30**	**9.18E-06**	**-0.26**	**11**	**2.30E-13**	-0.05	13	0.78
-1 std AF	-0.04	15	0.92	-0.03	16	0.56	**-0.09**	**14**	**0.03**	-0.04	21	0.99
+2 std AF	**-0.09**	**12**	**0.04**	**-0.16**	**9**	**2.69E-04**	**-0.29**	**6**	**5.56E-11**	0.00	2	0.55
-2 std AF	NaN	0	NaN	-0.09	3	0.33	0.01	2	0.40	-0.05	2	0.84
b_{bp}(443)												
+1 std AF	-1.85E-03	21	0.23	**-3.36E-03**	**28**	**1.82E-03**	**-4.34E-03**	**11**	**3.99E-03**	**-4.19E-03**	**10**	**5.77E-03**
-1 std AF	7.01E-05	12	0.41	6.90E-05	12	0.41	**-3.79E-03**	**14**	**4.25E-03**	**8.51E-04**	**16**	**0.08**
+2 std AF	-2.24E-03	10	0.24	**-6.17E-03**	**9**	**6.83E-05**	**-0.01**	**6**	**1.95E-04**	NaN	0	NaN
-2 std AF	NaN	0	NaN	-9.93E-04	3	0.93	-1.74E-03	2	0.73	NaN	0	NaN

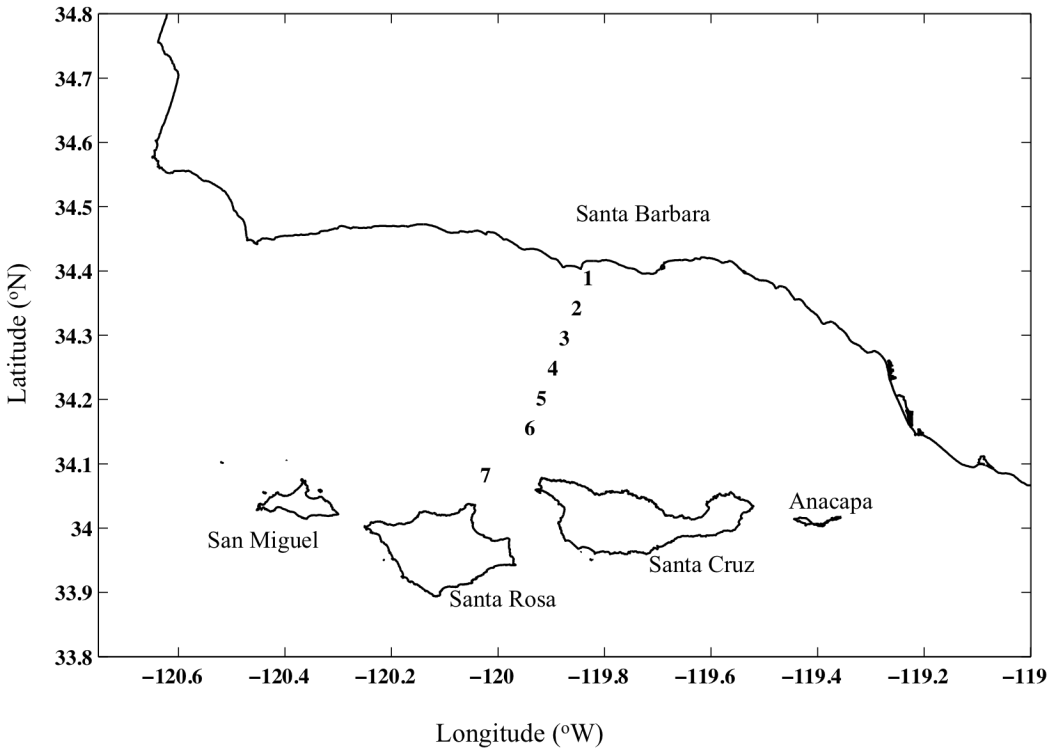

Figure 1. Map of the Santa Barbara Channel. Plumes and Blooms stations are indicated by their station number.

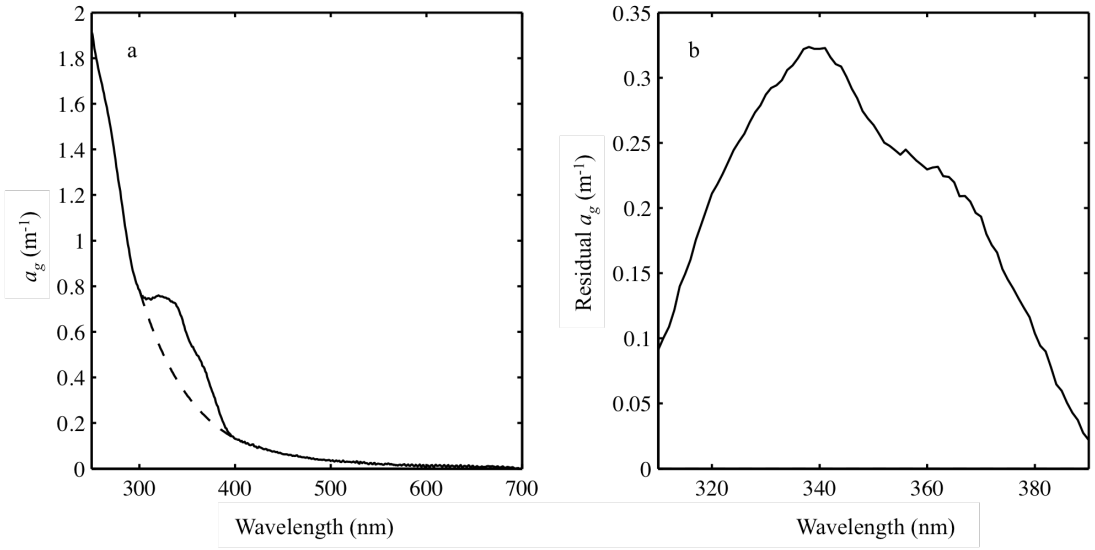

Figure 2. Example of MAA peak and MAA Index calculation: (a) CDOM absorption spectra for Sta. 5 on 24 January 2006 in the solid line and molded 'baseline' spectra (310-390 nm) in the dashed line and (b) residual between modeled $a_g(\lambda)$ and real $a_g(\lambda)$ data (310 – 390 nm).

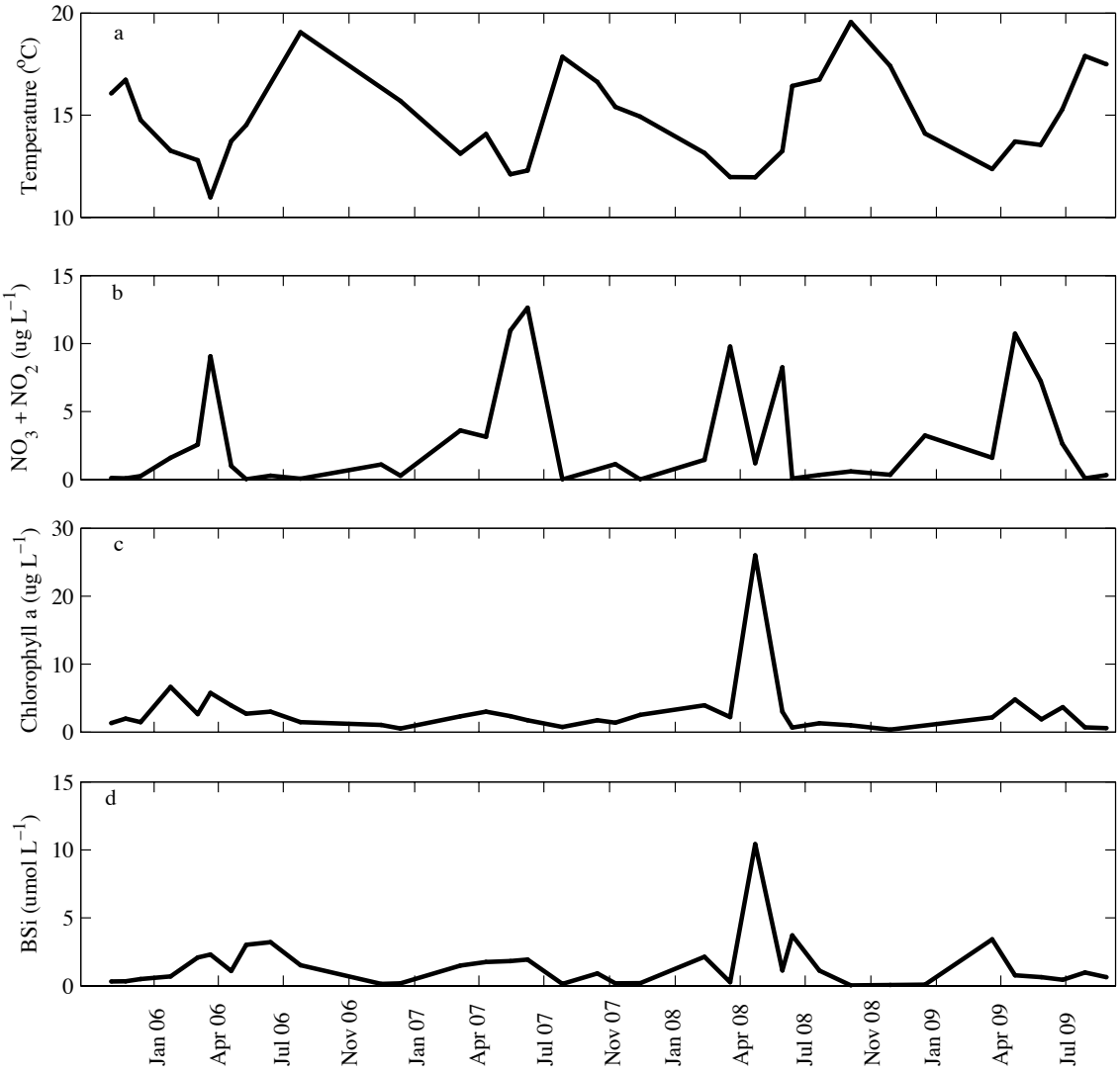

Figure 3. Surface seawater properties at Sta. 4: (a) Temperature, (b) Nitrate+Nitrite (NO_3+NO_2) concentration, (c) Chlorophyll *a* concentration – determined via HPLC and (d) Biogenic Silica (BSi) concentration.

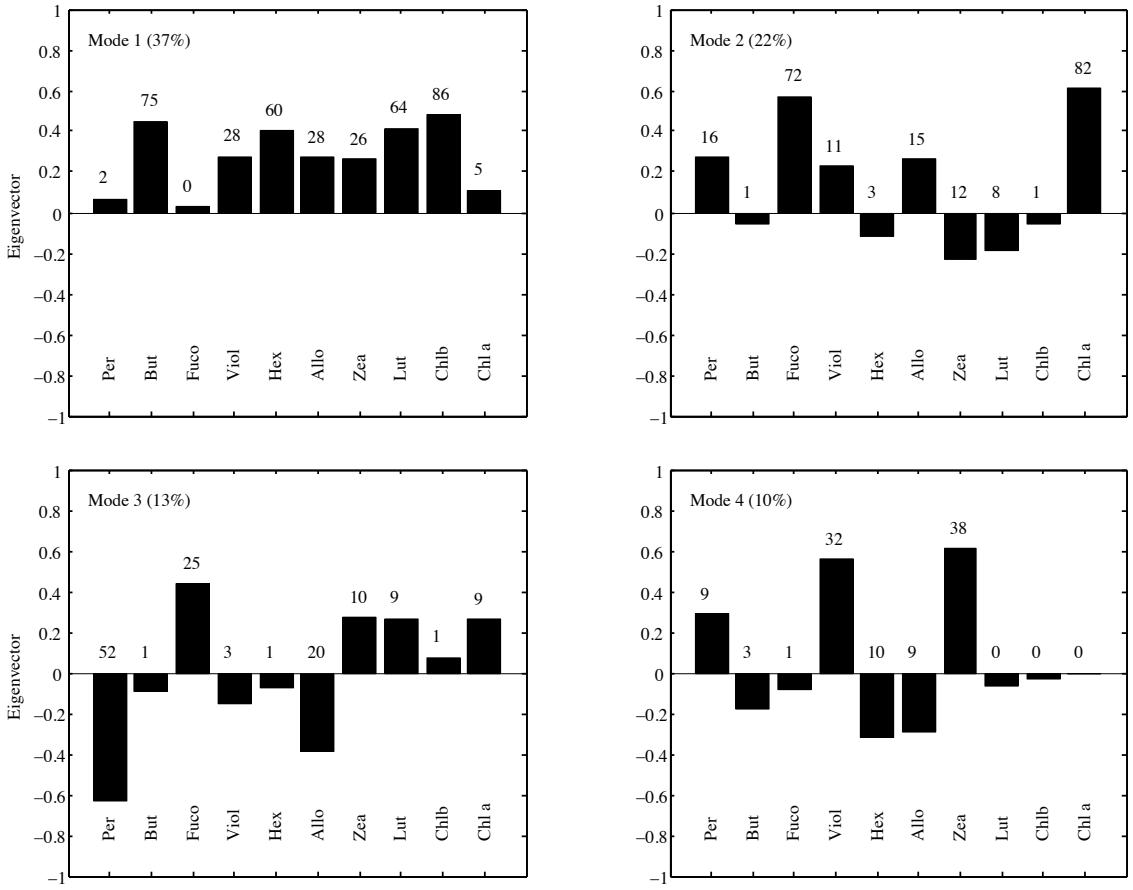

Figure 4. Eigenvectors for the 4 dominate EOF Modes. The percentile listed next to the titles are the percent of the phytoplankton diagnostic pigment co-variability captured by the given mode. The numbers listed above the eigenvector bars are r^2 x 100 of the linear regression between the respective pigment concentrations and the amplitude function for the given mode.

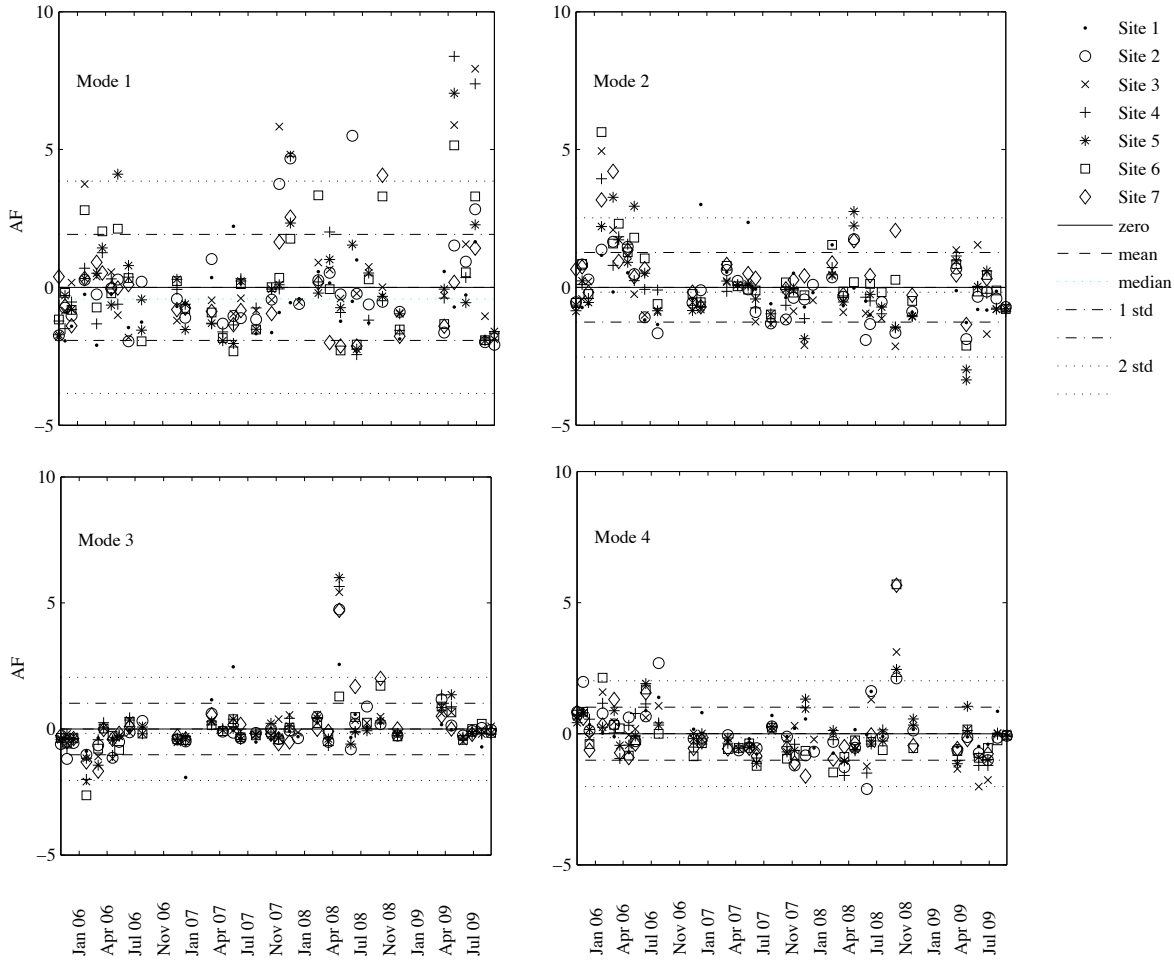

Figure 5. Amplitude functions for the 4 dominate EOF Modes. Figs highlight the mean and median AF, as well AF $\pm$1 standard deviation and $\pm$2 standard deviations from the mean.

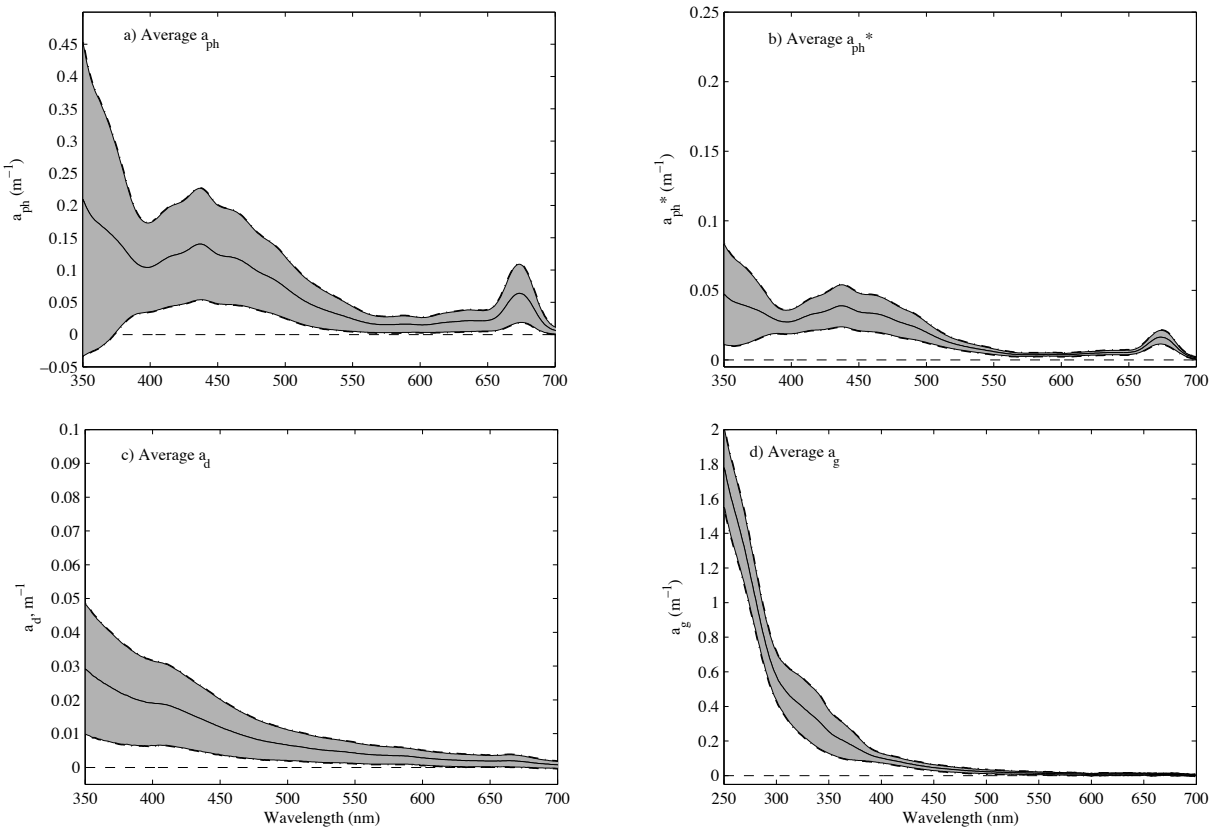

Figure 6. Average absorption properties of the Santa Barbara Channel for the study period: (a) phytoplankton absorption ($a_{ph}(\lambda)$), (b) phytoplankton specific absorption ($a_{ph}^*(\lambda)$), (c) detrital absorption ($a_d(\lambda)$), and (d) CDOM absorption ($a_g(\lambda)$).

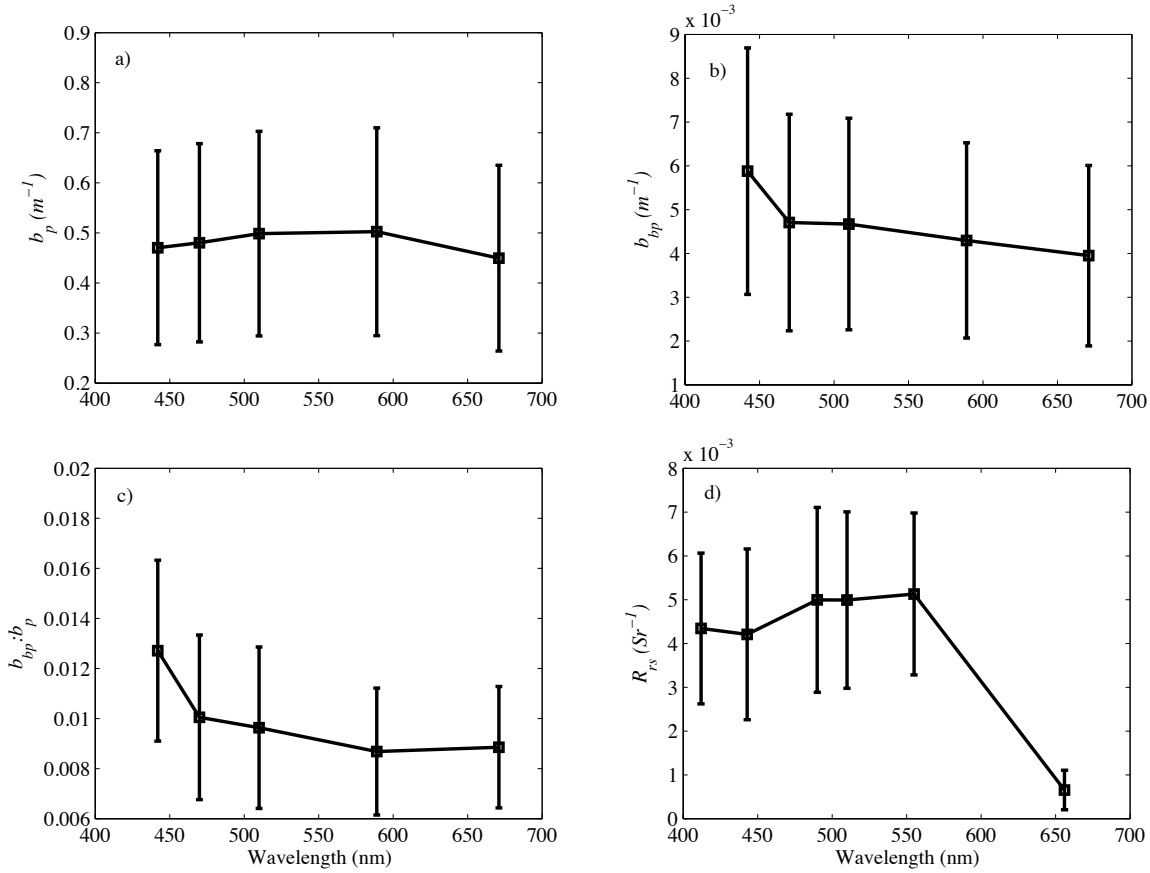

Figure 7. Average particle scattering properties and average ocean reflectance in the Santa Barbara Channel for the study period: (a) total particle scatter ($b_p(\lambda)$), (b) particle backscatter ($b_{bp}(\lambda)$), (c) particle backscatter normalized by total particle scatter ($b_{bp}(\lambda)$: $b_p(\lambda)$), and (d) Remote sensing reflectance – measured in situ with the PRR ($R_{RS}(\lambda)$).

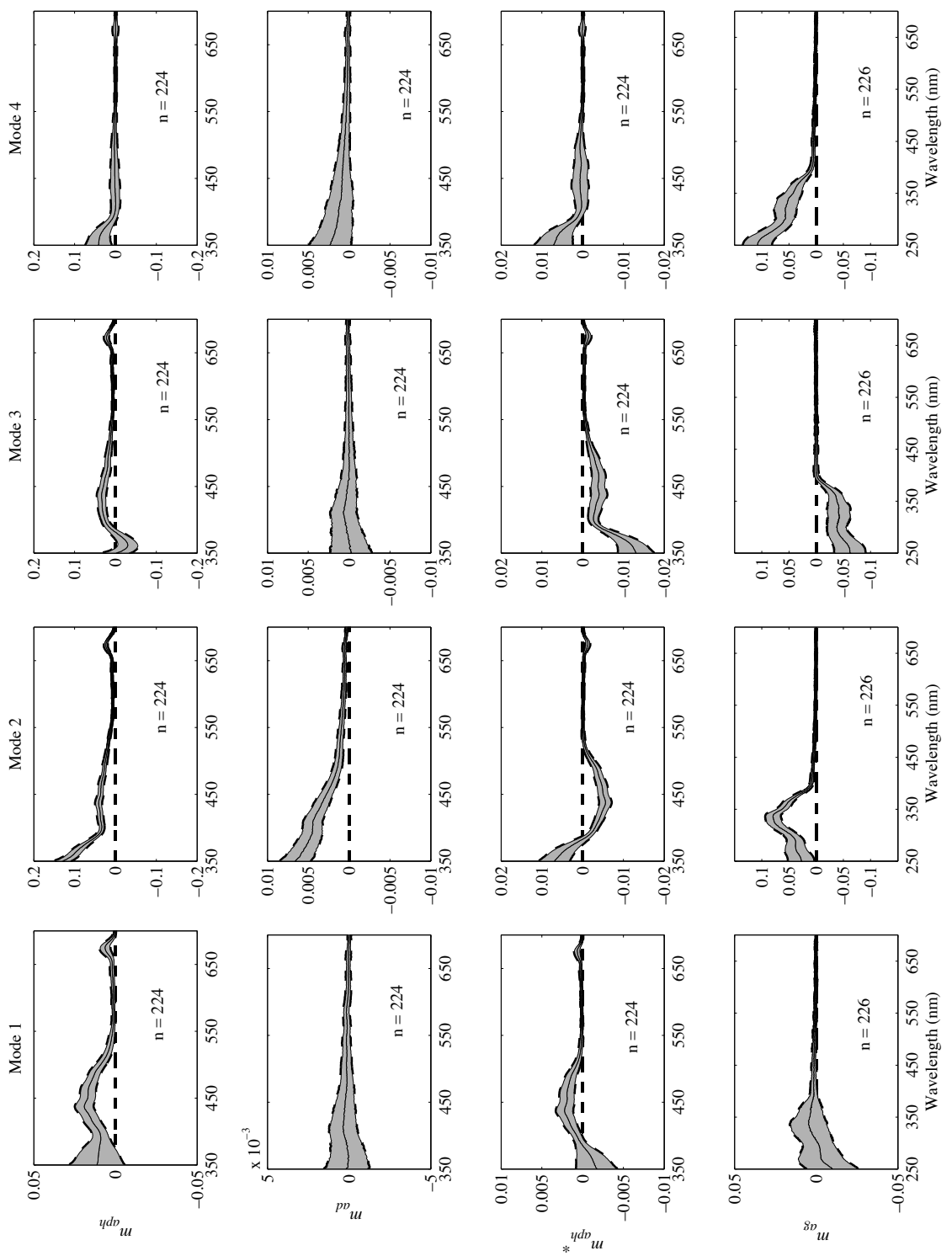

Figure 8.Figure 8. Slope diagrams for linear regressions of various absorption properties vs. EOF amplitude functions (AF) for each mode, where m_{IOP} refers to the term, m, in the linear equation $y=mx + n$.

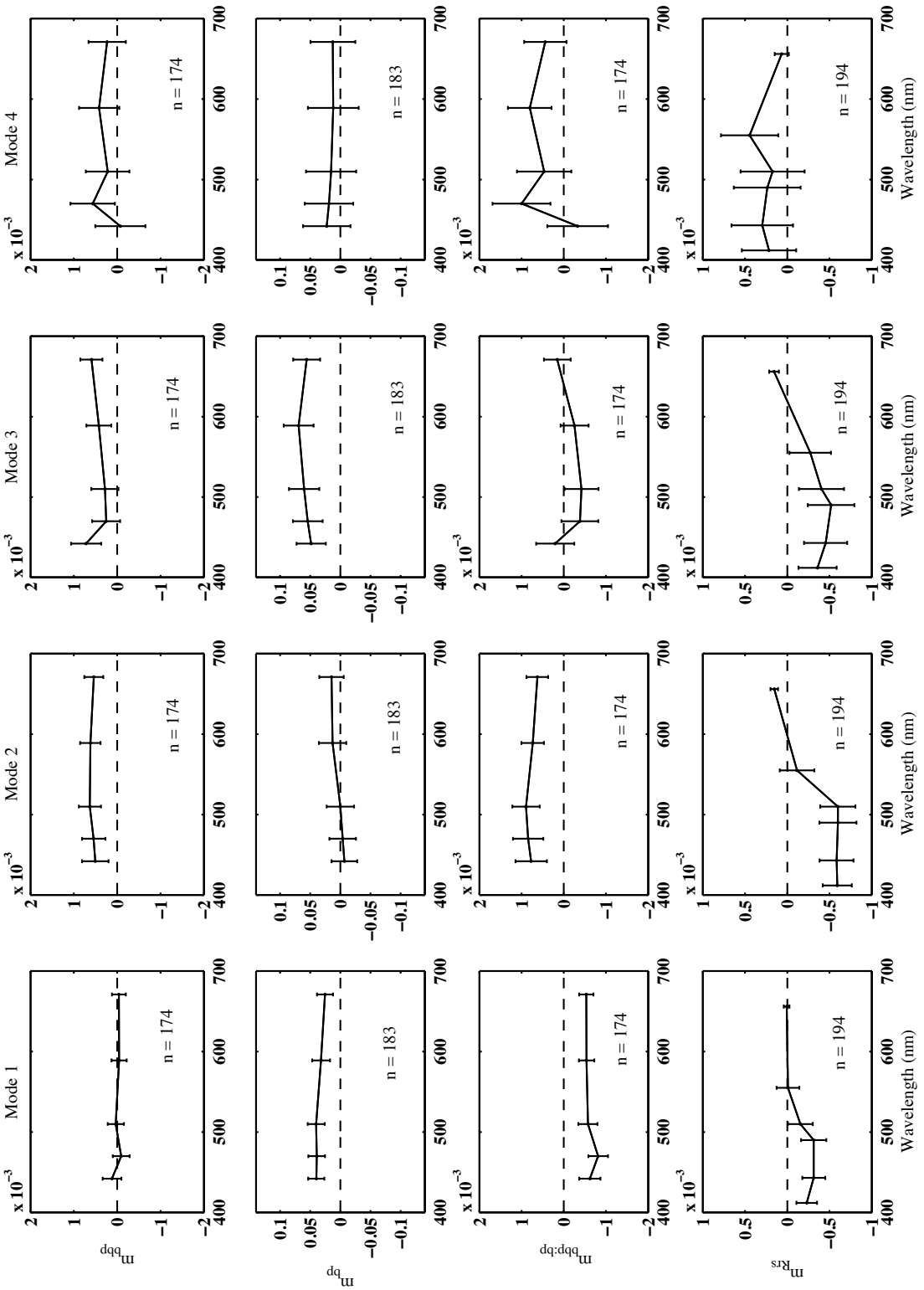

Figure 9. Slope diagrams for linear regressions of various scattering properties and $R_{RS}(\lambda)$ vs. EOF amplitude functions (AF) for each mode, where m_{IOP} refers to the term, m, in the linear equation $y=mx + n$.

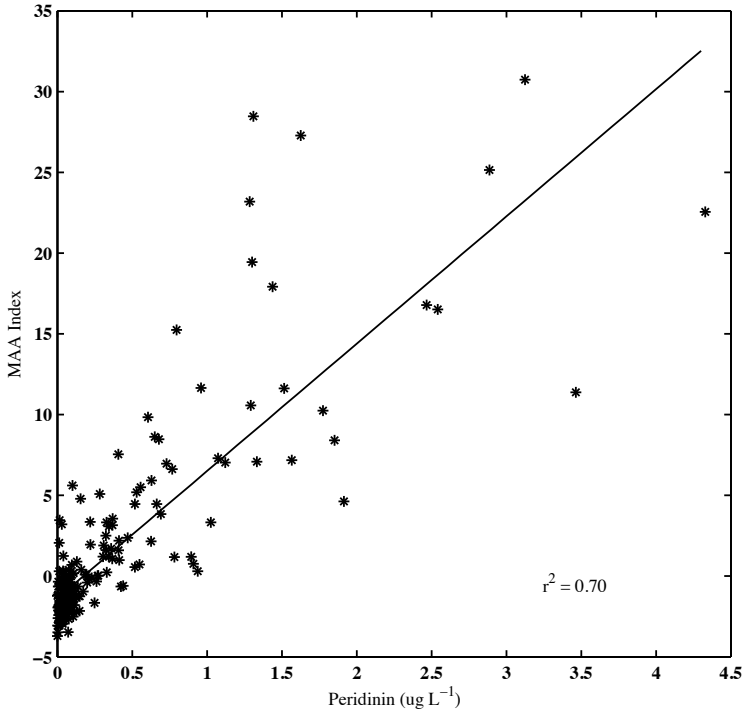

Figure 10. MAA index vs. Peridinin concentrations for the study period. MAA Index values represent the sum of the residuals of modeled baseline absorption from measured CDOM absorption over the wavelengths 310-390 nm.

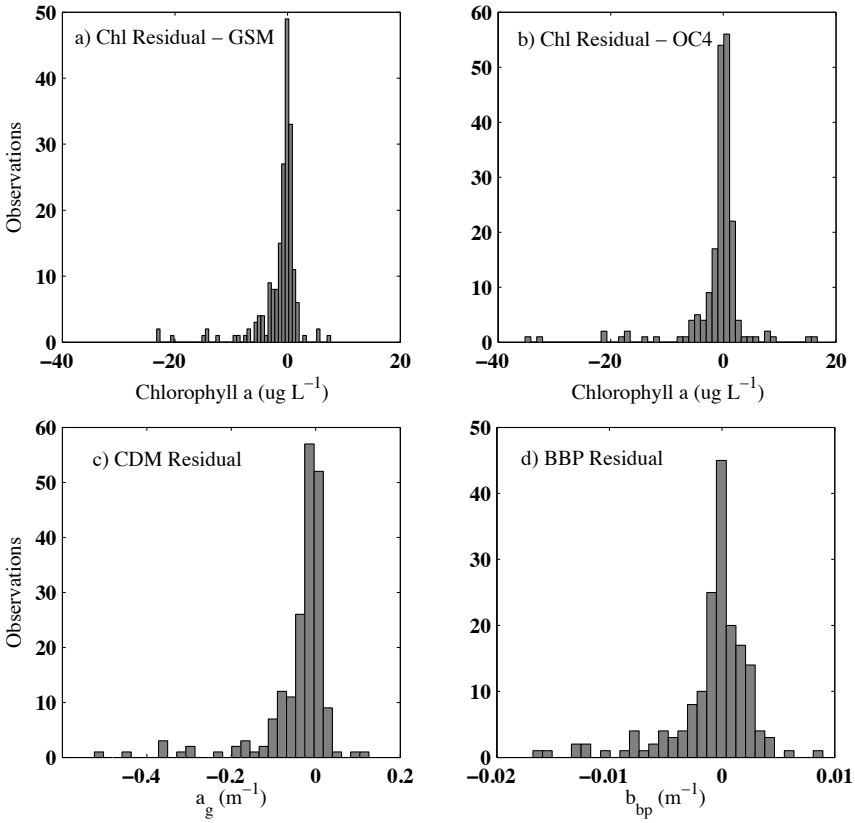

Figure 11. Model residuals for the OC4 version 6 and GSM-II models: (a) Chlorophyll *a* residual (μg L^{-1}) calculated from OC4 version 6, (b) Chlorophyll *a* residual (μg L^{-1}) calculated from GSM-II, (c) $a_{cdm}(443)$ residual (m^{-1}) calculated from GSM-II, and (d) $b_{bp}(443)$ residual (m^{-1}) calculated from GSM-II.

III. Colored dissolved organic matter dynamics in a nearly autochthonous coastal site

Rebecca K. Barrón, Dave Siegel, Norm Nelson and Nathalie Gulliocheau

Abstract

Colored dissolved organic matter (CDOM) is a ubiquitous component in the global ocean and is important for limiting light penetration in the surface ocean. Coastal ocean studies have show CDOM to be largely related to terrestrial organic matter loads, however studies of biological production of CDOM along the coastline have received much less attention. Data from a 15-year study in the Santa Barbara Channel (SBC), a productive coastal ecosystem, shows that phytoplankton community structure is strongly correlated to CDOM absorption, particularly in the UV range. Analysis of spectral CDOM data with an empirical orthogonal function (EOF) procedure highlighted seasonal and inter-annual trends in CDOM spectra, and allowed for separation of autochthonous vs. allochthonous sources. Increases in CDOM absorption coefficient were almost entirely related to autochthonous sources, particularly via the release of myosporine-like amino acids (MAAs). Phytoplankton abundance played a secondary role to community dominance in release of colored material. Allochthonous sources of CDOM to the surface SBC were almost entirely the product of seasonal deep-ocean upwelling. Deep-ocean upwelling resulted in decreased CDOM absorption in the surface via dilution despite the increased productivity associated with bloom species, e.g. diatoms. Freshwater inputs to the SBC resulted in no significant changes to the baseline CDOM absorption spectra

lower than λ = 280nm. The same EOF procedure was applied to the Global Ocean CDOM data set, and the three dominant modes of variability were similar in spectral shape to those found in the SBC. MAA Index values were well correlated to the global data set, particularly in regions of high-light adapted phytoplankton communities. Similarity of the EOF outcomes indicated that the SBC acts largely as an oceanic system despite the site's close proximity to the mainland.

Introduction

The study of colored dissolved organic matter (CDOM) has grown in attention in the oceanographic community over the past 20 years. CDOM is ubiquitous throughout the global ocean, dominates the absorption spectrum for wavelengths of light less than 500 nm and can be viewed from satellite remote sensors (Nelson and Siegel, 2013; Siegel et al. 2013). CDOM controls light energy penetration into the ocean and is therefore also important in regulating mixed layer depth. Due to the strong light-absorbing properties, CDOM acts as a sunscreen for aquatic plants and animals such as coral reefs. CDOM also plays a role in the biogeochemical cycles of dimethyl sulfide, carbon monoxide and hydrogen peroxide (Coble 2007). CDOM has semi-conservative properties, so it can also act as a tracer for ocean mass circulation (Nelson et al. 2007, 2010; Swan et al. 2009). Many of these applications have lead to the increased study of CDOM origin, fate, and transport in the ocean.

Terrestrial sources of CDOM are important in coastal areas, particularly those near large rivers, and can be observed from satellites (Siegel 2002). Early investigators theorized all oceanic CDOM to originate mostly from land soil and plant sources that were extracted and delivered to via the world's rivers in what we call "The Dirty Bathtub Ring" theory. More recent investigations have shown that very little terrestrial CDOM is present in the surface waters of the open ocean. Mannino et al. (2008) observed that allochthonous CDOM dominated composition in the coastal zone of the Mid-Atlantic Bight, and autochthonous sources became the main component of CDOM beyond the continental shelf break (Mannino et al. 2008). Twardowski et al. (2001) found that phytoplankton production accounted for 10% of CDOM composition in the East

Washington Sound, and the rest was attributed to terrestrial sources. Terrestrial contributions are dominant in coastal areas near large rivers or tributaries such as the Hudson, Amazon, Mississippi, Congo, Orinoco, and Yangtze Rivers, for example (Blough et al. 1993; Siegel 2002; Del Vecchio and Subramaniam 2004). Florida mangrove forests are an important source of CDOM in the surrounding coastal areas, however the magnitude varies largely by tidal influence (Maie et al. 2006). Many of the world's coastlines, however, do not have a large freshwater influence to carry heavy loads allochthonous materials out to sea. An increasing number of studies have shown that in situ processes to play an important role in coastal CDOM production and variability (Barron et al. 2014; Pavlov et al. 2014).

Open ocean CDOM is not correlated to dissolved organic matter (DOM) concentrations and represents a small, recalcitrant portion of the total DOM pool (Siegel et al. 2002; Nelson et al. 2007; Nelson and Siegel 2013). It is thought that heterotrophic microbes use autochthonous organic materials as substrate to produce much of the long-lived CDOM in the open ocean (Nelson and Siegel, 2013). CDOM in the surface ocean is primarily controlled by local production of heterotrophic bacteria, advection of water masses, and photodegradation as the primary loss mechanism (Siegel et al. 2002; Swan et al. 2009; Nelson et al. 2010). In addition to bacterial production, other autochthonous sources of CDOM in the surface ocean include direct excretion or byproducts from phytoplankton, zooplankton and macroalage (Steinberg et al. 2004; Nelson and Siegel 2013).

Many species of phytoplankton produce a UV-absorbing pigment called mycosporine-like amino acid (MAA) under conditions of high light stress. Some studies

have found MAA absorption features in CDOM spectra indicating direct release from phytoplankton cells (Whitehead and Vernet 2000; Barron et al. 2014; Pavlov et al. 2014). Morrison et al. (2004) theorized that MAAs potentially represent a significant portion of the CDOM absorption between 300-400 nm in the open ocean. Barron et al. (2014) identified large MAA features in CDOM spectra in the Santa Barbara Channel surface ocean that correlated strongly with dinoflagellate presence. Zooplankton have shown to excrete significant amount of CDOM directly into the water column as a waste product (Urban-Rich et al. 2006). Saba et al. (2009) found that the copepod *A. tonsa* excreted different DOM composition depending on diet, and a particularly high amounts of CDOM were excreted when the copepod fed on heterotrophic dinoflagellate species versus exclusive feeding on diatoms.

Oceanic CDOM at depth is formed by bacterial remineralization of sinking particulate organic matter (POM) (Nelson et al. 2007), and diffusion from the sediments at the continental shelf (Chen and Gardner 2004). Diffusion of CDOM from the deep ocean sediments does not appear to be significant, and the deep sediments are thought to be a permanent CDOM sink (Nelson and Siegel 2013). Seasonal mixing of subthermocline CDOM has proven to be an important allochthonous source for surface CDOM in the Atlantic Ocean (Nelson et al. 2004; Kitidis et al. 2006).

The questions this paper addresses are: How far does the "Dirty Bathtub Ring" extend, and how important are other sources of CDOM in a coastal ocean? This paper focuses on the Santa Barbara Channel, a coastal ocean with a narrow continental shelf and where terrestrial influence on oceanic properties is low, e.g. very low rainfall and river outflow. Yet many of the stations occupied are only a few kilometers from land.

Our goal is to assess the sources of CDOM at this site using a 15-year data set, and relate these coastal observations to global survey CDOM results. This work highlights the dominance of autochthonous sources of CDOM at this site, particularly that related to the dominance of dinoflagellates in the phytoplankton community. Finally, this research will show an example of a near-shore site with very little evidence of CDOM derived from terrestrial sources.

Methods

Data for this paper were collected as part of the Plumes and Blooms (PnB) program (Siegel et al. 2014). Observations were made at 7 stations in a transect across the Santa Barbara Channel starting from Goleta Point and extending to Santa Rosa Island. Stations 1 and 7 are located at the shelf break, approximately 50 m depth, and the rest of the sites are in deeper water, the deepest being Station 4 at approximately 550 m (Fig. 1).

This study used a 15-year data set starting in July 1997 through December 2012. An array of optical measurements was collected using *in-situ* profiling instruments on the PnB cruises as well as conductivity-temperature-depth measurements (e.g., Kostadinov et al. 2007; 2012; Antoine et al. 2011). Samples were taken at each station for laboratory analysis of inherent optical properties, and other chemical and biogeochemical parameters. Methods for the parameters used in this paper are described in detail below. More information of the Plumes and Blooms sampling scheme can be found on the project website (http://www-dev.eri.ucsb.edu/research/groups/plumes-and-blooms). It is noted that Plumes and Blooms has an annual monthly gap in the data time series each January, starting 2007, where there were no cruises conducted due to ship maintenance.

Discrete samples were taken using 5 liter Niskin bottles deployed on a rosette with a Seabird 9/11 conductivity-temperature-depth system. Samples that were taken at discrete depths were analyzed for nutrients, biogenic and lithogenic silica (BSi and LSi), particulate organic carbon (POC), phytoplankton accessory pigments, chlorophyll *a,* dissolved organic carbon (DOC), and CDOM. Nutrient samples were collected directly from the Niskin bottles and stored in a shipboard freezer, then transferred to the laboratory freezer until analysis on a Latchet QuikChem 8000 Flow Injection Analyzer. BSi and LSi samples were filtered shipboard onto 0.4 μm membrane filters and frozen until analysis using a NaOH extraction procedure described in (Shipe and Brzezinski 2001) and, more recently, in (Krause et al. 2013). DOC samples were filtered through pre-combusted GF/F filters directly from the Niskin containers into acid-leached high-density polycarbonate bottles and immediately placed in the shipboard freezer. The samples were kept frozen until analysis on a Shimadzu TOC-V using methods outlined in Hansell and Carlson (1998) and Carlson et al. (2004) (Hansell and Carlson 1998; Carlson et al. 2004).

Phytoplankton pigment data ranges from November 2005 – February 2012 (n = 306). The pigment samples were concentrated onto GF/F filters shipboard and immediately preserved in liquid nitrogen. The samples were shipped in liquid nitrogen to Horn Point Laboratory or NASA Goddard Space Flight Center where various pigments concentrations, including peridinin concentration, were determined via high performance liquid chromatography (HPLC) (Hooker et al. 2009; Barrón et al. 2014; see http://oceancolor.gsfc.nasa.gov/HPLC/).

The coefficient of absorption for colored dissolved organic matter (CDOM), $a_g(\lambda)$, was determined using surface water samples that were collected in glass amber bottles preconditioned for carbon analysis (e.g., Barrón et al. 2014). Samples were immediately stored in a shipboard refrigerator at 4°C. Samples were filtered through a 0.2 μm membrane filter in the laboratory via low-pressure vacuum filtration and analyzed on a Shimadzu 2401-PC spectrophotometer within 24 hours of collection. The data used for this paper ranged from July 2007 – December 2012.

Several large hump-like features in the ultraviolet spectral region were found in the CDOM absorption spectra from PnB (e.g., Barrón et al. 2014). An example of one of these hump-like spectra is shown in Figure 2a. The features are a departure from a typical CDOM spectrum, and were similar in shape to mycosporine-like amino acid (MAA) absorption signatures in CDOM spectra presented in other studies (Whitehead and Vernet 2000). The (presumably) MAA peaks in this study were quantified by modeling a 'baseline' CDOM spectrum by log-transforming the $a_g(\lambda)$ data (*see* Fig. 2a), then making a linear regression fit to the data points surrounding the MAA absorption region (300-310 nm and 390-400 nm). The procedure was similar to that of calculating the spectral slope using the log-linear method described in Nelson et al. (2007 and 2010), for the relationship:

$$a_g(\lambda) = a_g(\lambda_o)e^{-S(\lambda-\lambda_o)} \quad (1)$$

where $a_g(\lambda)$ is the CDOM coefficient at wavelength, λ, the reference wavelength λ_o and S is the spectral slope with units of nm^{-1}. S_{back} was used here to estimate what the CDOM spectra would appear to be if the MAA-like signal was not present. The modeled baseline spectra were then subtracted from the real $a_g(\lambda)$ data. The term 'MAA index' is defined

here as the summation of the residual between $a_g(\lambda)$ and the modeled baseline between λ = 310 – 390 nm (Barron et al. 2014).

The statistical characteristics of the Plumes and Blooms CDOM observations were compared with a global open ocean CDOM data set collected and analyzed by Nelson et al. (2012) and Nelson and Siegel (2013). CDOM collection and analysis methods are described in detail in Nelson et al. (2012).

The influence of terrestrial environments was measured using Ventura River discharge observations. Data were obtained from the United States Geographical Survey webbase for site USGS 1118500 for the entire range of the Plumes and Blooms data set. Seven-day cumulative discharge values were for the week prior to Plumes and Blooms sampling were used in the present statistical analysis.

Results

Oceanographic Variability in the SBC

The Santa Barbara Channel is embedded in the California Current and is influenced by coastal upwelling processes on basin and local scales (Harms and Winant 1998). Rainfall is sparse in the region, and river inputs are overall low and highly intermittent. Sea surface temperature (SST) in the SBC is warm in the summer, just above 20 ^{o}C, and is much cooler in the winter, as low as 10 ^{o}C (Figs. 3 and 4). The average sea surface salinity (SSS) is 33.6 PSU (Fig. 4). Vertical temperature and salinity seasonal trends at Station 4, the center of the channel, show characteristic spring upwelling events driven by regional winds, and stronger stratification as surface temperatures warm in the summer (Fig. 3). These upwelling events lead to cooler SST

and higher SSS values. Other significant inputs of subsurface waters are often the result of the cyclonic eddy that resides regularly in the center of the SBC (e.g., Harms and Winant, 1998). This eddy enhanced mixing caused isopycnal uplift, and is most important for subsurface transport in the fall months (Brzezinski and Washburn 2011). The El Nino/Southern Oscillation (ENSO) event of 1997/1998 was discernable in the temperature and salinity profiles, and the thermocline extended much deeper than usual, allowing warm surface water to penetrate past 75 m depth (Fig. 3). There appeared to be a cooling trend after the year 2000 that resulted in a shallower thermocline in the years that followed.

Surface temperature was nearly constant across the channel, with the exception of a few cruises where temperatures were cooler at stations 6 and 7, e.g. stations furthest from the mainland and closest to the Channel Islands (Fig. 4). Salinity was also close to constant across the channel with occasional lower salinities occurring at Stations 1 and 7, those closest to shore on either side of the channel (Fig. 4). Two low salinity events that reached across the SBC, March 1998 and January-February 2005, corresponded with high discharge events from the Ventura River and represents inputs from all streams and creeks that flow into the SBC (Warrick et al. 2004). Both of the high discharge events coincided with positive ENSO values, e.g. conditions for higher than average regional event-scale rainfall along the California Central Coast.

Nutrient concentrations were stratified most of the time with higher concentrations at depth due to microbial remineralization, and often depleted concentrations at the surface due to phytoplankton and microbial uptake. Wind-driven upwelling was responsible for the most significant nutrient inputs to the surface waters,

as seen in trends of nitrite + nitrate, referred to here after as just nitrate or NO_3, in Fig. 5. Eddy enhanced mixing was also responsible for entraining nutrients into the surface layer via isopycnal uplift. Brzezinski and Washburn (2011) found this mechanism to be most important for nutrient entrainment to the euphotic zone during the fall months, but was a notable transport mechanism anytime during the year when the water column was stratified and surface nutrient concentrations were low. As time went on, the apparent nutricline became shallower and higher concentrations of nitrate were observed at shallower depths throughout the year (Fig. 5). This corresponded with decreasing thermocline depth and increased isopycnal uplift. Surface nutrient gradients across the channel were considerably smaller, indicating that nutrient inputs to the surface waters were mostly due to coastal upwelling and eddy-enhanced isopycnal uplift of subsurface waters rather than river/stream inputs, e.g. physical properties as detailed in (Washburn et al. 2011).

Chlorophyll *a* concentrations in the SBC ranged from 0.16 μg/L to 28.7 μg/L, with an average of 2.72 μg/L. The chlorophyll max was usually shallow and most often observed at 10 m depth, but occasionally found as deep as 30 m (Fig. 5). The scale for chlorophyll *a* concentration in Figure 5 ranges 0 – 10 *μg/L*, and was chosen to highlight variability at low concentrations. Red shaded regions represent time and space points where chlorophyll *a* concentrations were $\geq$ 10 *μg/L*. Highest chlorophyll *a* concentrations were observed in the Spring in during upwelling, however elevated chlorophyll *a* was usually observed in response to surface mixing throughout the seasons.

Phytoplankton community composition analyses have been determined using phytoplankton accessory pigment analysis for subsets of Plumes and Blooms data by

Anderson et al. (2008) and Barron et al. (2014). As mentioned above, phytoplankton accessory pigment observations are available for only a portion of the PnB data set (after July 2005). According to Anderson et al. (2008) and Barrón et al. (2014), the phytoplankton community varied in correspondence to the physical and nutritional status of the SBC. A spring bloom is observed every year due coincident with the wind-driven upwelling of deep, nutrient-rich water to the euphotic zone. The Spring Bloom was correlated to the highest annual chlorophyll *a* concentrations, and the phytoplankton community was comprised of microplankton, mostly dominated by diatom groups as biogenic silica concentrations were highest this time of year (Barron et al. 2014). Dinoflagellate groups were often present during the spring bloom as well. Eddy enhanced mixing often resulted in dinoflagellate blooms most prevalent in the fall, and occasionally observed in the winter months (Brzezinski and Washburn 2011; Barron et al. 2014). However, recent studies have identified the associated blooms shifting to a more diatom-dominated community in recent years, most noteworthy the harmful diatom genus *Pseudo-nitzschia* (Sekula-Wood et al. 2011). During times of strong stratification, such as the summer months, the surface chlorophyll *a* values were low and the associated community was dominated by picophytoplankton and other high-light adapted species (Anderson et al. 2008; Barron et al. 2014).

CDOM in the SBC

Average surface CDOM absorption coefficients were relatively high throughout the spectra when compared to open ocean surface values, where surface values of $a_g(325)$ in the Eastern Pacific are around 0.15 m^{-1}, and around 0.05 m^{-1} in Pacific subtropical

gyres (Nelson et al. 2007; Swan et al. 2009). Plumes and Blooms CDOM was highly variable between wavelengths 300 – 390 nm (Fig 2b). The variability in this range was due to peak-like features in many of the SBC spectra with a peak centered between 325-335 nm, and often paired with a secondary peak centered around 360 nm. These features in the CDOM spectra were consistent with observations of mycosporine-like amino acids (MAAs) that were found in other studies to be correlated with the phytoplankton group dinoflagellates (Vernet and Whitehead 1996; Whitehead and Vernet 2000). Barrón et al. (2014) quantified this CDOM spectral feature as the MAA Index, defined as the sum of the difference between the measured CDOM spectra and a modeled CDOM spectra between $a_g(310)$ and $a_g(390)$ (Fig. 2b). The modeled spectra was calculated by a linear fit of the log transformed $a_g(\lambda)$ end-points surrounding the MAA affected region, 300-310 nm and 390-400 nm. MAA Index was then adjusted by a constant of 1.7 to center the mean value at 0, and values of MAA Index greater than 1 indicated significant MAA peaks present in the $a_g(\lambda)$ spectra. MAA Index correlated well to $a_g(325)$, with $r^2 = 0.49$ (Fig. 2c). There were 18 outliers from the linear regression fit shown in Figure 2c, in which increased $a_g(325)$ was observed without a corresponding increase in MAA index.

Surface $a_g(325)$ ranged from 0.1 – 1.1 m^{-1} with higher values sometimes found at Station 1 and/or Station 7, and the highest values observed across the channel from January - May 2006 (Fig. 6). This order-of-magnitude range in $a_g(325)$ spans the range of values found in the surface open ocean (Nelson and Siegel 2013) and those found in coastal regions with heavy terrestrial influence (Del Vecchio and Subramaniam 2004; Mannino et al. 2008; Carvalho et al. 2014). The highest values of $a_g(325)$ co-occurred with high values of MAA Index, e.g. MAA Index ≥ 2 in Fig. 6, indicating direct linkage

between phytoplankton and CDOM absorption at those times (Fig. 6). Most notable were the high $a_g(325)$ absorption and MAA Index values of 2006. Barrón et al. (2014) examined a subset of the Plumes and Blooms data (2005-2009) and found that dinoflagellate presence, as measured by the peridinin phytoplankton accessory pigment concentration, strongly correlated with MAA Index, $r^2 = 0.70$, and a large dinoflagellate bloom co-occurred with the increased $a_g(\lambda)$ values in 2006.

Relationships of CDOM absorption coefficient to oceanic properties were assessed using linear regressions with $a_g(\lambda)$ at different parts of the spectrum versus various surface properties (Table 1). Sea surface temperature (SST) was positively correlated to $a_g(250)$ and, more weakly, to $a_g(300)$. Salinity showed weak negative correlation with $a_g(250)$, very weak correlation to $a_g(300)$, and weak positive correlation at $a_g(400)$. Mixed layer depth (MLD) was negatively correlated with $a_g(\lambda)$ and stratification index as positively correlated with $a_g(\lambda)$, both most strongly at $a_g(300)$ with $r = -0.20$ and $r = 0.24$, respectively. Ventura River discharge showed very weak, but significant, positive relationships with $a_g(\lambda)$. Nitrate and phosphate concentrations were negatively correlated with $a_g(\lambda)$ at all wavelengths assessed, but most strongly at $a_g(250)$ followed by decreasing correlation coefficient as wavelength increased. Silicate concentrations were negatively correlated to $a_g(\lambda)$ at lower wavelengths. The significant negative correlations with the macronutrient concentrations measured and the positive correlations with SST indicate that freshly upwelled waters are not the source of elevated CDOM abundances. The relationship with the physical parameters, MLD and stratification index, showed that higher CDOM absorption coefficients were observed during stratified conditions, however, the relationships were weak throughout the spectra,

hence physical mixing processes were not likely the driving the factor for variability in the CDOM absorbance coefficient.

Dissolved organic carbon (DOC) concentration was well correlated with $a_g(\lambda)$, particularly at shorter wavelengths (Table 1). The correlation between $a_g(250)$ and DOC concentrations is among the highest seen in this analysis (Table 1). This high correspondence supports the recent analyses of Fichot and Benner (2011) where they related CDOM properties for wavelengths shorter than the solar spectrum to DOC concentrations.

Relationships between CDOM variability and phytoplankton-based sources of CDOM were also explored using the correlation analysis in Table 1. Chlorophyll *a* concentrations were positively correlated with CDOM, but only weakly (r = 0.17 – 0.30), suggesting that phytoplankton abundance is not driving CDOM variability. Peridinin, the indicator pigment for dinoflagellate populations, displayed strong positive correlation with $a_g(\lambda)$ at all wavelengths considered, the strongest being $a_g(350)$ with r = 0.84. Fucoxanthin, the indicator pigment for diatom presence, did not correlate as well with surface $a_g(\lambda)$, where the strongest relationship was observed at $a_g(400)$ with r = 0.26. Normalization by chlorophyll *a* only weakened the peridinin and fucoxanthin relationships, and resulted in lowered correlation coefficients across the spectrum. Lutein, an indicator pigment for high-light adapted phytoplankton, was negatively correlated with $a_g(250)$ and $a_g(300)$. Biogenic Silica (BSi), an indicator for diatom biomass, was weakly, positively correlated with $a_g(325)$ and $a_g(360)$, and had a slightly stronger positive relationship with $a_g(400)$. Lithogenic Silica (LSi), an indicator for land-derived

and re-suspended sediments, also showed weak, positive correlation with $a_g(300)$ and higher.

A surprising result from the calculations of MAA Index with the 15-year data set was that MAA peaks were discernable at very low absorption once the background CDOM was subtracted from the absorption spectra. MAA Index values greater than 1 were observed in approximately 16% of the data set, while MAA Index values greater than zero were observed in 63% of the data. MAA Index values between 0 and 1 indicate small MAA features that were mostly masked by background CDOM concentrations in the original spectra. MAA Index correlated very well with peridinin, r = 0.84, and more weakly to chlorophyll *a* concentration, hence normalizing peridinin concentration by chlorophyll *a* weakened the relationship (Table 1). A much weaker, but noteworthy, correlation of MAA Index to lithogenic silica, e.g. mineral particles, was also observed (Table 1). The LSi concentrations may have been related with sediment entrainment from the continental shelf during the eddy enhanced mixing events typically associated with elevated dinoflagellate populations (Brzezinski and Washburn 2011), thus higher MAA values. Weak positive correlation of MAA Index to DOC concentration was observed, however at r = 0.10, MAAs are not likely a large source of DOC for the SBC.

CDOM spectral shape was assessed using the exponential spectral slope parameter, *S*, as described in Equation 1. *S* can be calculated from a linear fit to the log-transformed $a_g(\lambda)$ data (Bricaud et al. 1981), or using a non-linear exponential model to the $a_g(\lambda)$ data (Twardowski et al. 2001). *S* is useful in determining the quality of CDOM in open ocean waters, where photobleaching of surface waters results in higher *S* values, such as observed in the subtropical gyres (Swan et al. 2012; Nelson and Siegel 2013). *S*

has also served as an end member indicator for freshwater-seawater mixing in coastal sites where lower *S* indicate freshwater sources of CDOM, and higher *S* indicate the oceanic end member (Stedmon et al. 2000; Del Vecchio and Blough 2004; Chen et al. 2007).

Values of the CDOM spectral slope were calculated for Plumes and Blooms using the end points for the MAA Index calculations and the linear fit of the log-transformed CDOM absorption coefficients from 300-310 nm and 390-400 nm (Fig. 2a). This modeled CDOM spectrum is referred to in this paper as the "background" CDOM spectra and the associated spectral slope will be referred to as S_{back}. Values of S_{back} for CDOM spectra without large MAA peaks, MAA Index ≤ 1, correlated very well with *S* values calculated from CDOM data with original data intact at wavelengths 300 – 400 nm, $r^2 = 0.98$. This procedure allowed for the calculation of spectral slope independent of the MAA peaks.

S_{back} was variable in the SBC, ranging from 0.01 – 0.029 nm^{-1} with an average value of 0.017 nm^{-1} and a standard deviation of 0.002 nm^{-1} (Fig. 6). Lower spectral slope values indicate flatter CDOM spectra, whereas higher values of *S* are indicative of CDOM spectral shapes closer to an exponential curve. Surface oceanic waters are often depleted in UV absorbing CDOM, and CDOM spectra in those regions typically have a higher spectral slope (Nelson and Siegel 2013). Therefore, higher spectral slope values could indicate prolonged exposure to the sun, e.g. photobleaching of the CDOM present at the surface. CDOM spectra from samples at depth in the ocean tend to have lower spectral slope values as well as waters rich in terrestrial DOM. The range of S_{back} observed in the SBC is indicative of periodic inputs of non-bleached, fresh CDOM

followed by periods of photobleaching during stratified conditions. Positive correlation of S_{back} to sea surface temperature and stratification index along with negative correlation to lutein was indicative of photobleaching during the warmer seasons of the year. Negative correlation of S_{back} to salinity, nutrients, BSi and positive correlation with peridinin indicate seasonal response to upwelling conditions with inputs of fresh CDOM to the surface.

EOF Analysis

Empirical orthogonal function (EOF) analysis is a tool used to elucidate patterns in multidimensional data sets by decomposing the variability of a large data set into independent, orthogonal functions, or modes (e.g., Emery and Thomson 1997). Here, an EOF analysis was applied to the mean-centered (in time) CDOM data set with wavelength range λ = 250-500 nm in effort to tease apart CDOM spectral features and their variation in time. The first four EOF modes explained nearly 100% of the observed variability in CDOM spectra. The shapes of the modal structures (Fig. 7), as well as the trends in amplitude function (AF) associated with the modes (Fig. 8) were used to diagnose and interpret relative meaning of each mode. Intensity of spectral mode structures or eigenvectors indicate the strength of the property in the covariance matrix, that is, the strength of the relationship of $a_g(\lambda)$ at adjacent wavelengths for that particular mode. Eigenvectors close to the zero line will not show a strong response and hence are not considered important for driving the variability for that mode.

Mode 1 accounts for 87% of the total variability in the Plumes and Blooms data set (Fig. 7). The spectral shape of Mode 1 decreased strongly with increasing wavelength

roughly similar to the average CDOM spectra (Fig. 2b). There were no negative values in the eigenvector associated with this mode, meaning that the spectral changes due this dominant mode of variability are coherent across the spectrum. Mode 1 amplitude function shows changes on interannual time scales where especially high Mode 1 contributions are seen in 2001-2002, 2005-2007 and 2011 (Fig. 8). Strongly positive AF values indicate times when the CDOM spectral shape most strongly resembled this mode.

Mode 2 accounted for 9% of the variability of the data set, and resulted in positive and negative values in the eigenvector, thus indicating an inverse dynamics between parts of the CDOM spectrum (Fig. 7). Spectral points of interest are found near 325 and 350 nm at which there were broad negative peaks in the eigenvector. Eigenvector values were positive for wavelengths less than 300 nm. Thus the second spectral mode illustrates a dynamic where increases in CDOM above 300 nm were negatively related with values near the peak at 330 nm and contributions for wavelengths greater than 400 nm were insignificant, e.g. eigenvector values close to zero (Fig. 7). The amplitude function for Mode 2 showed seasonal trends with positive values of AF observed in summer, typically during the month of August, and negative values were observed mostly in early spring, March – May, and late fall, around October (Fig. 8). The highest AF values were observed in 2006, coincident with the highest concentrations of $a_g(325)$ and MAA Index shown in Fig. 6.

Mode 3 accounted for 2% of CDOM variability and shared some of the same features as Mode 2 in that eigenvectors peaked at the MAA wavelengths (Fig. 7). However, Mode 3 was unique for the rest of the spectrum where eigenvectors were positive at wavelengths above $\lambda = 400$ nm and trended upward just after the MAA peak

to reach positive values, simply indicating that when MAA peaks are present the rest of the spectra is relatively low, e.g. higher S_{back}. Mode 3 amplitude function showed interannual variability where extreme values of AF (e.g. AF > 1 standard deviation from the mean) were mostly positive from 1997-2003 with the exception of a few negative values observed at stations 1 and 2. The positive AF values observed after 2003 occurred mostly at stations 6 and 7. The most extreme negative values of AF for Mode 3 occurred in early spring 2006 and corresponded to the highest frequency of MAA Index in the PnB time series (Fig. 6). Strong negative AF values were most frequently observed at station 1 from 2007 – 2012.

Mode 4, accounting for 2% variability of the data set as well where the eigenvector was mostly positive with a peak in the negative direction around λ = 310 nm (Fig. 7). Positive amplitude function indicated conditions where the CDOM spectra was depleted in the region around λ = 310 nm, and negative amplitude function were indicative of conditions of higher absorption in this area of the spectrum. Mode 4 amplitude functions displayed extreme values in both positive and negative direction Negative AF values were observed across all stations, but most often at station 7 particularly in 1997-1998, and fall of 2001 (Fig. 8). AF was mostly positive from 1998 – 2002 throughout the rest of the SBC. Seasonal trends were observed in extreme AF values where positive AF were more likely observed in the winter, however, the seasonal trends for Mode 4 were not as well defined at those in Mode 2 AF. More extreme values of Mode 4 AF were observed prior to 2006, and remain close to zero thereafter, indicating a loss of importance of this mode to $a_g(\lambda)$ properties in the SBC.

Linear regressions were performed using the amplitude functions of each mode against a suite of various seawater properties showed that each of the EOF modes were unique to particular oceanic conditions (Table 2). Mode 1 showed most pronounced positive correlation to SST, Peridinin, DOC, MAA Index, Stratification Index, and negative correlation to all nutrients, lutein and MLD (Table 2). The regression relationships of Mode 1 to seawater properties were similar to the relationships with $a_g(\lambda)$, thus indicating that changes in Mode 1 AF represented increases/decreases in CDOM absorption coefficient. Strong positive correlation with peridinin and weak correlation with chlorophyll *a* concentrations suggest that CDOM dynamics were strongly coupled with phytoplankton community structure, but surprisingly, phytoplankton biomass was not as important to changes in the CDOM absorption signal. Increased DOC observed in concert with positive changes in Mode 1 suggested that CDOM dynamics associated with this mode were representative of changes in the bulk DOC pool. The weak, but significant correlation with LSi suggests that terrestrial inputs or re-suspension of sediments might have had correspondence with Mode 1 as well. The weak significant correlation with salinity and discharge suggests that a terrestrial linkage was present, but their weak significance indicates that these factors are not likely the driver for CDOM variability for this mode.

The regression coefficients for Mode 2 AF vs. seawater properties displayed strong associations with seasonal dynamics when this mode was present (Table 2). Negative correlation with peridinin concentration, MAA Index, fucoxanthin, chlorophyll *a* concentration and all nutrients, and positive correlation with SST and stratification index show that Mode 2 is indicative of upwelling conditions in the SBC. These results

were reflective the seasonal trends in the AF data (Fig. 8), and the mixed microplankton/high chlorophyll phytoplankton community identified by Barron et al. (2014). DOC was positively correlated with Mode 2 AF, and consistent with the correlation of DOC with $a_g(250)$ in Table 1. Here, the positive correlation indicated that $a_g(250)$ was relatively lower when MAA peaks were present, as were corresponding DOC concentrations.

Mode 3 eigenvectors also displayed negative values in the MAA peak regions (Fig. 7); thus the observed negative correlation coefficients for regressions of Mode 3 AF vs. peridinin, MAA Index and *Sback* indicated positive relationships during times of MAA presence. DOC was negatively correlated to Mode 3 AF, and, again, indicative of the relationship between DOC concentration and $a_g(250)$. Increased DOC concentrations during times of negative AF signified new CDOM to the surface waters. Other notable relationships to Mode 3 were the lack of correlation to chlorophyll *a*, and the strong negative correlation to the absolute peridinin concentration as well as the peridinin concentration normalized by chlorophyll *a* (Peridinin/Chl *a* in Table 2). This indicates the community dominance of dinoflagellate populaitons co-occuring when this mode is positive. Fucoxanthin/Chl *a* along with BSi were positively correlated with this mode, a behavior mimicking that found in Barron et al. (2014), where a phytoplankton community alternating in diatom and dinoflagellate dominance significantly effected the variability of optical properties in Plumes and Blooms data from 2005-2009.

The most notable relationship in Mode 4 is that of Mode 4 AF and *Sback* (Table 2). With r = -0.83, the relationship was not only the strongest for Mode 4, but also the strongest relationship of all seawater properties with any EOF mode. Positive Mode 4 AF

indicated low *Sback*, e.g. increased absorbance in the UV region, and negative AF indicated high *Sback*, e.g. decreased absorbance in the UV region or bleached conditions (Fig. 8). Secondary relationships with Mode 4 include the weaker, negative correlation to MAA Index, and weak positive correlation to peridinin, fucoxanthin and chlorophyll *a*. Mode 4 is the only mode in which the MAA Index relationship and peridinin relationship do not have the same sign (Table 2). MAA index varied independently of microplankton populations for Mode 4, and appeared to be associated with $a_g(310)$ for this mode, e.g. the eigenvector peak at $\lambda = 310$ nm in Figure 7. There are many phytoplankton species other than dinoflagellate groups that produce MAAs. MAAs associated with higher S_{back} values may be attributed to species that dominate planktonic community composition during highly stratified periods.

In summary, each derived EOF mode of variability had a unique shape and corresponded to various physical and biogeochemical conditions. Mode 1 was comprised of all positive eigenvectors and resembled the average CDOM spectra. Mode 2 corresponded to upwelling conditions and AF varied on seasonal time scales. Mode 3 was strongly correlated MAA Index and dinoflagellate presence, and captured the high correspondence of DOC concentration to $a_g(250)$. Mode 4 was strongly correlated with *Sback*, thus trends in Mode 4 AF were indicative of CDOM spectral slope dynamics independent of MAA Index values and phytoplankton community structure.

Discussion

Autochthonous vs. Allochthonous Sources of CDOM in the Santa Barbara Channel

The 15-year Plumes and Blooms time series illustrated coastal CDOM dynamics throughout an array of physical and biological conditions. CDOM spectral properties

were highly variable on seasonal and interannual time scales. Spectral changes in surface CDOM absorption can be attributed to both autochthonous and allochthonous sources. The above results showed that MAA Index is the component most strongly correlated with CDOM absorption in the Santa Barbara Channel. Phytoplankton abundance played a secondary role to community structure as peridinin concentrations were by far the property most directly linked to $a_g(\lambda)$, thus strongly indicating the importance of dinoflagellate community dominance to CDOM dynamics in the SBC. High values of MAA Index co-occurred with high $a_g(325)$ indicating a direct phytoplankton source. EOF Mode 3 was well correlated to MAA Index, a good indicator for dinoflagellate presence, and the physical conditions typically associated with dinoflagellate blooms (Table 2). Mode 3 was also well correlated to DOC concentrations, indicating autochthonous production of CDOM in the surface ocean.

The SBC is particularly unique in that the MAA peaks in the dissolved phase are well defined for approximately 16% of the Plumes and Blooms data (Fig. 6). Whitehead and Vernet (2000) also observed well-defined MAA peaks in the dissolved pool off La Jolla Bay, Southern California during a red tide bloom of *Lingulodinim polyedrum* that persisted for two weeks. To our knowledge this is the only other study that has documented such large MAA absorption in the dissolved phase in situ, indicating that the intensity observed at the PnB study site must be due to fairly recent dinoflagellate exudation, e.g. $\geq$ 2 weeks.

The PnB data set illustrates weak evidence for allochthonous inputs to the surface CDOM pool. For example, weak, positive relationships are observed between LSi with $a_g(\lambda)$ along with a weak corresponding negative relationship with salinity at lower $a_g(\lambda)$

wavelengths (Table 1). However based solely on this evidence, it is not clear whether the CDOM is terrestrially linked, e.g. high $a_g(\lambda)$/low salinity input, or if this was a deep water signal, e.g. low $a_g(\lambda)$/high salinity input. Based on other relationships, e.g. those of MLD, temperature and nutrients, the salinity and LSi correlation correlations coefficients indicate the latter scenario, the deep upwelling source. Interestingly, the spectral slope parameter, S_{back} behaved as one would expect in a system with deep upwelling. That is, positive correlation of S_{back} to sea surface temperature and stratification index along with negative correlation to lutein concentrations was indicative of photobleaching. Negative correlation of S_{back} to salinity, nutrients, BSi and positive correlation with fucoxanthin concentration indicate seasonal response to upwelling conditions with inputs of deep CDOM to the surface.

To test for a terrestrial vs. a deep-water signal, e.g. 300 m, CDOM absorption coefficients collected at depth from May 2011 through June 2013 at Station 4 are compared with surface samples. Deep ocean water in the SBC was characterized by spectrally decreased CDOM absorption, and by decreased S_{back} (Figure 9). Mode 4 EOF captured the deep mixing/S_{back} relationship in the correlations with microplankton bloom indicators, e.g. positive correlation with fucoxanthin and peridinin. To test specifically for a terrestrial signal, a Student's two-tailed t-test was performed using the mean $a_g(\lambda)$ values corresponding salinity $\leq$ 32 PSU against the mean $a_g(\lambda)$ for the entire surface data set. In the 15-year study there were only 14 occurrences of low salinity points (Fig. 5). Low salinity observations points occurred across the channel in Spring 1998 and Winter 2005 following a high rainfall events, and other times were isolated to the sites nearest the coastlines of either the mainland or Santa Rosa Island. The t-test results indicated that

mean $a_g(\lambda)$ was significantly higher during low salinity events for wavelengths less than 280 nm. Freshwater inputs to the SBC are very sparse, and do not significantly alter CDOM absorption above the baseline conditions for optically significant wavelengths.

The main source of CDOM in the SBC was autochthonous and was directly linked to dinoflagellates. The CDOM associated with deep-water upwelling was largely allochthonous and associated with mixing of the deep-water end-member rather than production of new CDOM from bloom related species. Terrestrial CDOM was also present in the surface waters of the SBC, however the actual input of freshwater was very low - as little as 14 low-salinity events in 15 years, e.g. Salinity < 32 PSU. Thus, CDOM dynamics in the surface SBC are largely oceanic and driven by *in situ* biological activity and advection processes.

Global Perspective

The global CDOM data set (Nelson and Siegel, 2013) was analyzed using similar statistical techniques to gain perspective of how spectral properties of Santa Barbara Channel CDOM compared with the global surface ocean. The EOF analysis performed for the Global CDOM data set resulted 3 modes that look very similar to the first PnB modes (Fig. 10). Mode 1 accounted for 96.6% of the Global data and resembled the shape of the average CDOM spectra (Nelson and Siegel 2013). Mode 2, accounting for 3% of global variability, displayed positive eigenvectors at $\lambda < 300$ nm, and negative eigenvectors at $\lambda > \sim 300$ nm. Lastly, Mode 3, accounting for 0.09% of variability, also resulted with negative eigenvectors for the MAA region and positive eigenvectors

elsewhere in the spectra, indicating lower background CDOM absorption when increased absorption in the MAA regions was observed (Fig 10).

The MAA presence in the Global EOF Mode 3 was somewhat surprising since there were no obviously visible MAA peaks in the CDOM spectra (data not shown), although, Morrison and Nelson (2004) suggested that MAAs may be an important source of highly colored DOM in the off-shore regions of the ocean, and due to the nature of CDOM absorption (Del Vecchio and Blough 2004) distinct peaks are not often observed. Mode 2 was most strongly correlated with MAA Index with r = 0.61, and less so with Modes 1 and 3 with r = -0.39 and r = 0.32, respectively. Interestingly, MAA Index did not correlate well with $a_g(325)$ on a whole, r = -0.39, but showed strong correlation with the data collected from the Ross Sea, r = -0.68, and with the rest of the Global data set with the exclusion of data from the Ross Sea, r = -0.69 (Fig 11). The trends in Mode 2 AF and $a_g(325)$ were the opposite of the relationships observed in the SBC data set, in that MAA Index was associated with low CDOM absorption coefficient values. This was indicative of increased MAA production in the areas of the ocean with high-light adapted phytoplankton species, and photobleached background CDOM levels, and is in agreement with the hypothesis of Morrison and Nelson (2004). The very high MAA Index values observed in the Ross Sea, and separate correlation curve in Fig. 11 are likely due to the difference in phytoplankton community composition in the Southern Ocean where *Phaeocystis antarctica* have been observed to produce high levels of MAAs (Moisan and Mitchell 2001), whereas in the ocean gyres the community is dominated mostly by picoplankton species.

The Santa Barbara Channel EOF modes were surprisingly similar to the Global modes. Both first modes resembled the average CDOM spectra and represented full spectrum changes CDOM absorption. Also, both EOF analyses captured MAA signatures in the CDOM spectra and presented the prominence these MAA substances on a global scale. Dissolved MAA presence in the SBC was remarkably high due to the associated microplankton group, dinoflagellates, which is not so common in the open ocean (Alvain et al. 2005). However, the global data set showed that dissolved MAAs were present in other areas of the ocean in much more diluted intensity.

Conclusion

The SBC gives a unique opportunity to study the optical properties of a very near-shore oceanic site. Stations 1 and 7 are shallow and located just on the edge of the continental shelf, whereas the rest of the stations are off the shelf. Despite the proximity to the content/islands the CDOM dynamics are largely autochthonous. Furthermore, the autochthonous dynamics present in the SBC show that the "Dirty Bathtub Ring" of allochthonous CDOM may not extend as far into the World's oceans a previously thought. The EOF analysis of SBC $a_g(\lambda)$ and Global $a_g(\lambda)$ show that CDOM properties in the SBC strongly reflect those of the global ocean. This provides the unique opportunity to study autochthonous CDOM cycling properties relevant in the World oceans at a very near shore site. This would allow for less expensive field ventures along with the ability to sample more frequently and on shorter timescales.

References

Alvain, S., C. Moulin, Y. Dandonneau, and F. M. Bréon. 2005. Remote sensing of phytoplankton groups in case 1 waters from global SeaWiFS imagery. Deep Sea Res. Part I Oceanogr. Res. Pap. **52**: 1989–2004.

Anderson, C. R., D. A. Siegel, M. A. Brzezinski, and N. Guillocheau. 2008. Controls on temporal patterns in phytoplankton community structure in the Santa Barbara Channel , California. **113**: 1–16.

Barron, R. K., D. a. Siegel, and N. Guillocheau. 2014. Evaluating the importance of phytoplankton community structure to the optical properties of the Santa Barbara Channel, California. Limnol. Oceanogr. **59**: 927–946.

Biology, M. 1996. Release of ultraviolet-absorbing compounds by the red-tide dinoflagellate. 35–44.

Blough, N. V., O. C. Zafiriou, and J. Bonilla. 1993. Optical absorption spectra of waters from the Orinoco River outflow: Terrestrial input of colored organic matter to the Caribbean. J. Geophys. Res. **98**: 2271.

Bricaud, A., A. Morel, and L. Prieur. 1981. Absorption by dissolved organic-matter of the sea (yellow substance) in the UV and visible domains. Limnology Oceanography **26**: 43–53.

Brzezinski, M. a., and L. Washburn. 2011. Phytoplankton primary productivity in the Santa Barbara Channel: Effects of wind-driven upwelling and mesoscale eddies. J. Geophys. Res. **116**, doi:10.1029/2011JC007397

Carlson, C. A., S. J. Giovannoni, D. A. Hansell, S. J. Goldberg, R. Parsons, and K. Vergin. 2004. Interactions among dissolved organic carbon, microbial processes,

and community structure in the mesopelagic zone of the northwestern Sargasso Sea. Limnol. Oceanogr. **49**: 1073–1083.

Carvalho, M., A. M. Ciotti, S. M. Flores Gianesella, F. M. Prado Saldanha Correa, and R. R. Costa Perinotto. 2014. Bio-optical properties of the inner continental shelf off Santos estuarine system, Southeastern Brazil, and their implications for ocean color algorithm performance. Brazilian Journal of Oceanography **62**: 71–87.

Chen, R. F., and G. B. Gardner. 2004. High-resolution measurements of chromophoric dissolved organic matter in the Mississippi and Atchafalaya River plume regions. Mar. Chem. **89**: 103–125.

Chen, Z., C. Hu, R. N. Comny, F. Muller-Karger, and P. Swarzenski. 2007. Colored dissolved organic matter in Tampa Bay, Florida. Mar. Chem. **104**: 98–109.

Coble, P. G. 2007. Marine optical biogeochemistry: the chemistry of ocean color. Chem. Rev. **107**: 402–18.

Colleagues, D., O. Biology, P. Bontempi, N. Hq, R. Sensing, T. Team, S. Hooker, N. Calibration, V. Office, L. Van Heukelem, J. Perl, J. Dolan, L. C. Resources, R. Farnbach, R. F. Consulting, C. Trees, G. Fargion, C. Thomas, A. Neeley, and M. Russ. 2009. NASA Ocean Biology and Biogeochemistry GSFC Calibration and Validation Office 1450 S . Rolling Road , Halethorpe , Maryland 21227. 1–62.

Emery, W. J., and R. E. Thomson. 1997. Data analysis methods in physical oceanography., Pergamon.

Fichot, C. G., and R. Benner. 2011. A novel method to estimate DOC concentrations from CDOM absorption coefficients in coastal waters. Geophys. Res. Lett. **38**.

Hansell, D. A., and C. A. Carlson. 1998. Deep-ocean gradients in the concentration of dissolved organic carbon. Nature **395**: 263–266.

Harms, S., and C. D. Winant. 1998. Characteristic patterns of the circulationin the Santa Barbara Channel. J. Geophys. Res. **103**: 3041–3065.

Kitidis, V., A. P. Stubbins, G. Uher, R. C. U. Goddard, C. S. Law, and E. M. S. Woodward. 2006. Variability of chromophoric organic matter in surface waters of the Atlantic Ocean. Deep. Res. PART II-TOPICAL Stud. Oceanogr. **53**: 1666–1684.

Krause, J. W., M. A. Brzezinski, D. A. Siegel, and R. C. Thunell. 2013. Biogenic silica standing stock and export in the Santa Barbara Channel ecosystem. J. Geophys. Res. Ocean. **118**: 736–749.

Maie, N., J. N. Boyer, C. Yang, and R. Jaffe. 2006. Spatial, geomorphological, and seasonal variability of CDOM in estuaries of the Florida Coastal Everglades. Hydrobiologia **569**: 135–150.

Mannino, A., M. E. Russ, and S. B. Hooker. 2008. Algorithm development and validation for satellite-derived distributions of DOC and CDOM in the U.S. Middle Atlantic Bight. J. Geophys. Res. Ocean. **113**.

Moisan, T. a., and B. G. Mitchell. 2001. UV absorption by mycosporine-like amino acids in Phaeocystis antarctica Karsten induced by photosynthetically available radiation. Mar. Biol. **138**: 217–227.

Morrison, J. R., N. B. Nelson. 2004. Seasonal Cycle of Phytoplankton UV Absorption at the Bermuda Atlantic Time-Series Study (BATS) Site. **49**: 215–224.

Nelson, N. B., C. a Carlson, and D. K. Steinberg. 2004. Production of chromophoric dissolved organic matter by Sargasso Sea microbes. Mar. Chem. **89**: 273–287.

Nelson, N. B., and D. a Siegel. 2013. The global distribution and dynamics of chromophoric dissolved organic matter. Ann. Rev. Mar. Sci. **5**: 447–76.

Nelson, N. B., D. A. Siegel, C. A. Carlson, and C. M. Swan. 2010. Tracing global biogeochemical cycles and meridional overturning circulation using chromophoric dissolved organic matter. Geophys. Res. Lett. **37**, doi:10.1029/2009GL042325

Nelson, N. B., D. a. Siegel, C. a. Carlson, C. Swan, W. M. Smethie, and S. Khatiwala. 2007. Hydrography of chromophoric dissolved organic matter in the North Atlantic. Deep Sea Res. Part I Oceanogr. Res. Pap. **54**: 710–731.

Pavlov, A. K., A. Silyakova, M. A. Granskog, R. G. J. Bellerby, A. Engel, K. G. Schulz, and C. P. D. Brussaard. 2014. Marine CDOM accumulation during a coastal Arctic mesocosm experiment: No response to elevated pCO(2) levels. J. Geophys. Res. **119**: 1216–1230.

Saba, G. K., D. K. Steinberg, and D. A. Bronk. 2009. Effects of diet on release of dissolved organic and inorganic nutrients by the copepod Acartia tonsa. Mar. Ecol. Prog. Ser. **386**: 147–161.

Sekula-Wood, E., C. Benitez-Nelson, S. Morton, C. Anderson, C. Burrell, and R. Thunell. 2011. Pseudo-nitzschia and domoic acid fluxes in Santa Barbara Basin (CA) from 1993 to 2008. Harmful Algae **10**: 567–575.

Shipe, R. F., and M. A. Brzezinski. 2001. A time series study of silica production and flux in an eastern boundary region: Santa Barbara Basin, California. Global Biogeochem. Cycles **15**: 517–531.

Siegel, D. a. 2002. Global distribution and dynamics of colored dissolved and detrital organic materials. J. Geophys. Res. **107**: 1–14.

Stedmon, C. A., S. Markager, and H. Kaas. 2000. Optical properties and signatures of chromophoric dissolved organic matter (CDOM) in Danish coastal waters. Estuar. Coast. SHELF Sci. **51**: 267–278.

Steinberg, D., N. Nelson, C. Carlson, and a Prusak. 2004. Production of chromophoric dissolved organic matter (CDOM) in the open ocean by zooplankton and the colonial cyanobacterium Trichodesmium spp. Mar. Ecol. Prog. Ser. **267**: 45–56.

Swan, C. M., N. B. Nelson, D. A. Siegel, and T. S. Kostadinov. 2012. The effect of surface irradiance on the absorption spectrum of chromophoric dissolved organic matter in the global ocean. Deep. Res. PART I-OCEANOGRAPHIC Res. Pap. **63**: 52–64.

Swan, C. M., D. a. Siegel, N. B. Nelson, C. a. Carlson, and E. Nasir. 2009. Biogeochemical and hydrographic controls on chromophoric dissolved organic matter distribution in the Pacific Ocean. Deep Sea Res. Part I Oceanogr. Res. Pap. **56**: 2175–2192.

Twardowski, M. S., E. Boss, J. B. Macdonald, W. S. Pegau, A. H. Barnard, and J. R. V. Zaneveld. 2001. A model for estimating bulk refractive index from the optical backscattering ratio and the implications for understanding particle composition in case I and case II waters. J. Geophys. Res. **106**: 14129.

Urban-Rich, J., J. T. McCarty, D. Fernández, and J. L. Acuña. 2006. Larvaceans and copepods excrete fluorescent dissolved organic matter (FDOM). J. Exp. Mar. Bio. Ecol. **332**: 96–105.

Del Vecchio, R., and N. V Blough. 2004. On the origin of the optical properties of humic substances. Environ. Sci. Technol. **38**: 3885–91.

Del Vecchio, R., and A. Subramaniam. 2004. Influence of the Amazon River on the surface optical properties of the western tropical North Atlantic Ocean. J. Geophys. Res. **109**, doi:10.1029/2004jc002503

Warrick*, J. a., L. a. K. Mertes, D. a. Siegel, and C. Mackenzie. 2004. Estimating suspended sediment concentrations in turbid coastal waters of the Santa Barbara Channel with SeaWiFS. Int. J. Remote Sens. **25**: 1995–2002.

Washburn, L., M. R. Fewings, C. Melton, and C. Gotschalk. 2011. The propagating response of coastal circulation due to wind relaxations along the central California coast. J. Geophys. Res. **116**: 1–16.

Whitehead, K., and M. Vernet. 2000. Influence of Mycosporine-Like Amino Acids (MAAs) on UV Absorption by Particulate and Dissolved Organic Matter in La Jolla Bay. **45**: 1788–1796.

Table 1. Correlation coefficent (r) for the linear regressions of a_g with various seawater properties - areas in grey are not statistically significant (*p-value* > 0.05).

	ag(250)	ag(300)	ag(325)	ag(350)	ag(400)	MAA Index	S_{back}	n
SST	0.44	0.18	0.04	0.00	-0.05	-0.06	0.33	994
Salinity	-0.15	-0.06	-0.02	-0.03	0.09	-0.05	-0.18	975
NO3	-0.47	-0.24	-0.17	-0.15	-0.10	-0.05	-0.12	973
PO4	-0.48	-0.26	-0.19	-0.15	-0.09	-0.06	-0.16	973
SiO2	-0.36	-0.12	-0.05	-0.03	-0.05	0.06	-0.07	973
Chl *a*	0.04	0.17	0.27	0.30	0.26	0.23	-0.26	1042
DOC	0.55	0.36	0.21	0.19	0.26	0.10	0.10	283
Peridinin	0.33	0.60	0.75	0.83	0.40	0.84	0.10	371
Peridinin/Chl *a*	0.26	0.38	0.48	0.54	0.11	0.61	0.32	367
Fucoxanthin	-0.07	0.07	0.13	0.11	0.26	0.05	-0.38	371
Fucoxnathin/Chl *a*	-0.06	-0.02	-0.03	-0.06	0.20	-0.16	-0.39	367
Lutein	-0.21	-0.16	-0.13	-0.11	-0.07	-0.09	-0.13	307
BSi	-0.03	0.09	0.12	0.13	0.19	0.00	-0.18	544
LSi	0.10	0.12	0.17	0.22	0.14	0.18	-0.05	544
Discharge	0.07	0.10	0.10	0.09	0.08	0.04	-0.04	1074
MLD	-0.06	-0.20	-0.13	-0.12	-0.10	-0.03	-0.04	888
Stratification Index	0.00	0.24	0.10	0.08	0.05	0.00	0.18	906

Table 2. Correlation coefficent (r) for the linear regressions of AF with various seawater properties - areas in grey are not statistically significant (*p-value* > 0.05).

	Mode 1	Mode 2	Mode 3	Mode 4	n
SST	0.25	0.50	-0.16	-0.14	994
Salinity	-0.10	-0.20	0.15	0.08	975
NO3	-0.33	-0.37	0.20	0.02	973
PO4	-0.34	-0.37	0.19	0.07	973
SiO2	-0.19	-0.36	0.13	0.00	973
Chl *a*	0.16	-0.30	-0.03	0.12	1042
DOC	0.35	0.37	-0.18	0.05	283
Peridinin	0.59	-0.60	-0.68	0.25	371
Peridinin/Chl *a*	0.39	-0.32	-0.59	0.02	367
Fucoxanthin	0.03	-0.24	0.09	0.17	371
Fucoxanthin/Chl *a*	-0.05	-0.04	0.25	0.10	367
Lutein	-0.17	-0.04	0.12	0.10	307
BSi	0.07	-0.19	0.23	0.04	544
LSi	0.14	-0.11	-0.06	0.07	544
Discharge	0.09	-0.04	0.02	-0.02	1076
MLD	-0.21	-0.16	0.09	0.05	888
Stratification Index	0.24	0.32	-0.15	-0.10	906
MAA Index	0.43	-0.60	-0.63	-0.23	1071
S_{back}	-0.10	0.14	-0.30	-0.83	1067

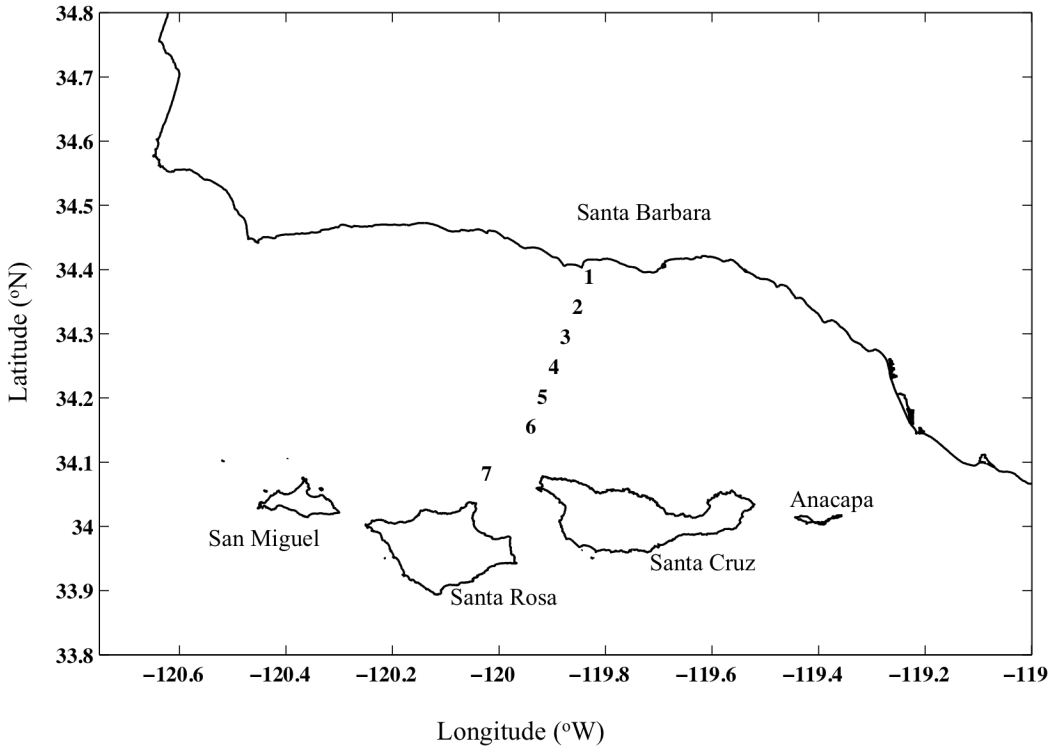

Figure 1. Map of Santa Barbara Channel. Numbers 1-7 indicate Plumes and Blooms station locations.

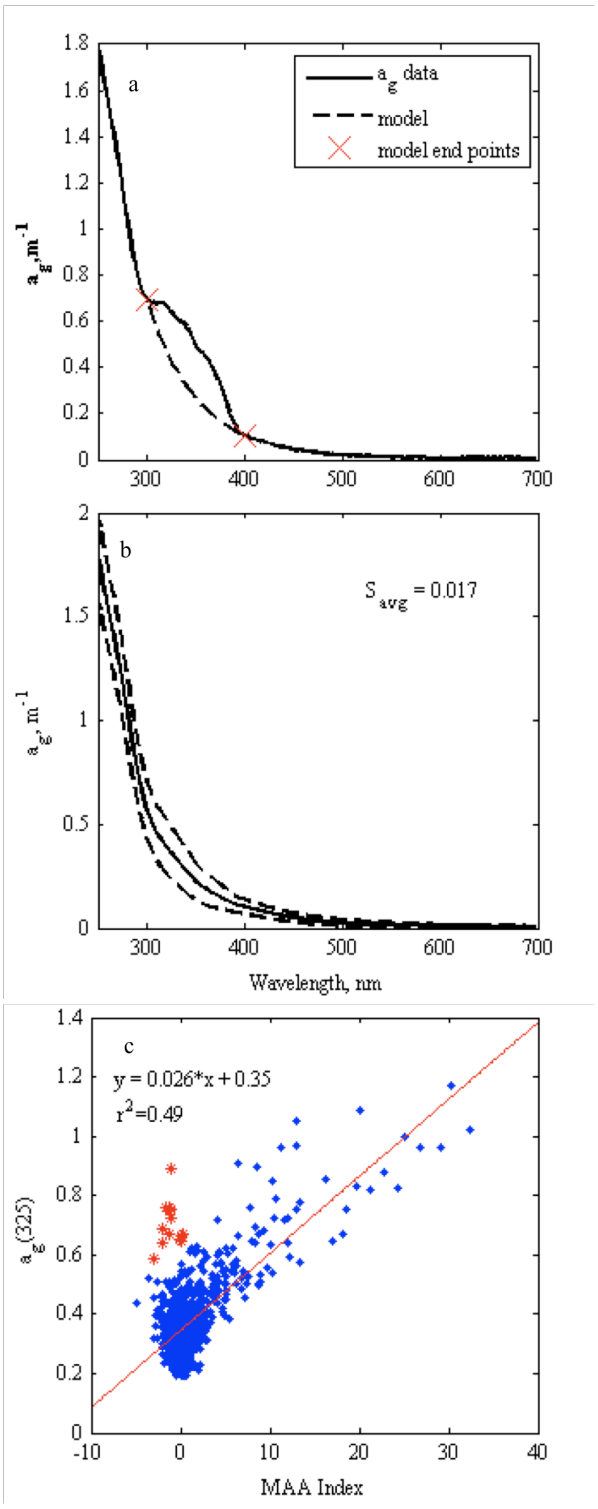

Figure 2. (a) Example $a_g(\lambda)$ spectra with MAA peaks. Dotted lines indicate modeled background $a_g(\lambda)$. (b) Average $a_g(\lambda)$ spectra. Dotted lines indicate 95% confidence intervals. (c) $a_g(325)$ vs. MAA Index. Red stars indicate outliers, where values of $a_g(325)$ > 0.5 nm^{-1} do not correlated with MAA Index.

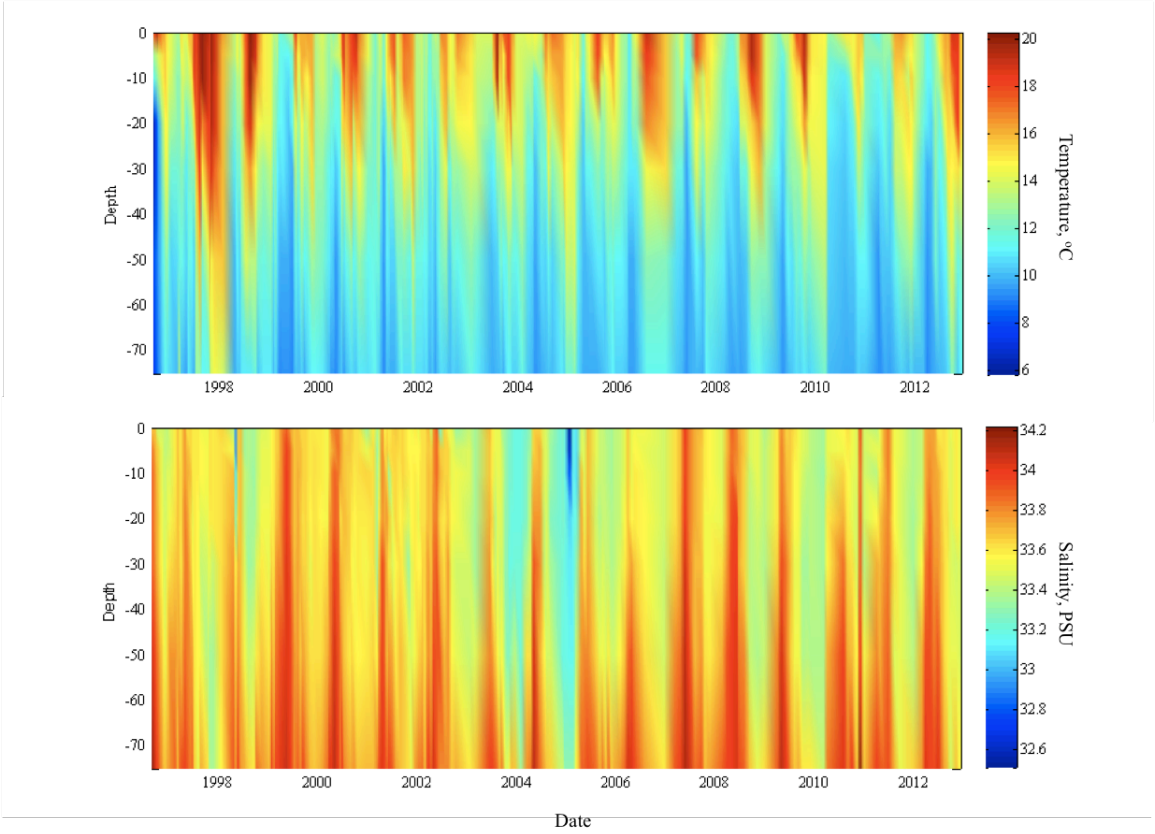

Figure 3. Plumes and Blooms Station 4 Temperature, ^{o}C and Salinity, PSU.

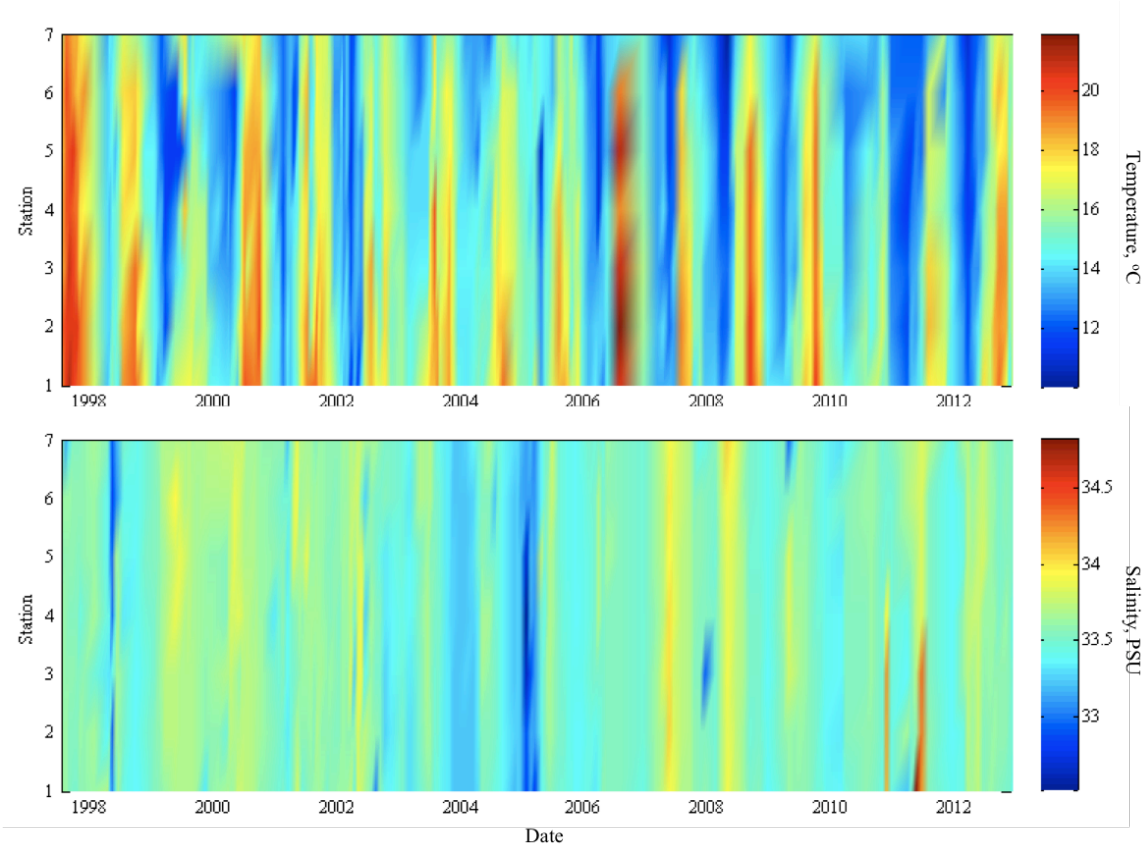

Figure 4. Plumes and Blooms surface Temperature, ^{o}C, and Salinity, PSU.

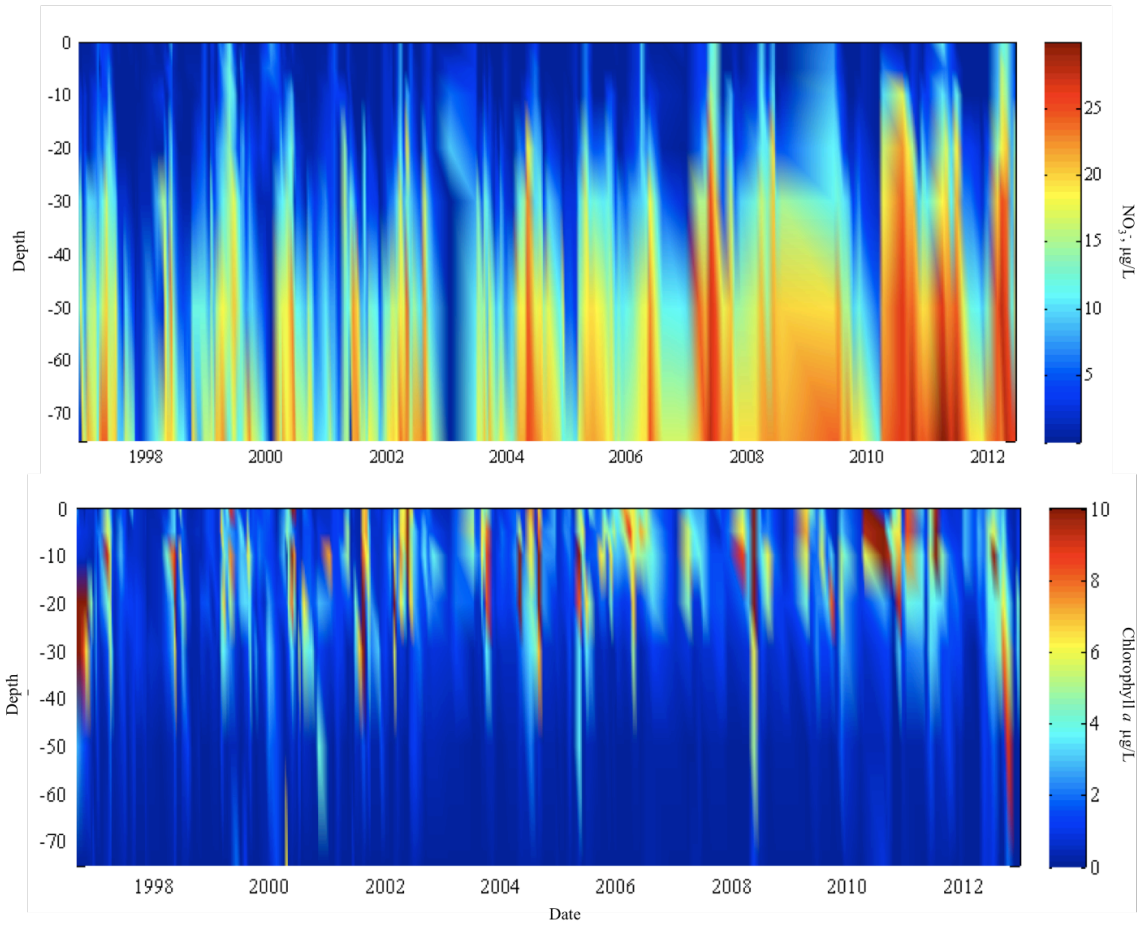

Figure 5. Plumes and Blooms Station 4 NO_3^-, μg/L and Chlorophyll *a*, μg/L.

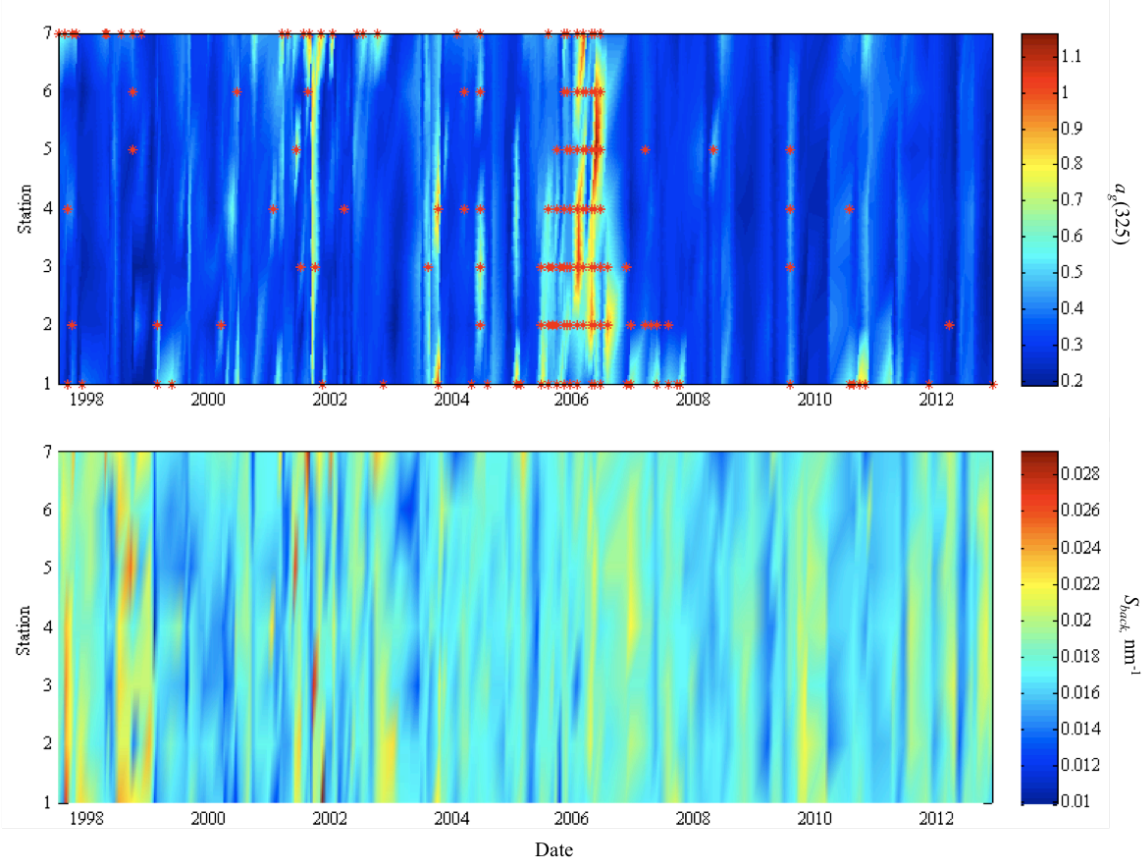

Figure 6. Top Panel: Plumes and Blooms surface $a_g(325)$. Red stars indicate time and location of samples where the surface MAA Index ≥ 2. Bottom Panel: Plumes and Blooms S_{back}, nm^{-1}.

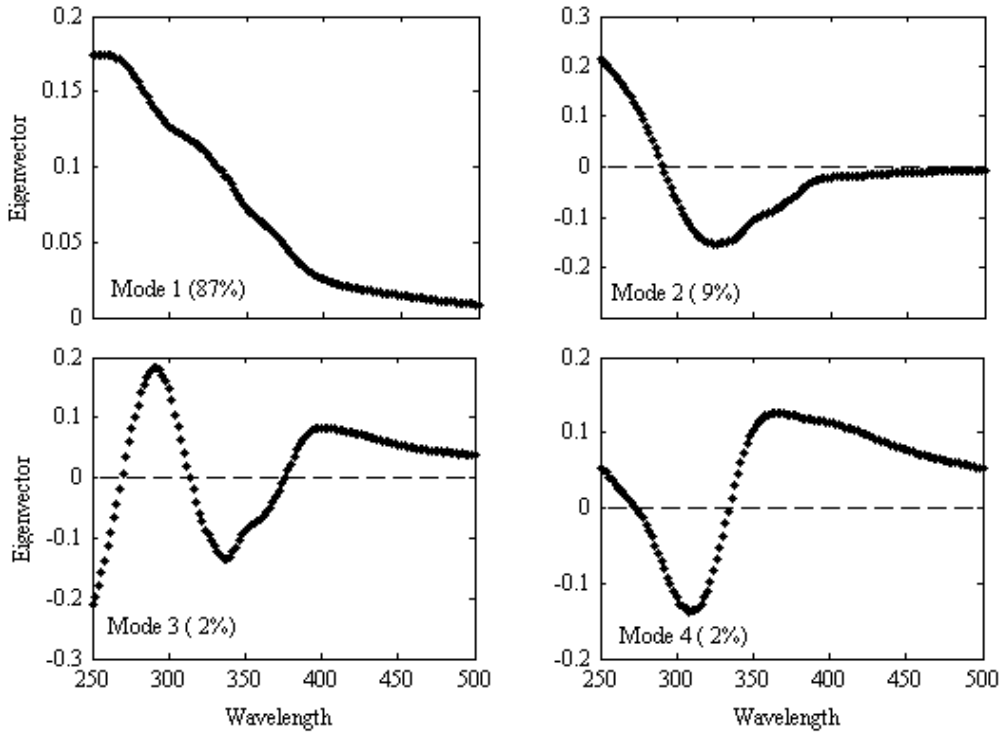

Figure 7. Plumes and Blooms EOF eigenvectors for the 4 dominant modes of variability for CDOM absorption coefficients from 1997-2012.

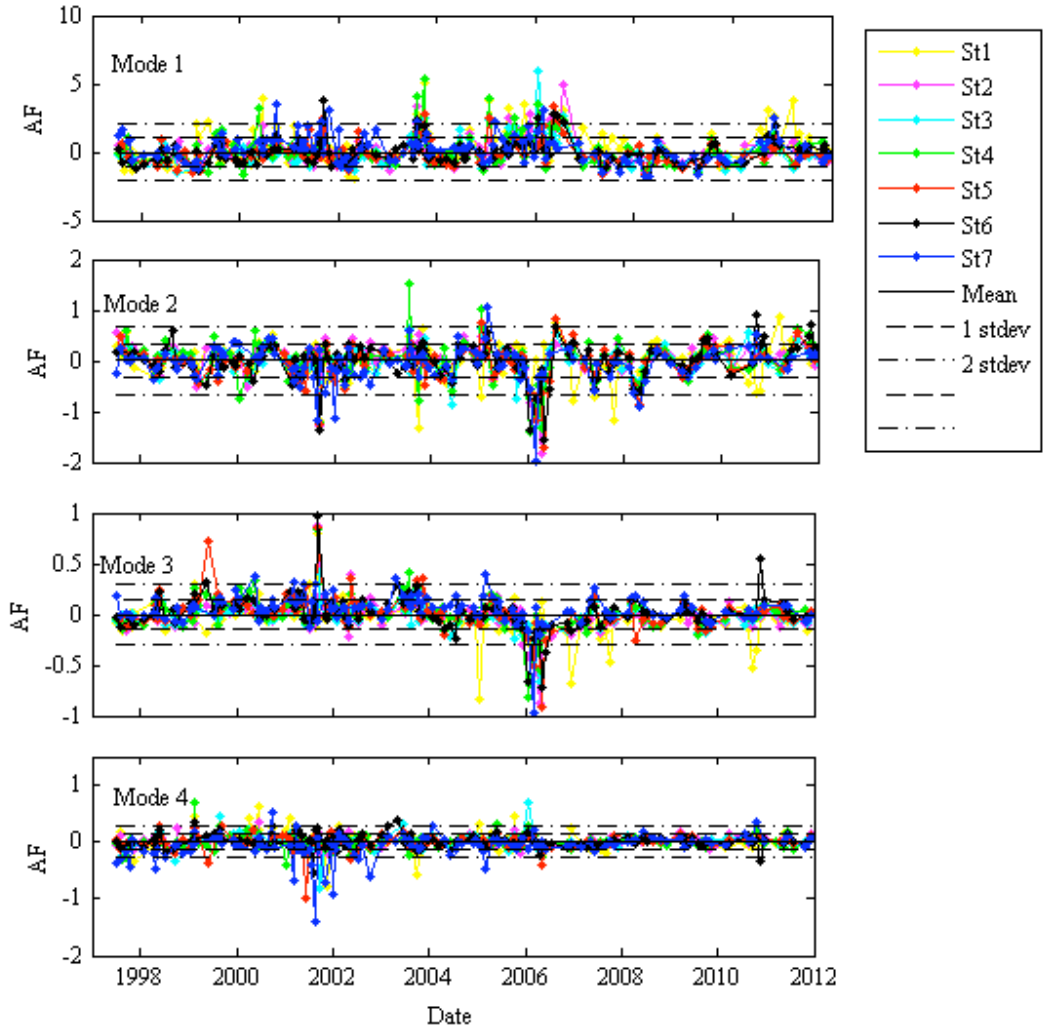

Figure 8. Plumes and Blooms EOF amplitude function (AF) for the 4 dominant modes of variability for CDOM absorption coefficients 1997-2012.

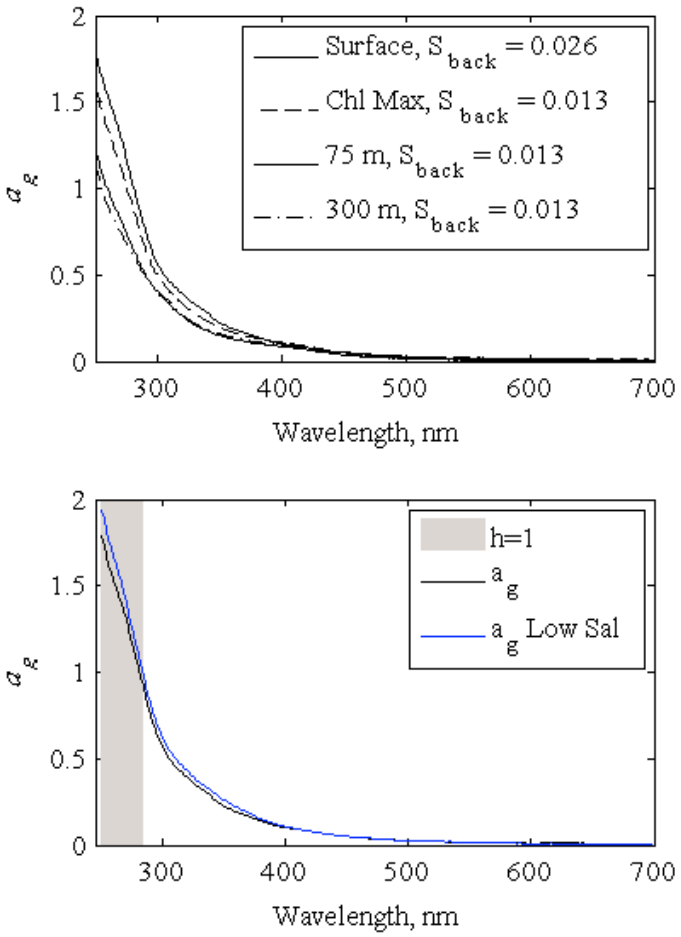

Figure 9. (a) Average $a_g(\lambda)$ at Station 4 for May 2011 through June 2013. (b) a_g1 = average surface $a_g(\lambda)$ for 1997 – 2012, a_g2 = average surface $a_g(\lambda)$ corresponding to salinity $\leq$ 32 PSU for 1997 - 2012. Grey shaded areas indicate Student's t-test results where the null hypothesis was rejected, h = 1, at *alpha* = 0.05.

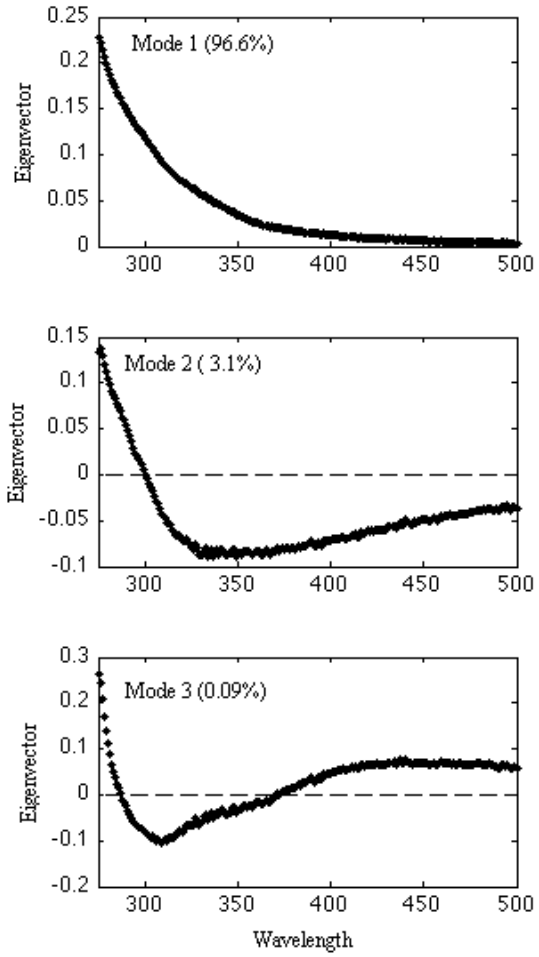

Figure 10. Global CDOM EOF eigenvectors.

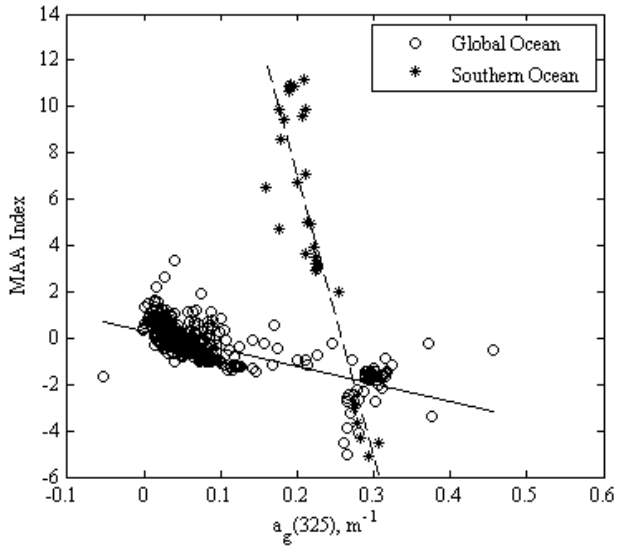

Figure 11. Global $a_g(325)$ vs MAA Index. Open circles indicate Global CDOM data excluding the Southern Ocean, r = -0.68. Southern Ocean indicated by stars, r = -0.69.

IV. Colored dissolved organic matter (CDOM) quality in a biologically productive coastal ocean

Rebecca K. Barrón, David Siegel, Norm Nelson and Nathalie Guillocheau

Abstract

Optical characterization of colored dissolved organic matter (CDOM) is useful in differentiating between CDOM sources and identifying dissolved organic matter (DOM) liability. CDOM samples were taken from three different environments in the Santa Barbara Channel, CA, including surface, deep-ocean (300 m) and kelp forest pelagic zone. Samples were analyzed for various CDOM properties. Slope ratio (S_R), specific UV-absorbance (SUVA), and mycosporine-like amino acid index, (MAA Index) all showed that the CDOM was primarily biologically derived from *in situ*, or "marine" sources. CDOM fluorescence measurements were made using excitation/emission spectroscopy (EEMS), and further indicated that the DOM sources in were highly biological. An empirical orthogonal function analysis was used to evaluate the EEMS data set, and constrained the variability into three dominate modes: Mode 1 (63.6%) was well related to phytoplankton biomass and indicative of productivity, Mode 2 (23.2%) was representative of the deep-water samples, and Mode 3 (4.65%) contained a unique kelp forest signature. The results of this work have shown that phytoplankton community structure is strongly linked to variability in CDOM absorption, whereas phytoplankton biomass is much more strongly related to CDOM fluorescence.

Introduction

The marine dissolved organic matter (DOM) pool is highly reactive and is important for microbial food webs. DOM quality and liability controls microbial production and therefore is important for ecosystem function (Hedges 2002). Carbohydrates and proteins serve as liable substrates for microbial consumption, while aromatic compounds such as fulvic acids and humic substances are more recalcitrant, and is important for photoprotection of aquatic organisms (Jaffé et al. 2008). The fraction of DOM pool that is light reactive is called chromophoric dissolved organic matter (CDOM) CDOM is ubiquitous in the global ocean (Nelson and Siegel 2013). Optical characterization of DOM is a very useful tool in determining the quality, and therefore function of DOM in a given aquatic system. Furthermore, CDOM characteristics are useful in determining DOM origin, fate and transportation through aquatic ecosystems, and application can range from small streams to a global-scale dynamics.

Some fraction of oceanic CDOM is thought to have derived largely from oxidation of marine organic matter as observed from the basin-wide correlation of CDOM absorption coefficient, $a_g(\lambda)$, with apparent oxygen utilization (AOU) in the global ocean (Swan et al. 2009; Nelson et al. 2010). CDOM also originates from terrestrial sources such as higher terrestrial or freshwater plants, and is exported to the oceans via rivers and streams. Specific chemical composition of CDOM is largely unknown as it is a mixture of organic chemicals. Terrestrially derived substances that are chromophoric include complex soil humic material, lignin, and other polyphenolic compounds leached from higher plants into freshwater systems. These materials are complex and largely recalcitrant in aquatic systems. Amino acid proteins and

polypeptides are also light reactive and are linked to heterotrophic processing of particulate organic matter. Amino acids are simple structures and are more readily available for bacterial uptake than terrestrially derived compounds.

CDOM quality dictates cycling and spectral shape properties, and this can be highly variable in coastal and estuarine ecosystems. Coastal areas with large river tributaries have can have significant terrestrial organic matter contribution, as much as 90% in the East Washington Sound (Twardowski and Donaghay 2001). Alternatively, Barrón et al (*In Prep*) has shown that freshwater influences had little to no discernable effect on CDOM absorption spectra in the Santa Barbara Channel.

Information about the chemical composition of DOM can be obtained from CDOM spectra. Lower molecular weight compounds with simpler structures absorb at shorter wavelengths, while larger, more complex compounds with higher substitution and conjugation absorb at higher wavelengths and broaden absorption spectra. Due to the charge attraction properties of the CDOM matrix, some of the higher wavelength absorption can be attributed to simple compounds, however. The addition of sodium borohydride inhibits charge transfer attractions between the chromophores making up the CDOM pool, thus resulting a reduction of the long wavelength absorption (Ma et al. 2010; Andrew et al. 2013). Andrew et al (2013) attributed the remaining long-wavelength absorption, e.g. at wavelengths greater than 400 nm, to terrestrially derived substances.

CDOM absorption coefficient is characterized by higher absorption in the UV portion of the spectrum, and decreasing absorption with increasing wavelength resembling an exponential curve (Nelson and Siegel 2013). The smooth tail in the visible end of the CDOM spectrum has been attributed to charge transfer between the

chromophores of organic compounds making up the CDOM pool (Del Vecchio and Blough 2004). In oceanographic and freshwater literature, there is a suite of spectral properties that can be used to characterize CDOM. The spectral shape of the CDOM absorption coefficient, $a_g(\lambda)$, can be described by the equation:

$$a_g(\lambda) = a_g(\lambda_o)e^{-S(\lambda-\lambda_o)} \quad (1)$$

where S is the spectral slope over the wavelength range λ_o - λ. Spectral slope calculations are made at over different wavelength ranges in literature, some spanning UV – visible wavelengths, and some only spanning wavelengths in the UV spectrum. This makes it difficult to compare CDOM properties between studies. However, S in general has been shown to have an inverse relationship with CDOM molecular weight (Green and Blough 1994).

Slope ratio, S_R, is calculated as $S_{275\text{-}295}$: $S_{350\text{-}400}$, and has been found to inversely correlate with molecular weight, where $S_R < 1$ is indicative of terrestrially derived CDOM compounds, and $S_R > 1.5$ is indicative of marine derived CDOM (Helms et al. 2008; Stedmon and Nelson 2015). Helms et al. (2008) found that higher S_R was related to increased UV-light exposure, while decreased S_R was observed for dark incubated samples due to bacterial production of CDOM.

Specific UV absorption (SUVA) is calculated as short wavelength CDOM absorption normalized by dissolved organic matter (DOC) concentration, and has demonstrated to correlate with molecular weight and aromaticity of CDOM compounds (Weishaar et al. 2003). SUVA has shown to be a useful and reliable parameter for cross-site comparison of DOM quality (Jaffé et al. 2008). Near shore SUVA values for the Santa Barbara Channel were comparatively low with respect to those found in multiple

inland aquatic ecosystems, reflecting the high CDOM absorption and (comparatively) low DOC values in coastal systems (Jaffé et al. 2008).

A fraction of CDOM is also fluorescent, sometimes referred to FDOM in literature. Aromatic compounds emit light when transitioning from excited to ground state, thereby giving off fluorescence. As substitution and conjugation on aromatic rings increase and organic molecules become more complex, the wavelength of fluorescent emission also increases. Excitation Emission Matrix Spectroscopy (EEMS) is a common analytical tool for characterizing FDOM in aquatic systems (Coble 2007; Nelson and Siegel 2013). Specific regions of fluorescence in EEMS have been identified with groups of compounds including terrestrially derived humic materials, marine-derived humic materials and amino acid compounds such as the proteins tryptophan and tyrosine. Humic materials display longer wavelength fluorescence emission than proteins, and CDOM quality is easily discerned between these broad categories. Multivariate statistical techniques, such as the parallel factor analysis (PARAFAC) technique developed by Stedmon et al. (2003) and refined by Cory et al. (2005), are useful for identifying hidden features in the 3-D EEMS, and teasing out organic compound fingerprints in large EEMS data sets (Cory and McKnight 2005; Cory et al. 2007). The model developed by Cory and McKnight (2005) uses a predetermined set of EEMS markers taken from a variety of environments, mostly from soil and freshwater samples, in attempt to represent a global CDOM model. This model, however, is limited by the rigid use of the predetermined peaks, and does not work well in open ocean systems where many of the fluorescence features are not found.

The Santa Barbara Channel, located along the central California coast, is a productive coastal upwelling system, and bulk optical properties are strongly influenced by phytoplankton community composition (Barron et al. 2014). Surface CDOM absorption is strongly influenced by phytoplankton functional type, and less so by phytoplankton biomass (Barron et al. *In prep*). Here we examine CDOM quality in the surface waters, at depth, and in adjacent kelp forest ecosystems using spectral CDOM characteristics as well as fluorescence techniques. In paper we use a multivariate statistical technique called an empirical orthogonal function (EOF) analysis to identify CDOM end members in EEMS samples from the three regimes. This paper shows that both deep water and pelagic kelp forest ecosystems have unique fluorescent biomarkers associated with respective sampling locations. Furthermore, the results show that although phytoplankton composition is linked to spectral CDOM absorption characteristics, phytoplankton biomass is much more strongly related to CDOM fluorescence.

Methods

Plumes and Blooms

Data for this paper were collected from August 2009 – June 2013 as a subset of a much larger data set called the Plumes and Blooms program beginning in 1996 and extending through the present time, December 2014. Plumes and Blooms (PnB) sampling consisted of optical and biogeochemical measurements taken at 7 stations extending across the center of the Santa Barbara Channel (Fig. 1). A suite of optical measurements was collected using *in-situ* profiling instruments on the PnB cruises as well as

conductivity-temperature-depth measurements (Kostadinov et al. 2007, 2010; Barron et al. 2014). Discrete surface water samples were taken at each station, and at depth at Station 4, for laboratory analysis of inherent optical properties, and other chemical and biogeochemical parameters. Methods for the parameters used in this paper are described in detail below. More information of the Plumes and Blooms sampling scheme can be found on the project website (http://www.oceancolor.ucsb.edu/plumes_and_blooms/).

Discrete samples were taken using 5 liter Niskin bottles deployed on a rosette with a Seabird 9/11 conductivity-temperature-depth system. Samples that were taken at discrete depths were analyzed for nutrients, biogenic and lithogenic silica (BSi and LSi), particulate organic carbon (POC), phytoplankton accessory pigments, chlorophyll *a,* dissolved organic carbon (DOC), and CDOM. Nutrient samples were collected directly from the Niskin bottles and stored in a shipboard freezer, then transferred to the laboratory freezer until analysis on a Latchet QuikChem 8000 Flow Injection Analyzer. BSi and LSi samples were filtered shipboard onto 0.4 μm membrane filters and frozen until analysis using a NaOH extraction procedure described in (Shipe and Brzezinski 2001) and, more recently, in (Krause et al. 2013). DOC samples were filtered through pre-combusted GF/F filters directly from the Niskin containers into acid-leached high-density polycarbonate bottles and immediately placed in the shipboard freezer. The samples were kept frozen until analysis on a Shimadzu TOC-V using methods outlined in Hansell and Carlson (1998) and Carlson et al. (2004) (Hansell and Carlson 1998; Carlson et al. 2004).

Phytoplankton pigment samples were concentrated onto GF/F filters shipboard and immediately preserved in liquid nitrogen. The samples were shipped in liquid

nitrogen to Horn Point Laboratory or NASA Goddard Space Flight Center where various pigments concentrations, including peridinin concentration, were determined via high performance liquid chromatography (HPLC) (Hooker et al. 2009; Barrón et al. 2014; see http://oceancolor.gsfc.nasa.gov/HPLC/).

CDOM Characterization

Samples for colored dissolved organic matter (CDOM) analysis were collected in glass amber bottles preconditioned for carbon analysis (e.g., Barrón et al. 2014). Samples were immediately stored in a shipboard refrigerator at 4^{o}C. Within 24 hours of collection, samples were filtered through a 0.2 μm membrane filter in the laboratory via low-pressure vacuum filtration and analyzed for absorbance, A, on a Shimadzu 2401-PC spectrophotometer using a 10 nm path length cuvette. The coefficient for CDOM absorption was calculated as $a_g(\lambda) = 2.303A/l$, where l is the path length of the cuvette in m, and $a_g(\lambda)$ has units of m^{-1}.

Several large hump-like features in the ultraviolet spectral region were found in the CDOM spectra from PnB and were described in Barrón et al. (2014) and Barrón et al. (*In Prep*) as dissolved mycosporine-like amino acid (MAA) absorbance features. The (presumably) MAA peaks in this study were quantified using the MAA Index parameter (Barrón et al., 2014). Baseline CDOM was modeled using the log-transformed $a_g(\lambda)$ data, and making a linear regression fit to the data surrounding the MAA region (300-310 nm and 390-400 nm). MAA Index is calculated as the sum of residual between the modeled and observed $a_g(\lambda)$ at λ = 310 – 390 nm plus a constant of 1.7 (Barrón et al, 2014). The constant of 1.7 was taken from Barrón et al. (*In Prep*) to center the mean of the MAA

Index calculated with a 15-year PnB surface CDOM data set (1997-2012). MAA Index values > 1 indicates significant MAA peak observations.

Discrete CDOM samples were also analyzed for fluorescence using excitation emission matrix spectroscopy (EEMS) using a Horiba Jobin Yvon Fluoromax FM4 following the recommended practice in Nelson and Coble (2009). Excitation and emission wavelength accuracy were checked for drift prior to each analysis session by running a single excitation scan without a sample, and single emission scan using deionized (DI) water from a milli-Q system. The FM4 rarely showed drift, but on occasion it was corrected if needed. DI water blanks were analyzed with each analysis session, and subtracted from sample EEMS to normalize for Raman scattering. Quinine sulfate standard was used to calibrate for excitation/emission, and run each analysis day. The quinine sulfate standard was kept in a light-tight glass bottle and stored in the refrigerator for up to one year. Quinine sulfate dilution series was run each time a new batch of standard was made.

After filtration and analysis on the Shimadzu spectrophotometer, the CDOM samples were transferred in to 40 mL glass amber bottles, acid washed and pre-combusted for carbon analysis, and stored in a 4 ^{o}C refrigerator. Samples were analyzed on the FM4 within 1 week to 1 year of collection. Duplicate samples were analyzed with every session, and duplicates were kept in the refrigerator and reanalyzed throughout study period. Duplicate samples showed little to no differences in fluorescence intensity, and no differences shifting in absorption peaks over time. If duplicates showed higher than 10% difference in fluorescence intensity, all samples from the same analysis day

were reanalyzed. Samples with sharp peaks, typically due to bubbles in the sample cuvette, were removed from the data set and reanalyzed if possible.

Discrete water samples were taken on June 6, 2013 at sites belonging to the Santa Barbara Coastal Long Term Ecological Research (LTER) program at 5 kelp forest ecosystem monitoring sites including the Arroyo Quemado, Naples, Mohawk, Carpentaria and Arroyo Burro Reefs (Fig. 1). CDOM samples were taken surface, 5 m and 10 m (where applicable) using the same bottle and handling protocols as PnB CDOM sampling. Samples were analyzed for $a_g(\lambda)$ within 24 hours of collection and EEMS within 1 week of collection.

Results

Oceanographic Conditions

The Santa Barbara Channel has been characterized by two dominant physical regimes that include wind-driven deep-water upwelling during spring, and stably stratified periods punctuated by eddy-driven isopycnal uplift (Brzezinski and Washburn 2011; Washburn et al. 2011). During the study period, sea surface temperatures ranged from 10 – 20 ^{o}C, and average sea surface salinity was 33.6 PSU (Fig. 2). Seasonal changes were observed in vertical density structure, where deep wind-driven upwelling occurred in the spring forcing cold/high salinity water to the surface. Stratification was observed most strongly in the summer months where surface waters were characterized by warm/lower salinity water in the upper 10 – 20 m, and cooler/higher salinity waters were observed at depth (Fig. 2).

Nutrient concentrations were highest in spring, and lowest in late-summer and winter periods as evidenced by the surface-averaged dissolved nitrate, NO_3^+, and phosphate, PO_4^{+3}, concentrations depicted in Figure 3. Ocean upwelling was the primary transport mechanism for nutrients into the euphotic zone, and resulted in spring phytoplankton blooms where increased chlorophyll *a* concentrations were observed across the channel (Fig. 3). Dissolved silicate (SiO_2^{-2}) concentrations mimicked those of dissolved nitrate. The phytoplankton community structure was dominated by diatoms during the spring bloom periods, but diatoms have historically co-occurred with increased dinoflagellate presence during spring blooms (Anderson et al. 2008; Barron et al. 2014).

Isopycnal uplift due to a cyclonic eddy residing in the center of the channel was often an important transport mechanism any time stratified/low surface nutrient conditions were observed. Eddy-enhanced nutrient entrainment was often observed in the fall months when a secondary microplankton bloom was sometimes observed and was typically dominated by dinoflagellate groups (Brzezinski and Washburn 2011; Barron et al. 2014). Note there was a gap in sampling from April – June 2010, so the spring bloom may not have been adequately sampled during that year (Fig. 3). Phytoplankton community structure largely influences the optical properties in the Santa Barbara Channel, and community composition has shown to be more important than phytoplankton abundance in influencing CDOM absorption (Barron et al. *In Prep*).

CDOM absorption properties

CDOM samples were collected for $a_g(\lambda)$ analysis at all surface sites for the entire study period, at Station 4 at depth starting from April 2011, and just inside 5 kelp forests

off the shore of mainland California on June 6, 2013. Mean $a_g(\lambda)$ for PnB surface samples, shown in the upper panel of Figure 4, displayed greater variability surrounding the absorption band between wavelengths λ = 300 – 400 nm, and was much less variable for the rest of the spectrum. Variability in the in the UV-A region of the spectrum was due to the presence of mycosporine-like amino acid (MAA) absorption features present in the $a_g(\lambda)$ data. Barrón et al. (2014) quantified these MAA-like absorption peaks as the MAA Index. In surface samples in the SBC MAA Index was well correlated to peridinin concentration, $r^2 = 0.73$; peridinin is the indicator pigment for dinoflagellate groups (Barron et al. 2014). Mean $a_g(\lambda)$ taken at 10 m depth plotted very similar to the mean surface $a_g(\lambda)$, and the mean $a_g(\lambda)$ at 75 and 300 m depth were much lower across the entire spectrum (Fig. 4). Mean $a_g(250)$ and mean S_{back} decreased with decreasing depth for PnB samples. Mean $a_g(\lambda)$ was higher across the spectrum for the kelp forest samples, as was mean S_{back} where flattening of the mean $a_g(\lambda)$ from λ = 300 – 400 nm was pronounced.

Previous studies have shown that the spectral slope parameter, spanning UV – visible wavelengths, is inversely correlated with molecular weight of CDOM compounds (Green and Blough 1994; Siegel et al. 2013). The S_{back} parameter, however, only extends from 310-390 nm, and, since it is considering modeled "background" absorption, relationship with molecular weight cannot necessarily be assumed. Another spectral measure of CDOM quality and composition is the spectral slope ratio (S_R), and was calculated as:

$$S_R = \frac{S_{275-295}}{S_{350-400}} \quad (2)$$

where $S_{275\text{-}295}$ and $S_{350\text{-}400}$ are the spectral slope parameter in Equation 1 calculated from wavelengths $\lambda = 275 – 295$ nm, and $\lambda = 350 – 400$, respectively. The observed data was used for $a_g(350) – a_g(400)$ rather than modeled background absorption coefficient, as in S_{back}, so the S_R parameter is not entirely free from MAA influence in samples where the secondary MAA peak, centered at $a_g(360)$, was observed. S_R was used in previous studies as an indicator for terrestrially derived CDOM ($S_R < 1$) versus marine endmember CDOM ($S_R > 1.5$). Terrestrially derived CDOM compounds are assumed to have a higher molecular weight, whereas marine CDOM is assumed to have extensive photodegradation, thus loss in the UVB portion of the spectrum (Helms et al. 2008; Stedmon and Nelson 2015). Slope ratio for the SBC mostly displayed values of $S_R > 1.5$, e.g. oceanic. A few surface samples displayed $S_R < 1$, however they coincided with high MAA Index, e.g. MAA Index > 1, and (Fig. 5). Two samples from the kelp forest displayed $S_R < 1.5$, not quite in the terrestrial range, but these samples also had values of MAA Index > 1. There was only one sample free from MAA influence that displayed $S_R < 1$,which was a deep-water sample in May 2011, and was likely an outlier. The rest of the SBC CDOM would've been considered "oceanic" by the S_R results. This is consistent with the analysis of Barrón et al. (*In Prep*), where a study using 15-years of CDOM absorption data in the SBC showed insignificant evidence that surface $a_g(\lambda)$ was affected by terrestrial inputs.

SUVA is a frequently used parameter to evaluate CDOM quality in freshwater and estuarine research, where higher values of SUVA indicate higher aromaticity and molecular weight compounds, e.g. lignin and humic materials (Weishaar et al. 2003; Helms et al. 2008; Stedmon and Nelson 2015). SUVA ($m^2\ gC^{-1}$) was calculated as:

$$SUVA = \frac{A(254)}{[DOC]}, \quad (3)$$

where A, m^{-1}, is the decadal CDOM absorbance at $\lambda = 254$ normalized to pathlength, and [DOC] is the DOC concentration, gC m^{-3}. DOC data was available for PnB samples from April 2009 – April 2012. Mean SUVA for the SBC was 0.87 $\pm$ 0.1 m^2 gC^{-1}, and, like S_R, there was no real discernable difference between surface and deep-water samples (Fig. 5). SUVA was typical for an oceanic system, compared with reported value of Pacific Ocean SUVA = 0.6 m^2 gC^{-1} by Weishaar et al. (2003), and SUVA $\leq$ 1 m^2 gC^{-1} for the SBC "coastal" sample by (Jaffé et al. 2008). . Lowest SUVA values were observed coincident with high MAA Index in 2010. SUVA values presented in Figure 5 indicated that the DOM pool in the SBC is composed more so of low molecular weight compounds, e.g. proteins, per unit DOC compared with an area with significant terrestrial influence, like a freshwater lake or stream, and support the findings of Barrón et al. (*In Prep*) that CDOM dynamics in the coastal area are largely oceanic.

CDOM Fluorescence

CDOM fluorescence can be particularly useful for coastal research in determining CDOM quality and origin. SUVA values are can be paired with CDOM fluorescence measurements, as in Jaffé et al. (2008), where the fluorescence data aids in determining terrestrial VS microbial origin of the DOM considered.

Fluorescence markers in EEMS spectra include humic materials that emit fluorescence in visible wavelengths, and proteins that emit in the UV part of the spectra. Table 1 was taken from Stedmon and Nelson (2015) lists previously identified EEMS peaks in aquatic literature (mostly those from Coble (2007)). Proteins in EEMS spectra indicate

biologically derived compounds, which may have greater bioavailability to the surrounding heterotrophic bacteria than humic materials. Therefore, proteins represent fresh CDOM more likely produced *in situ*. Humic materials are much more recalcitrant remain dissolved in the water for long periods of time, and A-peaks in particular have historically been associated with terrestrial humic material. C and M peaks have historically been designated as "marine humic" material in that the compounds have humic-like fluorescence, but have are thought to have been derived from oceanic precursors rather than terrestrial plant precursors (Coble 2007).

Figure 6 shows an example EEMS spectrum for a surface sample taken at Station 4 in August 2009. The A and N peaks were quite common for Santa Barbara Channel surface waters, where A-peak represents terrestrial humic material and the N-peak represents amino acids associated with phytoplankton (Coble 2007). There was also increased absorption in the longer excitation/emission area of the EEMS, denoted by the M and C peaks. The intensity of fluorescence was determined in quinine sulfate equivalents (QSE) and was variable in time for given regions of the EEM spectrum (data not shown).

Multivariate statistical procedures are very useful in analyzing large EEMS data sets, because they are able to identify trends now discernable to the eye. Parallel factor analysis (PARAFAC) is a commonly used technique in freshwater and coastal CDOM research and can be useful in identifying key EEMS compounds. The Global Cory-McKnight PARAFAC model is commonly used to analyze EEMS data, as it identifies pre-set FDOM compounds found from various environments (Cory and McKnight 2005). A subset of the Plumes and Blooms surface samples were analyzed using the Cory-

McKnight model, however the model did not fit well to the oceanic data set compared with results typically found by the original authors of the PARAFAC model using data sets it was developed for (results not shown). Thus an empirical orthogonal function analysis (EOF) was used to identify EEMS features and trends. The EOF is ideal for this type of analysis because identifies patterns in time and space using a series of basis functions to decompose a large data set is into a set of orthogonal modes. Basis functions of the data are determined by calculating eigenvectors of the covariance matrix. The PnB surface water samples, Station 4 deep-water samples and kelp forest water samples were all input to the EOF analysis. Each EEMS data matrix was mean-centered with respect to time, decomposed into a single file string, and input to the EOF model so that the covariance matrix accounted for variability in time and space. The EOF analysis resulted in eigenvectors describing the EEMS signature associated with each mode of variability. The eigenvector strings were reconstructed into a 3-D matrix and plotted with EEMS identifiers (Fig. 7). Amplitude functions (AF) for each mode indicated the intensity of the pattern in time and space, where extreme AF (AF > 1 std from the mean, Fig. 7) indicated strong presence of the associated fluorescence pattern. Rather than separating the eigenvector peaks of interest, as done in the Cory and McKnight (2005) PARAFAC model, the 3-D pattern was considered as a whole in describing SBC data. There are benefits to doing the procedure both ways, but the nature of the EOF allows for more information about the spectral signatures to be considered in a given AF string.

The EOF analysis captured 91.45% of the EEMS variability within the first 3 modes (Fig. 7). Mode 1 (63.6% variability) was reflective of the most common EEM markers found in the data set, with well-defined peaks near the A and N markers, and

broad emission in the visible wavebands, e.g. “marine humic” region. Mode 1 eigenvectors were all positive, indicating positive co-variability among the fluorescence peaks. Mode 1 AF was mostly positive as well, and most extreme AF values were observed in the spring/early summer (Fig. 8). Box plots in Figure 9 emphasize the spatial variability of modal amplitude function. The box plots for Mode 1 AF overlap the mean AF line for all of the spatial points considered signifying that the EEMS patters represented by Mode 1 were not isolated to a particular spatial region (Fig. 9).

Mode 2 (23.2% variability) displayed a dipole between the protein and humic fluorescence signals with the protein peak on the negative axis and humics on the positive axis. Mode 2 AF showed distinct separation between the surface-water and deep water samples, where positive AF were observed for all deep-water samples and negative AF were observed for most of the surface samples, including those collected in the kelp forest (Fig. 9). Figures 8 and 9 showed that Mode 2 was clearly capturing a deep-water, 10 – 300 m, signature. The standard deviation line for mean AF of samples taken at 10 m depth overlapped the mean AF line in Figure 9. This was likely because the depth of the chlorophyll *a* maximum was often found at 10 m depth, and there were some protein peaks found at 10 m during the study.

Mode 3 (4.7% variability) displayed a unique protein peak with ex/em centering at approximately 275 nm /350 nm, and inverse co-variation with a humic-like peak centering around 310 nm /350 nm (Fig. 7). The terms “protein-like” and “humic-like” are used very loosely here, because there are no previously identified substances that fluoresce at these peak locations. Due to their proximity to the protein and marine humic regions, speciation can be assumed. Furthermore, the “humic-like” peak was very close

to the protein-humic border, and may have been an artifact or simply an anti-fluorescence, e.g. low fluorescence area, for the area just adjacent to the protein peak observed. The most extreme AF for Mode 3 was observed in the kelp forest samples in the positive direction, and Mode 3 was therefore interpreted as a kelp forest signature (Fig. 9).

The EOF effectively separated the EEMS into three modes that describe the environments considered (Fig. 9), with Mode 1 representative of a productive marine signature, Mode 2 representative of the deep-water signature and Mode 3 representative of the kelp forest signature. To gain more perspective as to the dynamics of the modes in the SBC, linear regressions were performed with CDOM absorption and various seawater properties using Plumes and Blooms data only (Tables 2 and 3). Due to the lack of overlapping DOC data, relationships with modal amplitude function and SUVA and DOC were not assessed. Kelp forest samples were not included in the linear regression analysis, and results for Mode 3 regressions represent only PnB data.

Mode 1 was well correlated to all $a_g(\lambda)$, with higher correlation coefficient at longer $a_g(\lambda)$ wavelengths, and displayed negative correlation with S_{back}, indicating that Mode 1 was associated with increased CDOM absorption across the spectrum (Table 2). Mode 2 was weakly correlated with CDOM absorption properties, and the strongest correlation was with S_{back} with r = -0.23. Negative correlation of Mode 2 AF with S_{back} indicates decreased S_{back} associated with deep-water CDOM, which is consistent with the results observed above (Fig. 2). Lastly, Mode 3 was well correlated with $a_g(\lambda)$, more so at shorter wavelengths, S_R, and with MAA Index (Table 2). MAAs are aliphatic and do not exhibit fluorescence, thus the peak in Mode 3 eigenvectors is not a MAA peak. The relationship here is reflective of the prevalence of MAAs in the kelp forest, (Fig. 5) and

the strong association of Mode 3 with the kelp forest EEMS samples. The relationship with S_R could have indicated an association with terrestrial materials, given the proximity to the shoreline. However, due to the MAA prevalence in the SBC it is difficult to interpret relationships with S_R.

Mode 1 was most strongly correlated with chlorophyll *a* and biogenic silica concentrations with r = 0.30 and 0.31, respectively, indicating positive correlation with diatom blooms (Table 3). Interestingly, the regression analysis did not show a significant correlation between the Mode 1 AF with fucoxanthin, the indicator pigment for diatoms. There are gaps in both the BSi and the fucoxanthin data, so it is possible that the relationships are characterizing two different time periods within the study period. Mode 2 showed the strongest positive correlation with lithogenic silica concentration, r = 0.28, and secondary relationships with biogenic silica and chlorophyll *a* concentrations. The positive correlation with LSi is consistent observations made in Barrón et al (*In Prep*) where CDOM relationships with mineral particles were indicative of sediment re-suspension from shoaling on the continental shelf (Barrón et al. *In Prep*). Mode 2 also displayed significant negative correlation with 19'hexanoyloxy-fucoxanthin concentration, the indicator pigment for chromophytes and other green nanoflagellates (Vidussi et al. 2001). Previous studies have found these phytoplankton groups present in the baseline community phytoplankton community, and not typically associated with increased chlorophyll *a* concentrations (Anderson et al. 2008; Brzezinski and Washburn 2011; Barron et al. 2014). Negative correlation with Mode 2 AF indicated positive correlation with the protein peak (plotted as a negative in Fig. 7). Mode 3 was negatively correlated with nutrient concentrations, indicating that the kelp forest endmember signal was

prevalent in the rest of the SBC when nutrient concentrations were low. Halewood et al. (2012) observed DOC retention in the inner shelf of the Santa Barbara Channel during stratified months, e.g. summer, and release in the fall/winter months. The relationship between Mode 3 AF and nutrients could have been indicative of that mechanism; but due to lack of a more complete kelp forest data set, there was no way further assess that hypothesis.

Discussion

Pelagic connections with CDOM quality

CDOM quality in the SBC was assessed using an array of optical and statistical techniques. CDOM absorption and fluorescence properties provided a wealth of information about DOM cycling and partitioning in the productive coastal site, and each method gave specific insight to the dynamics of the pelagic ecosystem. CDOM absorption coefficient was heavily influenced by dissolved MAAs and accounted for much of the increased UV-A absorbance. High values of MAA Index clearly influenced S_R values, where low S_R was only observed coincident with increased MAA presence. Barrón et al. (2014) found values of the MAA index to strongly correlate with peridinin concentrations, and Barrón et al. (*In Prep.*) showed that peridinin concentration was most strongly related to CDOM dynamics in the SBC. Furthermore, Barrón et al. (*In Prep*) found that phytoplankton community composition was much more important for changes/increases in CDOM absorption than was phytoplankton abundance. Dinoflagellates are major contributors to CDOM cycling in the SBC despite rarely dominating the phytoplankton community (Barron et al. 2014). Previous studies have

found that zooplankton sloppy feeding mechanisms release more DOM when dinoflagellates serve as their food source over other phytoplankton groups (Saba et al. 2009). Such ecosystem dynamics could play a major role in determining CDOM composition in the pelagic coastal system.

Interestingly, SUVA values were well within range of oceanic values, and indicated the DOM in the SBC was primarily composed of low molecular weight (Weishaar et al. 2003; Jaffé et al. 2008). The SUVA calculation was free of MAA influence as it included only $a_g(254)$. There was no obvious connection of SUVA to MAA Index, hence no connection of SUVA to dinoflagellate presence in the SBC (Fig. 5). This is consistent with the results of Barrón et al. (*In Prep*) where DOC concentrations for a larger subset of PnB data (2007 – 2011) correlated very poorly with MAA Index. SUVA dynamics further confirmed the observation that dinoflagellate presence does not appear to have much influence on bulk DOC concentrations, but does influence CDOM spectral shape in the UVA portion of the spectra. These results impact the accuracy of using optical instrumentation for biogeochemical measurements in the ocean. Careful choice of wavelength would determine which information to get from an optical measurement, e.g. phytoplankton community composition information measured within the UVA region (Barron et al. 2014), or DOC composition and/or concentration information contained in the UVB region (Fichot and Benner 2011).

CDOM fluorescence measurements proved to be a rich complementary measurement to the CDOM absorption measurements routinely made in the Plumes and Blooms program. MAAs are not fluorescent, therefore the EEMs were able to capture the CDOM dynamics in the absence of MAA signal contamination. EOF Mode 1 for the

EEM data set was reflective of the SUVA values, in that it showed a strong biological signal. Mode 1 was most strongly correlated with chlorophyll *a* concentration, but showed very weak correlation with phytoplankton pigment markers. Thus, phytoplankton biomass was much more important to increased CDOM fluorescence than community composition. These results were consistent with the findings of Rochelle-Newall and Fisher (2002), where CDOM fluorescence was linked more strongly to bacterial production, and that phytoplankton did not directly contribute to the fluorescent DOM pool. The negative correlation of Mode 2 AF with nanoflagellate groups indicated that the strong protein signal was correlated with the baseline phytoplankton community, as determined in Barrón et al. (2014).

Mode 2 and 3 represent allochthonous sources of for the pelagic surface SBC, in that Mode 2 represented the deep-ocean, up to 300 m, signal and Mode 3 the near-shore kelp forest signal. Correlation with LSi for the EEMS Mode 2, with deep-water CDOM in indicators in Barrón et al. (*In Prep*), and with the upwelling phytoplankton community in Barrón et al. (2014) all indicate that terrestrially derived material in the SBC enters via the sediments on the continental shelf through upwelling rather than via stream/river flow. Rainfall and river flow is very sparse in the Santa Barbara region, and previous studies have shown little to no correspondence with the river discharge and terrestrial optical signatures in the surface waters. Furthermore, recent studies in the SBC have shown very good correlation between wave height and particle scattering in the shallow areas along the continental shelf (*F. Hendrickx and D. Siegel pers. commun. 2014*).

The kelp forest signal in of Mode 3 was apparently devoid of terrestrial humic material despite the very close proximity of the kelp forests to the mainland, and

represented DOM production through biological sources. It is unclear if the DOM from the kelp forest is associated with the pelagic community of the kelp forest or from exudations of the kelp itself. At this time there are no studies using direct measurement of fluorescent DOM of the giant kelp, *Macrocystis pyrifera*, or similar species. Laboratory leaching experiments of clipped kelp blades were attempted during the course of this study, however the kelp blades did not fare well in the lab. It is likely that the EEM signature for the kelp forest was indicative of bacterial processing of unique kelp-derived DOM compounds. *In situ* measurements of kelp DOM would be much more useful to identify a specific source.

Conclusion

The Santa Barbara Channel is a productive coastal system with unique optical properties. The CDOM properties S_R, SUVA and MAA Index were very useful in telling different stories about CDOM variability. Phytoplankton community structure has a strong influence on CDOM absorption properties in the SBC, where dinoflagellates are particularly related to absorption in the UVA region of the spectrum. On the other hand, CDOM fluorescence was more strongly linked to phytoplankton abundance, and community structure played a secondary role. The EOF analysis was useful in identifying DOM sources in the SBC, and showed that the majority of the DOM was of bacterial origin. The kelp forest samples displayed a unique EEMS signature indicative of a protein-like substance associated with the pelagic kelp forest ecosystem. It is unclear if this signature is a direct source from the giant kelp species, *Macrocystis pyrifera*, or from bacterial processing of a unique DOM precursor. Results from this study will be useful for larger scale application of optical measurements, as they demonstrate the various

parameters useful differentiating DOM origin.

References

Anderson, C. R., D. A. Siegel, M. A. Brzezinski, and N. Guillocheau. 2008. Controls on temporal patterns in phytoplankton community structure in the Santa Barbara Channel , California. **113**: 1–16.

Andrew, A. a., R. Del Vecchio, A. Subramaniam, and N. V. Blough. 2013. Chromophoric dissolved organic matter (CDOM) in the Equatorial Atlantic Ocean: Optical properties and their relation to CDOM structure and source. Mar. Chem. **148**: 33–43.

Barron, R. K., D. a. Siegel, and N. Guillocheau. 2014. Evaluating the importance of phytoplankton community structure to the optical properties of the Santa Barbara Channel, California. Limnol. Oceanogr. **59**: 927–946.

Brzezinski, M. a., and L. Washburn. 2011. Phytoplankton primary productivity in the Santa Barbara Channel: Effects of wind-driven upwelling and mesoscale eddies. J. Geophys. Res. **116**, doi:10.1029/2011JC007397

Carlson, C. A., S. J. Giovannoni, D. A. Hansell, S. J. Goldberg, R. Parsons, and K. Vergin. 2004. Interactions among dissolved organic carbon, microbial processes, and community structure in the mesopelagic zone of the northwestern Sargasso Sea. Limnol. Oceanogr. **49**: 1073–1083.

Coble, P. G. 2007. Marine optical biogeochemistry: the chemistry of ocean color. Chem. Rev. **107**: 402–18.

Colleagues, D., O. Biology, P. Bontempi, N. Hq, R. Sensing, T. Team, S. Hooker, N. Calibration, V. Office, L. Van Heukelem, J. Perl, J. Dolan, L. C. Resources, R.

Farnbach, R. F. Consulting, C. Trees, G. Fargion, C. Thomas, A. Neeley, and M. Russ. 2009. NASA Ocean Biology and Biogeochemistry GSFC Calibration and Validation Office 1450 S . Rolling Road , Halethorpe , Maryland 21227. 1–62.

Cory, R. M., and D. M. McKnight. 2005. Fluorescence Spectroscopy Reveals Ubiquitous Presence of Oxidized and Reduced Quinones in Dissolved Organic Matter. Environ. Sci. Technol. **39**: 8142–8149.

Cory, R. M., D. M. McKnight, Y.-P. Chin, P. Miller, and C. L. Jaros. 2007. Chemical characteristics of fulvic acids from Arctic surface waters: Microbial contributions and photochemical transformations. J. Geophys. Res. **112**: 1–14.

Fichot, C. G., and R. Benner. 2011. A novel method to estimate DOC concentrations from CDOM absorption coefficients in coastal waters. Geophys. Res. Lett. **38**.

Green, S. A., and N. V Blough. 1994. Optical-absorption and fluoresence properties of chromophoric dissolved orgainc-matter in natural-waters. Limnol. Oceanogr. **39**: 1903–1916.

Hansell, D. A., and C. A. Carlson. 1998. Deep-ocean gradients in the concentration of dissolved organic carbon. Nature **395**: 263–266.

Hedges, J. I. 2002. Biogeochemistry of Marine Dissolved Organic Matter, Elsevier.

Helms, J. R., A. Stubbins, J. D. Ritchie, E. C. Minor, D. J. Kieber, and K. Mopper. 2008. Absorption spectral slopes and slope ratios as indicators of molecular weight, source, and photobleaching of chromophoric dissolved organic matter. Limnol. Oceanogr. **53**: 955–969.

Jaffé, R., D. McKnight, N. Maie, R. Cory, W. H. McDowell, and J. L. Campbell. 2008. Spatial and temporal variations in DOM composition in ecosystems: The importance of long-term monitoring of optical properties. J. Geophys. Res. **113**: G04032.

Kostadinov, T. S., D. a. Siegel, and S. Maritorena. 2010. Global variability of phytoplankton functional types from space: assessment via the particle size distribution. Biogeosciences Discuss. **7**: 4295–4340.

Kostadinov, T. S., D. a. Siegel, S. Maritorena, and N. Guillocheau. 2007. Ocean color observations and modeling for an optically complex site: Santa Barbara Channel, California, USA. J. Geophys. Res. **112**: 1–15.

Krause, J. W., M. A. Brzezinski, D. A. Siegel, and R. C. Thunell. 2013. Biogenic silica standing stock and export in the Santa Barbara Channel ecosystem. J. Geophys. Res. Ocean. **118**: 736–749.

Ma, J., R. Del Vecchio, K. S. Golanoski, E. S. Boyle, and N. V Blough. 2010. Optical Properties of Humic Substances and CDOM: Effects of Borohydride Reduction. Environ. Sci. Technol. **44**: 5395–5402.

Nelson, N. B., and P. G. Coble. 1994. Optical Analysis of Chromophoric Dissolved Organic Matter, p. 79–96. *In* Oliver Wurl [ed.], Practical Handbook of Seawater Analysis. CRC Press.

Nelson, N. B., and D. a Siegel. 2013. The global distribution and dynamics of chromophoric dissolved organic matter. Ann. Rev. Mar. Sci. **5**: 447–76.

Nelson, N. B., D. A. Siegel, C. A. Carlson, and C. M. Swan. 2010. Tracing global biogeochemical cycles and meridional overturning circulation using chromophoric dissolved organic matter. Geophys. Res. Lett. **37**, doi:10.1029/2009GL042325

Rochelle-Newall, E. J., and T. R. Fisher. 2002. Production of chromophoric dissolved organic matter f luorescence in marine and estuarine environments : an investigation into the role of phytoplankton. Mar. Chem. **77**: 7–21.

Saba, G. K., D. K. Steinberg, and D. A. Bronk. 2009. Effects of diet on release of dissolved organic and inorganic nutrients by the copepod Acartia tonsa. Mar. Ecol. Prog. Ser. **386**: 147–161.

Shipe, R. F., and M. A. Brzezinski. 2001. A time series study of silica production and flux in an eastern boundary region: Santa Barbara Basin, California. Global Biogeochem. Cycles **15**: 517–531.

Siegel, D. a., M. J. Behrenfeld, S. Maritorena, C. R. McClain, D. Antoine, S. W. Bailey, P. S. Bontempi, E. S. Boss, H. M. Dierssen, S. C. Doney, R. E. Eplee, R. H. Evans, G. C. Feldman, E. Fields, B. a. Franz, N. a. Kuring, C. Mengelt, N. B. Nelson, F. S. Patt, W. D. Robinson, J. L. Sarmiento, C. M. Swan, P. J. Werdell, T. K. Westberry, J. G. Wilding, and J. a. Yoder. 2013. Regional to global assessments of phytoplankton dynamics from the SeaWiFS mission. Remote Sens. Environ. **135**: 77–91.

Stedmon, C. a, S. Markager, and R. Bro. 2003. Tracing dissolved organic matter in aquatic environments using a new approach to fluorescence spectroscopy. Mar. Chem. **82**: 239–254.

Stedmon, C. A., and N. B. Nelson. 2015. The Optical Properties of DOM in the Ocean. 481–508.

Swan, C. M., D. a. Siegel, N. B. Nelson, C. a. Carlson, and E. Nasir. 2009. Biogeochemical and hydrographic controls on chromophoric dissolved organic

matter distribution in the Pacific Ocean. Deep Sea Res. Part I Oceanogr. Res. Pap. **56**: 2175–2192.

Twardowski, M. S., and P. L. Donaghay. 2001. Separating in situ and terrigenous sources of absorption by dissolved materials in coastal waters. J. Geophys. Res. **106**: 2545.

Del Vecchio, R., and N. V Blough. 2004. On the origin of the optical properties of humic substances. Environ. Sci. Technol. **38**: 3885–91.

Vidussi, F., H. Claustre, B. Manca, A. Luchetta, and J.-C. Marty. 2001. Phytoplankton pigment distribution in relation to upper thermocline circulation in the eastern Mediterranean Sea during winter. **106**: 939–956.

Washburn, L., M. R. Fewings, C. Melton, and C. Gotschalk. 2011. The propagating response of coastal circulation due to wind relaxations along the central California coast. J. Geophys. Res. **116**: 1–16.

Weishaar, J. L., G. R. Aiken, B. a. Bergamaschi, M. S. Fram, R. Fujii, and K. Mopper. 2003. Evaluation of Specific Ultraviolet Absorbance as an Indicator of the Chemical Composition and Reactivity of Dissolved Organic Carbon. Environ. Sci. Technol. **37**: 4702–4708.

Table 1. Common regions of fluorescence maxima

Type	Label	Excitation (nm)	Emission (nm)
Visible - Humic	A	260	400-460
Visible - Humic	M	290	370-410
Visible - Humic	C	320-360	420-460
UVA - Protein	N	280	370
UVA - Protein	T	275	305
UVA - Protien	B	275	340

Adapted from Stedmon and Nelson (2015).

Table 2. Correlation coefficent (r) for amplitude functions (AF) vs $a_g(\lambda)$ properties. Values in bold represent significance of p-value < 0.05.

	Mode 1	Mode 2	Mode 3	N
$a_g(275)$	**0.38**	**-0.11**	0.43	144
$a_g(325)$	**0.46**	0.06	**0.36**	145
$a_g(350)$	**0.47**	0.11	**0.33**	145
$a_g(400)$	**0.49**	0.13	**0.23**	145
S_{back}	**-0.33**	**-0.23**	0.11	145
S_R	-0.08	-0.01	**-0.25**	144
MAA Index	**0.14**	0.09	**0.25**	145

Table 2. Correlation coefficient (r) for AF vs biogeochemical properties. Values in bold represent significance of *p-value* ≤ 0.05.

	Mode 1	Mode 2	Mode 3	N
NO3	0.05	0.10	**-0.21**	131
PO4	0.03	0.12	**-0.19**	131
SiO2	0.02	0.06	**-0.19**	131
Chl a	**0.30**	**0.20**	0.05	131
BSi	**0.31**	0.17	0.08	107
LSi	0.16	**0.28**	-0.11	107
Peridinin	0.04	0.05	0.02	122
Fucoxanthin	0.05	-0.10	0.02	122
19'hexanoyloxy-fucoxanthin	-0.11	**-0.24**	-0.02	122
Zeaxanthin	0.01	-0.04	0.02	122

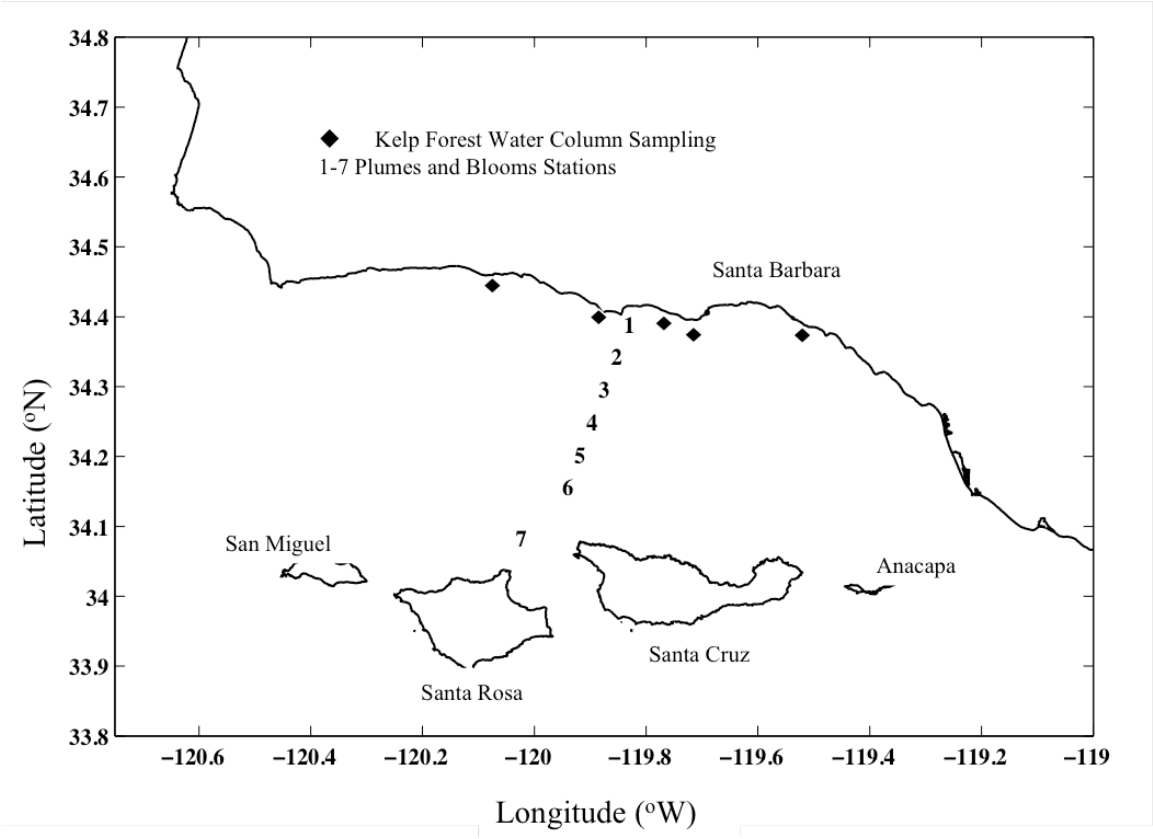

Figure 1. Map of Santa Barbara Channel, CA. Plumes and Blooms sampling locations are marked by numbers, and kelp forest sampling sites are marked by diamonds.

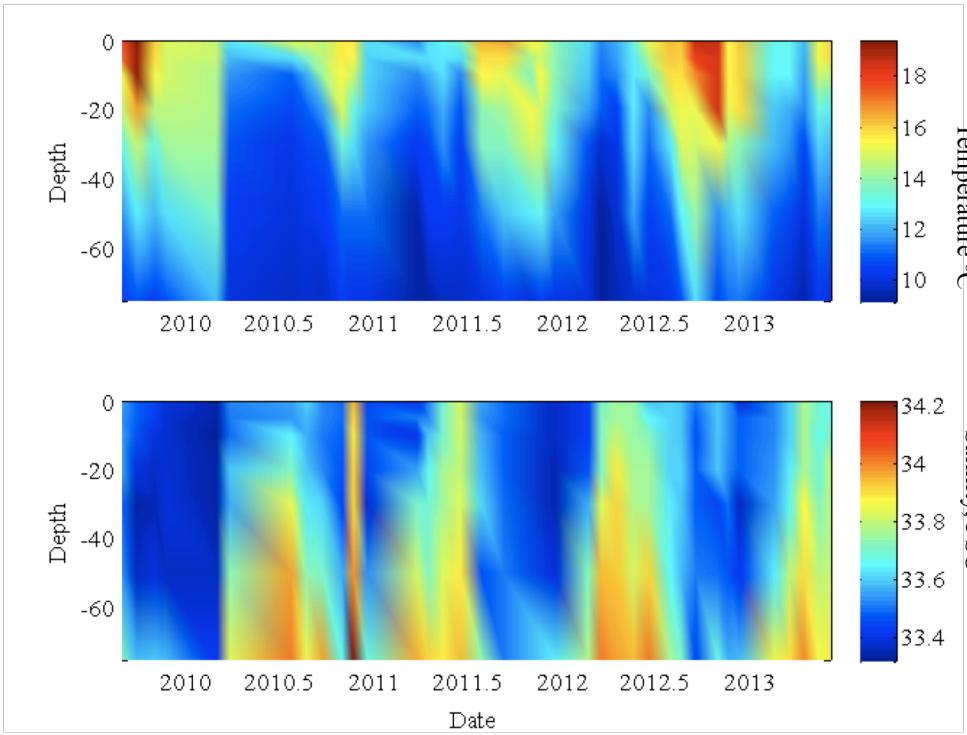

Figure 2. Vertical profiles of temperature, ^{o}C, and Salinity, PSU, at Plumes and Blooms Station 4.

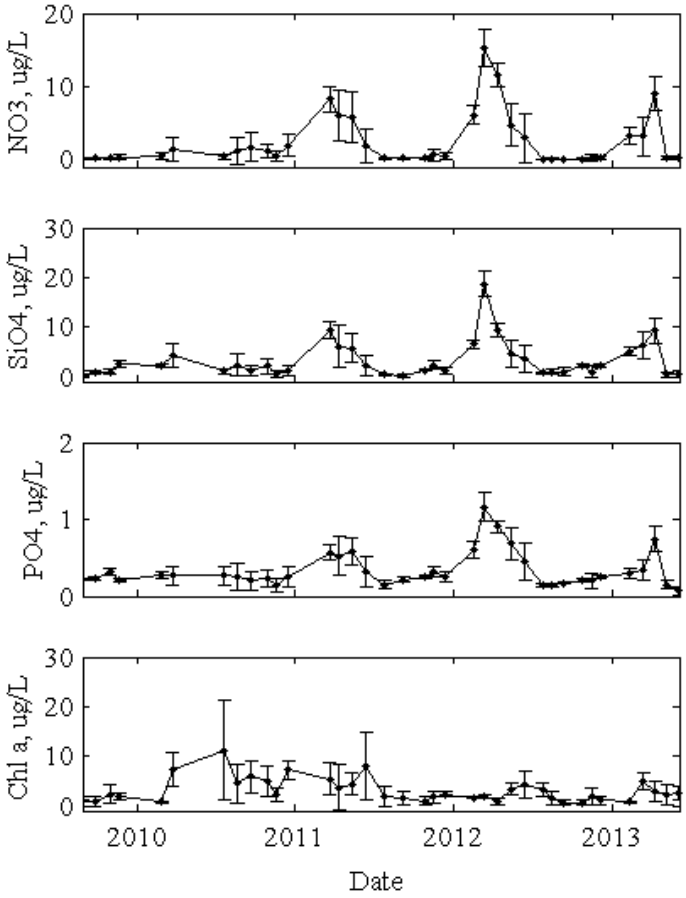

Figure 3. Surface average nitrate, NO3, chlorophyll *a*, Chl a, concentrations for Plumes and Blooms Stations 1 – 7.

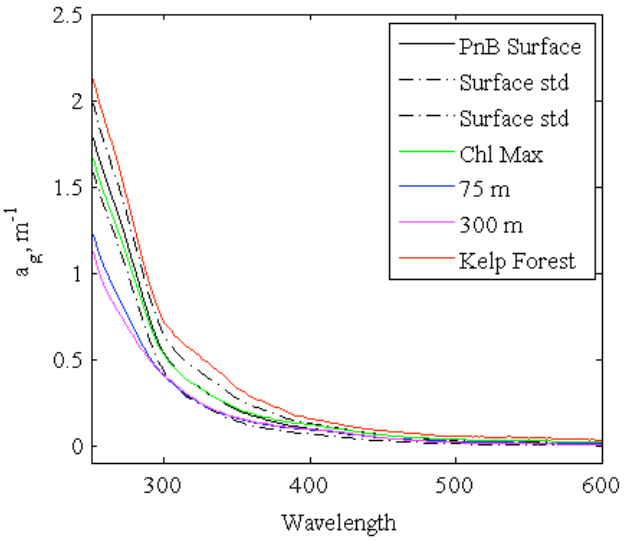

Figure 4. Mean $a_g(\lambda)$: Plumes and Blooms surface, Stations 1 – 7; Station 4 Chlorophyll *a* Max depth (10 m), 75 m, 300 m; Kelp Forest, Arroyo Quemado, Naples, Mohawk, Carpentaria and Arroyo Burro.

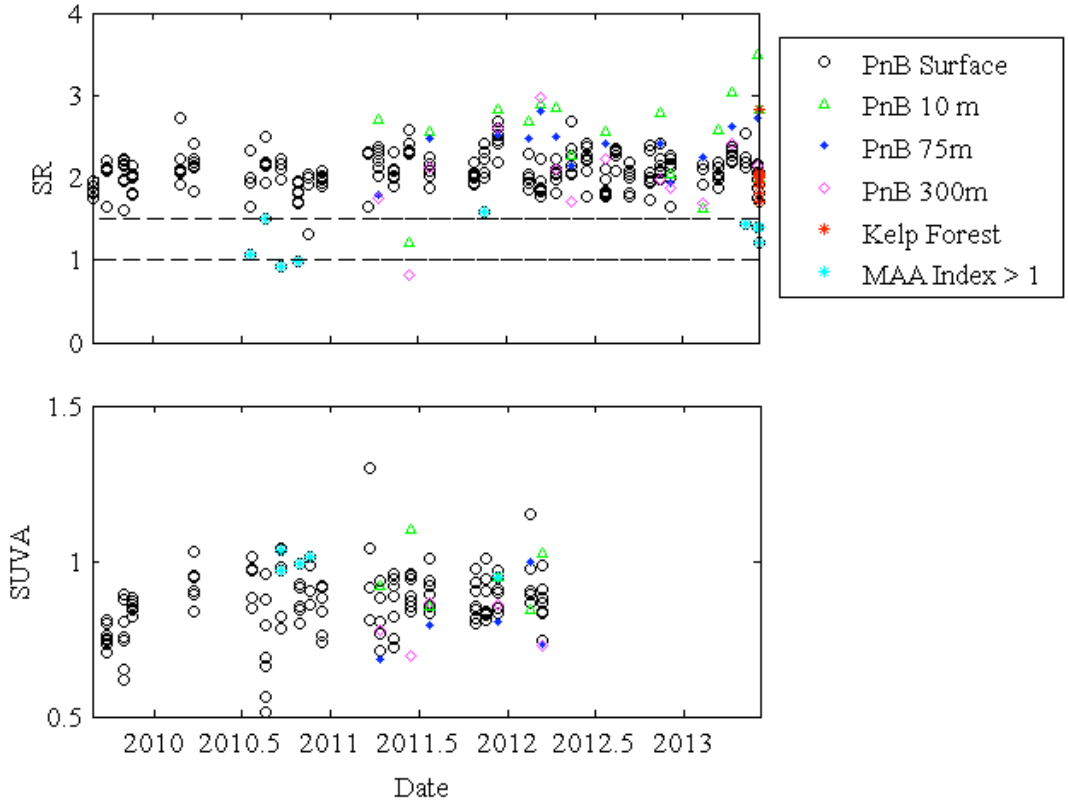

Figure 5. S_R and SUVA for Santa Barbara Channel CDOM samples.

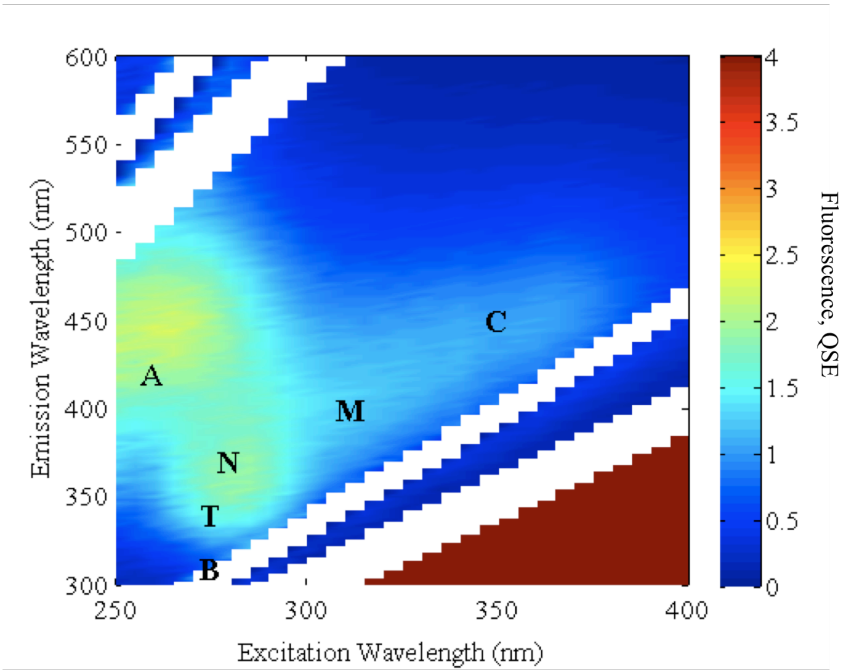

Figure 6. Example EEMS from Plumes and Blooms Station 4, 27-August, 2009.

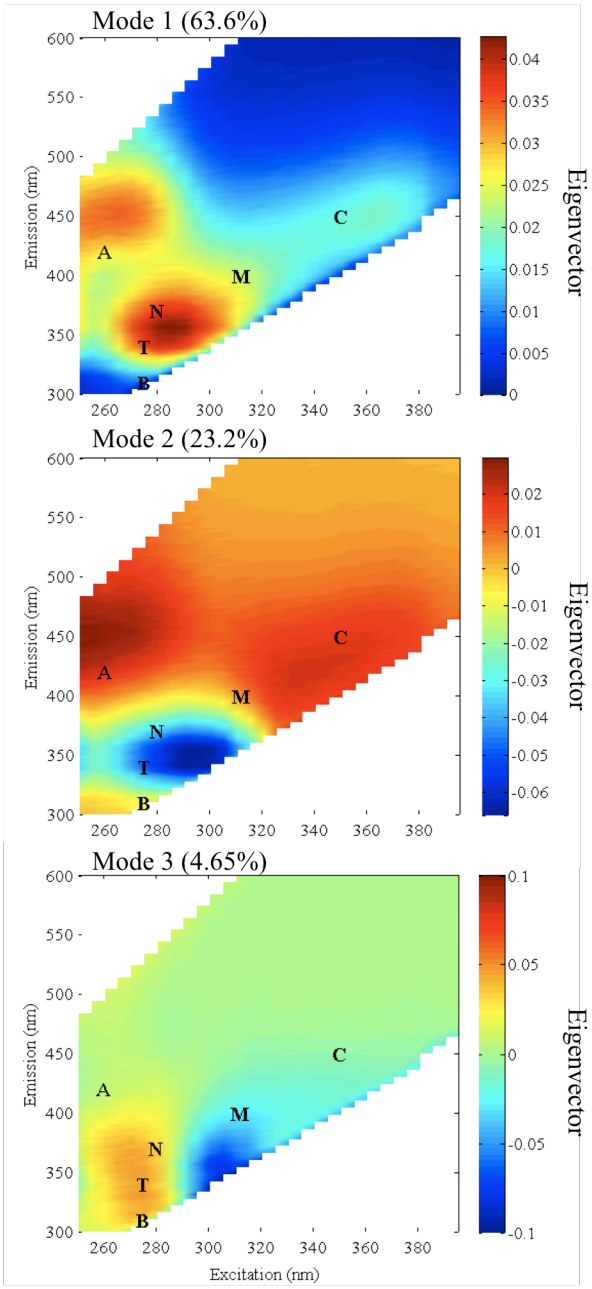

Figure 7. Eigenvectors for EOF output using EEMS data for the SBC.

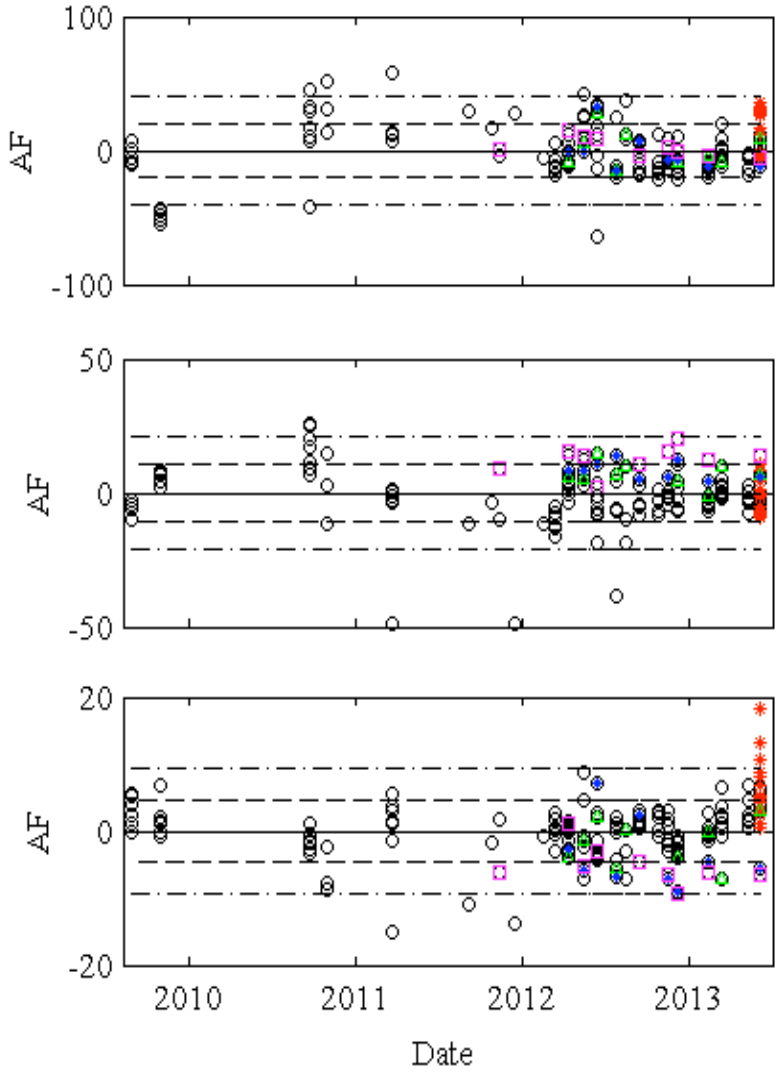

Figure 8. EOF amplitude function (AF).

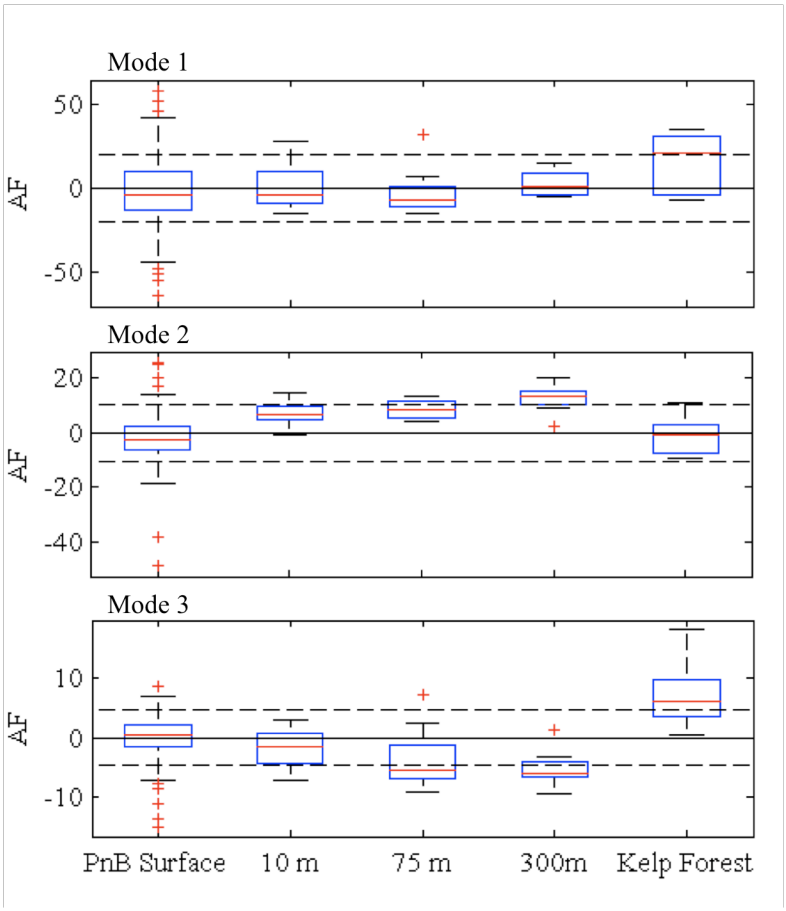

Figure 9. Mean AF for PnB Surface samples (Station 1 – 7), Station 4 at 10m, 75 m and 300 m depth, and Kelp Forest.